UNIVERSITÀ
DEGLI STUDI
FIRENZE

DOCTORAL PROGRAMME IN INDUSTRIAL ENGINEERING
DOTTORATO DI RICERCA IN INGEGNERIA INDUSTRIALE

XXXII

Application of Austempered Ductile Irons to structural components of railway vehicles

ING/IND-14

Doctoral Candidate
Gianluca Megna

Supervisors
Prof. Andrea Bracciali

External Referees
Prof. Carlo Rosso
Prof. Angelo Mazzù

Dean of the Doctoral Programme
Prof. Maurizio De Lucia

Years 2016/2019

Summary

The development of new materials for railway structural components represents a very challenging topic. Especially in the last year, the research and the development focused the attention to lighter components in order to reduce mass, energy consumption and damages of both rails and wheels. However, conservative and proved in service solutions for safety critical components are today the main choice of the railway vehicle manufacturers. This is often dictated by the current frame regulation, which not only gives the guidelines for the design process but also imposes the material to be used. An example is the axle that together with the wheels composes the wheelset, which represents the main component of a railway vehicle. In this context, a great effort must be done to bring innovative solutions.

Since the last decade of 19th century, steel technology has grown rapidly, replacing early cast iron railway components that were very cheap but also very brittle. The interest in cast iron technology for structural components slowly restarted only after the development of ductile irons (DIs) in 1948, and more recently with the development of Austempered Ductile Irons (ADIs), whose mechanical properties are today comparable with the ones of high strength steel. ADI has been commercialized for the first time in 1972, and it is obtained by a special heat treatment (called *austempering*) of ductile iron improving its characteristics in terms of strength and toughness. The use of this material is today very spread as replacement of steel in automotive industries, gear manufacturing, earth moving vehicles and all that applications in which high strength, low weight and wear resistance are needed.

In this thesis, a state of the art of the structural components of railway vehicles and the material used for their manufacturing is analyzed in order to find possible new applications for ADI. The main scope of the research is therefore to demonstrate that high stressed steel components of railway vehicles can be replaced by casted ADI components. After a survey of the possible components to be produce in ADI, three possible applications were found: wheel centre for tyred wheels, bogie frame, couplers for heavy haul operation. A feasibility analysis was performed and after a preliminary design the project has been focused in the development of an optimized tyred wheel as replacement of the current wheel for an existing Diesel Multiple Unit (DMU). Prototypes of this wheel have been finally manufactured and tested in order to demonstrate the feasibility of the application of ADI to the structural components of railway vehicles.

Contents

Introduction

A railway system can be generally described as the composition of several subsystems: the vehicle, the track (or generally speaking the infrastructure), the energy supply system and the signalling system. A good interaction between these subsystems is needed to guarantee a successful railway service, considering its three main pillars: safety, regularity and punctuality. For this high valuable interaction between very different and critical components, the whole railway system is conventionally known as a "complex system". However, complex systems often need compromises in order to guarantee a good interaction in all conditions. The most famous example regarding the way a vehicle runs on the track is the conflict between steering and stability. In fact, it is nearly impossible to guarantee a stable run at high speed in straight track and at the same time to guarantee the ability of the vehicle to run in tight curves without generating wear and damages of both wheel and rail.

On the other side, a complex system needs to be regulated in order to guarantee a safe operation in every possible condition and between different countries. In fact, today modern railways are interoperable with the aim to harmonize the available technology all along these countries. This is particularly true in Europe, where the European Commission released the first Technical Specification for Interoperability (TSI) for high speed in 2002 [1]. Nowadays, these legal documents represent the state of the art of the entire railway system covering the main aspects such as passenger and freight rolling stock, infrastructures, energy supply, signalling and traffic management. The Technical Group 256 of the European Committee for Standardization (CEN) is currently active to supply standards supporting the guidelines dictated by the TSI's. In this work, the EN standards are therefore taken as the basis for the evaluation of the current technologies used in railway vehicles. Despite the very strict safety rules that regulate the railway system, a continuous technical research is necessary in order to develop new solutions that help to increase the efficiency of the transport, to reduce the costs related to production, maintenance, operation of the components and to reduce the environmental impact of the transport.

Materials to be used in safety critical components is one of the main research topics as the application of modern technologies would let to reduce the mass or increasing the whole life of the components. However, it is a very sensitive point and the aforementioned rules give specific indications to be followed by the manufactures. This is especially true if a component belonging to a subsystem interacts with another component that belongs to a different subsystem. The main example is the case of *wheel/rail contact*, a steel to steel rigid and often unlubricated contact in which high pressure is reached and important tangential forces arise.

Understanding rolling contact fatigue (RCF) behavior and more in general wear related to this contact is still today an open issue [2] and introducing new materials would need years of research and years of testing, in order to guarantee a safety level as high as the current one. For this reason, even if different materials have been tested in the past, today the research is concentrated in developing advanced steel grades for specific applications.

Therefore, in order to focus about the motivations that led this project, it is possible to introduce the main research question: *in which structural components of railway vehicle is possible to apply innovative materials? In particular, is it possible to replace steel with Austempered Ductile Iron for those components that are highly stressed?*

To answer this question is preliminary needed to perform an extensive state of the art analysis, that includes:

- **Standards analysis** based on the current European regulation frame for the approval of railway vehicles. TSI Loc&Pas [3], gives the main guidelines and it supported by European Norms (ENs) drafted by CEN (European Committee for Standardization), CENELEC (European Committee for Electrotechnical Standardization) and ETSI (European Telecommunications Standards Institute).

- **Market analysis** of casted components currently used in the railway market, based on a survey performed at most important trade fair of railway sector (InnoTrans 2016).

- **Technical review** based on a literature research of technical and academic papers about past and present ADI applications.

ADI is in fact a quite recent material, but its outstanding properties led to a rapid and extensive spreading in automotive and earth moving machines. Some applications can be found also in railway vehicles, but only few and simple products have reached a commercial success. However, ADI can bring to a considerable mass reduction thanks to the low density, the high-performance mechanical properties and the incomparable easiness of producing complex shapes. However, the market is almost covered by few manufactures and it could be very difficult for new or small companies to emerge in a field in which products are proven in service since many years.

Therefore, this research, founded by *Zanardi Fonderie S.p.A.*[1], a worldwide leader company in cast iron product and austempering, has the main scope to demonstrate that the application ADI in structural components of railway vehicles is feasible and that innovative components can be designed according to the current standards, developed, tested and commercialized.

[1] *Zanardi Fonderie S.p.A.* is a family firm based in Minerbe (Verona) that has now reached its fourth generation. The production consists of ductile iron and ADI castings formed in green sand. Company production is mainly of medium size series with an average of 22000 tons of iron every year, of which 10000 ADI, with unit weight casts between 1 and 120 kg.

1. Railway vehicles

1.1. Structural components of railway vehicles

The main component of a railway vehicle is the *wheelset* that is made of two wheels connected by a rigid axle. If two or more wheelsets are grouped together in a frame the vehicle is a bogied vehicle and this frame is called *bogie frame*. The connection with the wheelsets is guaranteed by an axlebox (which houses the roller bearing) and a set of springs called *primary suspension* gives a certain flexibility in *x, y, z* directions. All these components, together with the braking system and the traction system, are usually called in one word *running gear*. The bogie is then connected to the carbody by another set of springs, called *secondary suspension*. Depending on the kind of vehicle and the peculiarity of service, the arrangement of these components can be different, and a range of solution exists. For example, freight bogies do not usually have the secondary suspension and the connection with the carbody is made of a spherical pivot and two side bearers used as anti-roll system.

Therefore, is possible to identify three structural components of a railway vehicle: the wheelset, the bogie frame (usually it includes the axleboxes) and the carbody. Considering that the carbody production technology lays outside the scope of this work, in the following paragraphs the other components, which are part of the running gear of a railway vehicle, will be analyzed.

According to the definition from [4], the running gear is the system that provides safe motion of the vehicle along railway track. Equalization of vertical loads, guidance of the vehicle and transmission of the braking and traction forces are the main functions of this system. Stability in straight track at high speed, curving ability during curve negotiation together with the control and damping of dynamic forces must be guaranteed by a proper design of the running gear. Even if the choice of the suspension system is critical in order to optimize the vertical, lateral and longitudinal dynamic behavior, the structural design of the wheelset and the bogie frame play a very important role if the aim is to achieve a light and safe running gear. The interaction between wheels and rails is strongly influenced by the ability of a running gear to be as friendlier as possible while running over curves and track irregularities.

However, all of these are safety critical components and their design and manufacturing process is often standardized to provide proven in-service components, which must be able to guarantee a safe service between different countries, availability in short time with known

maintenance and simple inspection procedures. In the following paragraphs the state of the art of wheelsets and bogies production technology will be described. EN standards are taken as starting point considering also the necessary procedures that new components must comply to be introduced in the market.

Attention is paid for casted products, which is a common practice in North America, where casted steel is used to produce wheels, bogie frames and couplers, even for heavy haul vehicles. Respect to cast iron, it is known that the castability of steel is quite poor as the liquid steel cools rapidly as it enters in the mould. Thin sections are therefore difficult to be produced reducing the freedom in component design and increasing the possibility of internal porosity in the zones subjected to shrinkage. Association of American Railroads (AAR) regulations defines very demanding tasks for the approval of the casting processes. These complicated procedures are balanced by the very low-cost production of a high number of casted products. Moreover, castings let the production of simpler products. For example, the three-pieces bogie (the most common freight bogie in USA, Russia, South Africa and Australia) is made of two casted side frame and one casted bolster, connected by friction wedges and a nest of spring, reducing the manufacturing time and costs respect to welded structures. Even if today the tendency to produce bogies as a mix of casted parts and welded parts is quite spread, in Europe the practice of steel foundry has been abandoned very early, due to the difficult to control the quality of the products.

Wheels can be either tyred or monobloc. The first kind is composed by three components: the wheel centre, the tyre and the retaining ring. The tyre is the wearable part and it is shrink fitted on the wheel centre heating the tyre up to a temperature sufficient to recover the mechanical interference. The retaining ring is then applied. Simpler is the second kind: monobloc wheels, as the name say, have no need to be assembled after their manufacturing, with lower costs for mounting and maintenance. However, as the tyre is not removable, when it is worn, the whole wheel must be scrapped. Figure 1, shows the difference between the two kinds of wheels.

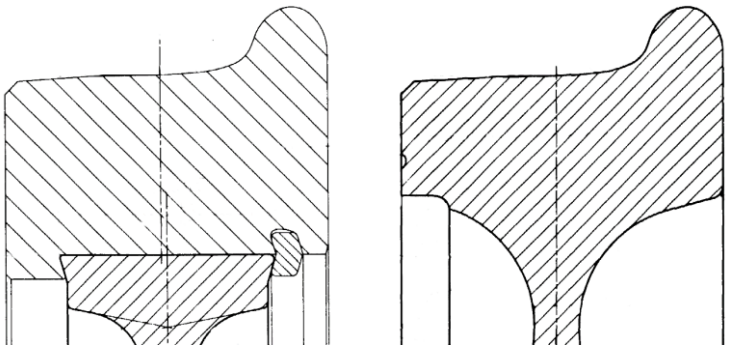

Figure 1**.** Drawings of a tyred (left) and monobloc (right) wheel with the same external diameter of 940 mm. Tread and flange profile is the same for both wheels.

Even if railway vehicles were born with tyred wheels, today monobloc wheels are mainly used in almost all kind of vehicle. Monobloc wheels give advantages for high-speed applications and where tread brakes are used, but they are replacing tyred wheels also in urban and suburban trains. The reasons can be explained considering the lengthy and expensive

maintenance procedures and the higher unsprung mass respect to a monobloc wheel with the same diameter.

The wheels are therefore fitted by mechanical interference on a common axle. The axle connecting the two wheels is the most stressed part of railway vehicle, as it is subjected to alternate bending during its rotation, and its mechanical design and maintenance procedure is very critical. As the wheels are rigidly connected, the two wheels rotate at the same angular speed, and the wheelset is therefore able to self-centering when a lateral displacement occurs. Bearings placed inside or outside the wheels, allow the wheelset assembly to freely rotate respect to the bogie frame. Depending on the arrangement of axle, wheels and bearings, different kinds of wheelset can be found, as shown in Figure 2.

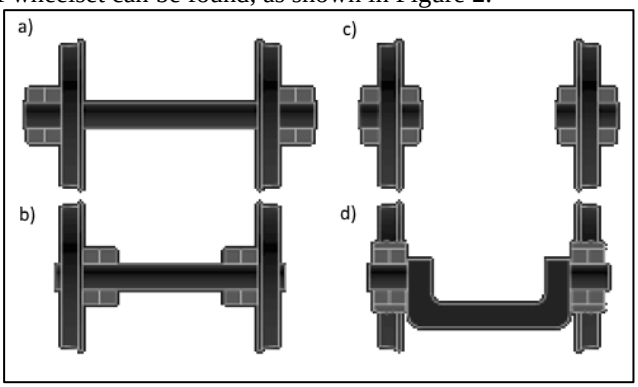

Figure 2. Different kinds of wheelsets [5] a) with outboard bearings; b) with inboard bearings; c) independently rotating wheels with bearings on both sides; d) independently rotating wheels with no-rotating axlebridge.

The bogie frame groups the wheelsets (usually two) to improve the steering ability of a railway vehicle and at the same time letting to produce longer wagons. Two-axle vehicles are today very rare respect to vehicles with four axles grouped in two bogies. The bogie design and its connection to the wheelsets is central in the dynamic behavior of the vehicle. The main parameters that influence the running dynamics are given by the bogie wheelbase (distance between the two wheelsets) and the primary suspension stiffness in longitudinal direction. As shown in Figure 3, low values of this parameters guarantee a better behavior while running in small radius curves, but they can reduce the stability at high speed.

However, dynamics of a bogie in curves is quite complex as in most conditions the leading wheelset of a bogie shows higher angle of attack α respect to rear one. Running in curves is also related to other parameters, as the running speed, the curve radius, the cant and the gauge of the track.

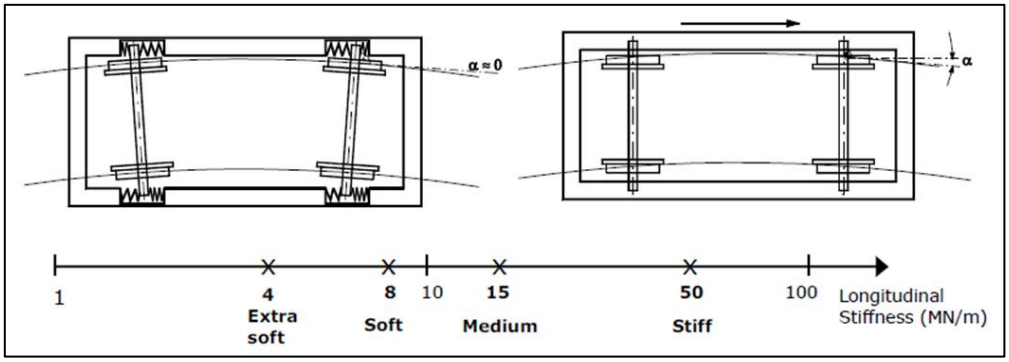

Figure 3. Different curving behaviour between a "flexible" bogie with soft suspensions (left) and a "stiff" bogie with rigid suspensions (right) [6] plotted vs. the typical values of longitudinal primary stiffness for passenger vehicles [7]. The angle α is called angle of attack and it is considered as representative parameter for a curving ability of wheelset.

Finally, the connection between the bogie frame and the wheelsets is completed by the axleboxes, which house the bearings and sustain the primary suspensions, while on the other side the bogie is connected to the wagon body by the secondary suspensions and a bolster that can rotate unless Flexcoil springs are used.

Bogie design and manufacturing technology is today very advanced, and inboard bearings bogies represent the state of the art in these field, as with their lower weight and moment of inertia around the vertical axis let to adopt short wheelbase with maximum speeds up to 250 km/h. On the contrary bogie frames for freight wagons are not so advanced and old technologies are still used, as low production and maintenance costs must be guaranteed. Several alternatives to the Y25 (the most common freight bogie in Europe) have been proposed and tested, but due to the very demanding tasks of freight wagons market these bogies have never been serious competitor of the Y25.

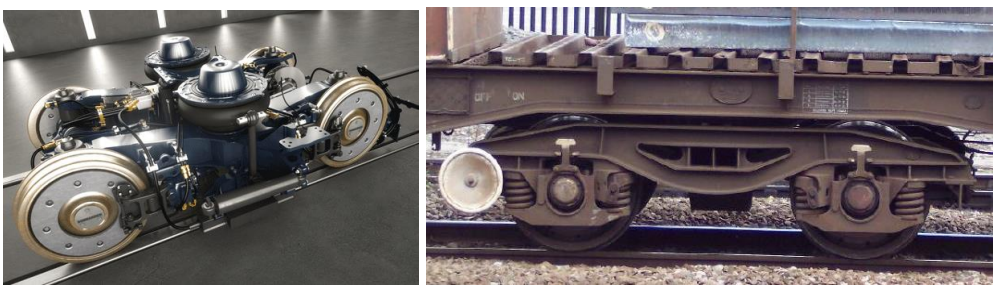

Figure 4**.** On the left the most advance passenger bogie (Bombardier *Flexx Eco*) [8] and the most common freight bogie (right) [9].

1.2. Current regulation frame

To give the manufactures all the necessary means for a correct and safe design and a high-quality production, the European legislation have provided a number of technical specification (Technical Specification for Interoperability or TSI for short), that every National Safety Authority (NSA) must adopt as guidelines for the Authorization for the Placing In Service (APIS) of each new vehicle. This is the result of a complex legislation program started in 2001 with the 1st Railway Package, which has the aim to guarantee a more efficient transport system by stimulating a real competition between operators, opening the market between the different countries and improving European train paths. In 2016 the 4th Railway Package has been approved to hopefully complete this process[2].

In this context, TSI related to vehicle design are supported by several technical standards drafted by CEN. For the purpose of this research only few standards will be described, considering that only wheelsets and bogies are relevant.

1.2.1. Standards for wheels

Relevant standards for wheels are drafted by the Working Group 11 of the Technical Committee 256 of CEN and are mainly divided between standards for design methods and standards for product qualification. Wheels manufacturing is regulated by:

- EN 13979-1:2003+A2:2011 - Railway applications - Wheelsets and bogies - Monobloc wheels - Technical approval procedure - Part 1: Forged and rolled wheels
- EN 13262:2004+A2:2011 - Railway applications - Wheelsets and bogies - Wheels - Product requirements

Firstly, such standards are specifically defined for monobloc wheels. Therefore, tyred wheel does not exist anymore for the European legislation. About this choice there is not a technical reason, but it is related to the fact that the first TSI, and consequently the first EN standard, has been drafted only for high-speed vehicles, for which tyred wheel are not considered suitable due to the relevant centrifugal force and the related risk of losing the tyre. However, even if a TSI also for conventional rail has been developed later, tyred wheels have never been reintroduced as possible application. Modern vehicles are always equipped with monobloc wheels, as ENs are today used from all manufactures and operators even if not specifically required and tyred wheels are limited to old fleets. For example, metro vehicles are often designed according to these standards considering them as the state of the art.

[2] European Commission. Fourth railway package of 2016. Available at: https://ec.europa.eu/transport/modes/rail/packages/2013_en (accessed on 10.07.2019).

Secondly, the standards define the methods and the materials that must be used for wheel manufacturing. EN 13262 provides all the necessary procedures for the qualification of the product (the monobloc wheel) and its production process. It is applicable only to forged and rolled wheels which are made from vacuum degassed steel and with the heat-treated rim. This heat treatment, called rim chilling or rim hardening, is required to generate compressive residual circumferential stresses in the rim by water spraying, to reduce wear and tread damages [10]. However, the actual benefits of this process are still field of debate for mainly two reasons. The first one is that these compressive residual stresses have a limited duration, due to the thermo-mechanical stresses due to tread braking in freight wagons [11] or the re-profiling processes to restore the correct tread profile in both passenger and freight vehicles. The second one is that if the rim is in compression, on the other side the wheel web has consequently tensile residual stresses. This is shown in Figure 5 for an AAR casted wheel, but the same happens in wheels designed according to EN 13262.

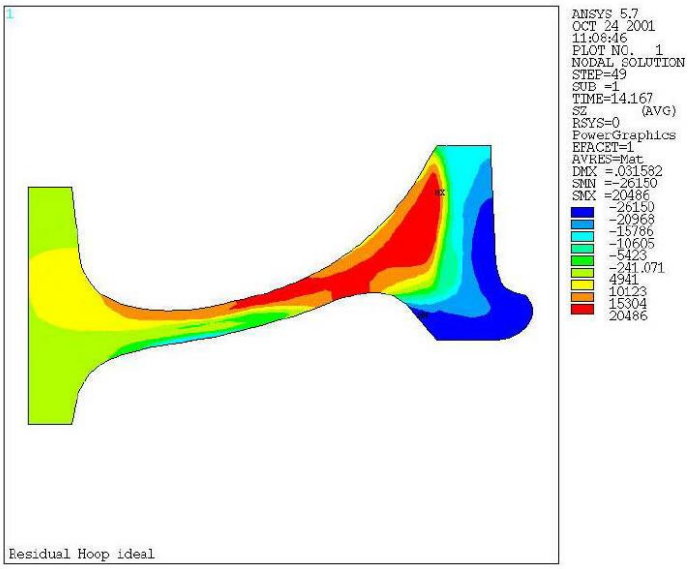

Figure 5. Residual circumferential (hoop) stresses on an AAR casted wheel with diameter of 36 inches = 914 mm, after the process of rim quenching. Maximum tensile stress is 20486 psi = 141.3 MPa [12].

These tensile stresses have an impact on the fatigue behavior of the wheel, which however are always not considered during the design assessment stage.

Data of interest are the mechanical properties to be achieved to consider a steel qualified for the wheel production. Chemical content of single elements to be achieved for admitted steels are show in Table 1, while values required during tensile test are shown in Table 2.

Table 1. Required chemical composition of steels according to EN 13262.

Steel grade	Maximum content [%]										
	C	Si	Mn	Pb	S	Cr	Cu	Mo	Ni	V	Cr+Ni+Mo
ER6	0,48	0,40	0,75	0.02	0,015	0,30	0,30	0,08	0,30	0,06	0,50
ER7	0,52	0,40	0,80	0,020	0,015	0,30	0,30	0,08	0,30	0,06	0,50
ER8	0,56	0,40	0,80	0,020	0,015	0,30	0,30	0,08	0,30	0,06	0,50
ER9	0,60	0,40	0,80	0,020	0,015	0,30	0,30	0,08	0,30	0,06	0,50

Table 2. Required values to be achieved during tensile according to EN 13262

Steel grade	Rim			Web	
	R_{eH} [MPa]	R_m [MPa]	A_5 [%]	R_m [MPa]	A_5 [%]
ER6	500	780÷900	15	680÷800	16
ER7	520	820÷940	14	710÷830	16
ER8	540	860÷980	13	740÷860	16
ER9	580	900÷1050	12	770÷920	14

Others important parameters are those regarding the toughness of the material. For all wheels the impact strength of specimens from the rim must be evaluated according to Charpy test at 20°C (K_u) and -20°C (K_v). The required average values are shown in Figure 6.

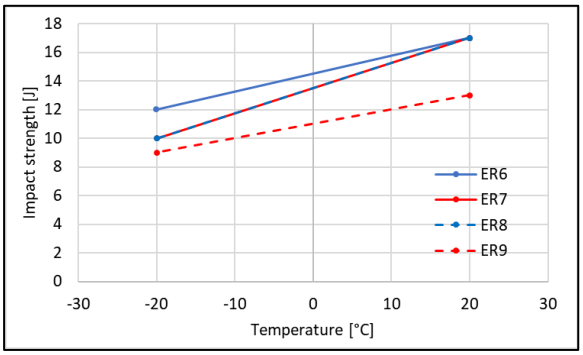

Figure 6. Average values to be achieved during the Charpy tests at 20°C (K_u) and -20°C (K_v) from notched specimens from the wheel rim. For ER7 and ER8 the same values are required.

However, even if notch-impact tests could be useful for the evaluation of *ductile-to-brittle temperature transition*, it is not the correct parameter to predict the capabilities of structures and components containing cracks to continue to carry loads [13]. In this case only the *fracture mechanics theory* can be used with high confidence. In fact, to limit the failure conditions, the knowledge of macroscopic material characteristics like yield stress or elongation at fracture is not enough and the stress-intensity factor K has to be evaluated. This value is measured in MPa$\sqrt{m}$ and depends from the shape of the crack and the stress level to which the crack is subjected according to (1), where σ is the applied stress, a is the main length

crack and *Y* is the geometric factor depending on the ratio between the length *a* of the crack and the length of the specimen *w*.

$$K = \sigma(\sqrt{a})Y(\frac{a}{w}) \tag{1}$$

Even if this value is strongly influenced by the complexity of the crack geometry and loading condition, is it possible to determine a unique value, called critical stress-intensity factor K_c, at which fracture become unstable. Starting from the hypothesis that the plastic region around the crack tip is smaller enough respect to dimension of the specimen, measuring this value with specific tests and specimen's configurations, defined in standards such as [14], the resistance to crack propagation can be therefore evaluated, plotting the force against the crack growth.

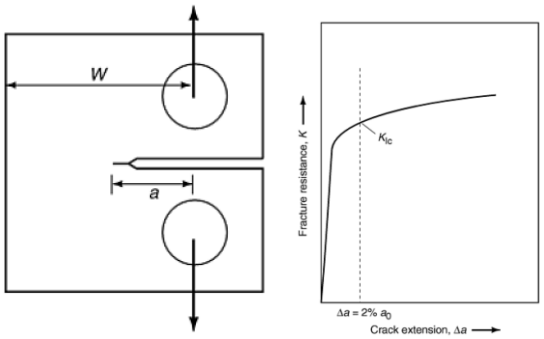

Figure 7. One of the pre-cracked CT (Compact Tension) specimens defined by ASTM E399 [14] (left) for the evaluation of critical stress-intensity factor K_{Ic}. Schematic representation of fracture resistance plot (right) [15].

Independently from the behavior of the material (ductile or brittle) the deformation of the crack measured during the test, can be linear-elastic or non-linear due to the occurrence of plastic deformation at the crack tip. In the second case other parameters can be derived for the description of the fracture, such as the *J-integral*, the *CTOD* (Crack Tip Opening Displacement) or the *CTOA* (Crack Tip Opening Angle) [16]. All these tests are quite expensive respect to notch-impact tests and correlations between the results of impact tests and the K_{Ic} have been developed in the past to reduce the time of experimental process. However, these correlations are dimensionally incompatible, ignore the different influence of the loading rate and the notch acuity, and are valid only for limited types of materials and ranges of data [15].

The standard EN13262, only require the measure of the stress-intensity factor for block braked wheels made of ER6 and ER7 steels. Minimum values to be achieved are respectively 80 MPa√m and 70 MPa√m. The reason of this evaluation can be found in [17], in which extensive research has shown that monobloc wheels can break due to the thermo-mechanical stresses due to continuous braking if the fracture toughness of material is not enough to prevent crack growth. An example is shown in Figure 8.

More interesting for general solid wheel design (disc braked, or tread braked) is the fatigue limit of the materials. EN13262 gives the minimum required values of total stress variation $\Delta\sigma$, independently from the steel grade: 450 MPa (±225 MPa) for wheels with machined web and 315 MPa (±157.5 MPa) for wheels with as rolled web, for 10^7 cycles and a probability of survival equal to 99.7%. The verification of this mechanical property must be proven on the wheel itself, applying radial stresses on the web by means of full-scale fatigue test bench. Usually, the previous characteristics are verified on two wheels without statistical evaluation applying a radial stress level of ±240 MPa for wheels with machined web and ±168 MPa for wheels with as rolled web, and no crack must be visible on the wheel web after 10^7 cycles.

Fatigue limits to be applied during the design stage according to EN13979 are shown in Table 3 and compared with the previous values. These values were obtained by several full-scale tests described in [19], and applying safety coefficients equal to 1.36 for wheels with machined web and 1.2 for wheels with as rolled web.

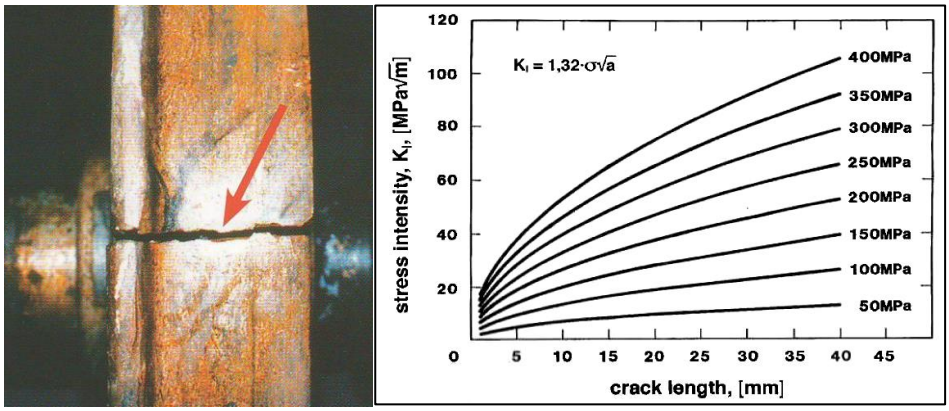

Figure 8. Broken wheel due to radial crack opening. The red arrow shows the opening point on the tread (left) [18]. Stress-intensity factor plotted against the crack length of a semi-elliptical crack for different stress values. For a K_I value of 70 MPa√m and a stress of 350 MPa, the critical length results between 20 and 25 mm (right) [18].

Table 3. Summary of the fatigue limits and stress levels to be used for the design and product qualification.

Wheel web state of delivery	Fatigue limit according to UIC510-5 [MPa]	Minimum $\Delta\sigma/2$ required by EN13262 [MPa]	Radial $\Delta\sigma/2$ for full-scale tests applied on two wheels [MPa]	Design $\Delta\sigma/2$ required by EN13979 [MPa]
Machined	246	225	240	180
As rolled	175	157.5	168	145

The standard EN 13979 also provides the methods to be used for the FEM evaluation of the stresses due to in service loads. The *maximum principal stress method* (MPSM) is defined in the EN13979, but it is explicitly applicable only to the assessment of axisymmetric

wheels, for which the radial stress is usually dominant with respect to circumferential stress in the wheel web, and therefore the stress distribution due to three load cases that can be observed at the wheel-rail contact (shown in Table 4) repeated for different angular positions, is reduced to a uniaxial load case to be compared with the permissible stress. Principal stresses and directions are calculated for each node, finding the maximum principal stress σ_{max} and its direction. The smallest minimum principal stress for all load cases is then projected (σ'_{min}) in the direction of σ_{max}. The alternate stress is therefore $\sigma_a = \Delta\sigma/2 = (\sigma_{max}-\sigma'_{min})/2$, while the mean value is $\sigma_m = (\sigma_{max}+\sigma'_{min})/2$. This procedure is repeated for all the principal directions and the resulting pairs (σ_m ; σ_a) are plotted in the Haigh diagram, shown in Figure 9. It is worth to highlight that the Haigh diagram is quite unusual, as the mean stress has no effect on the alternating stress, likely due to the hypothesis of absence of surface defects that could lead to high stress concentrations.

Table 4. External loads and load cases to be applied during the design of the wheel. The three load cases are the representation of three different kinds of contact that could occur at the wheel-rail interface. A= vehicle running on straight track; B= vehicle running on curved track; C= vehicle running on crossings.

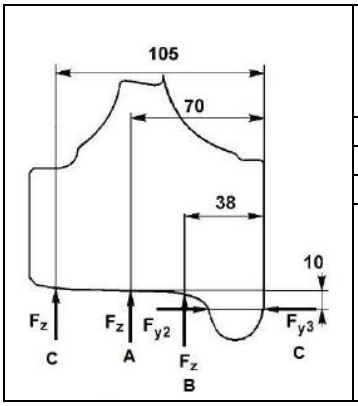

	Load Case A (Straight track)	Load Case B (Curved track)	Load Case C (Check rail)
Vertical force F_z	1.25*P*	1.25*P*	1.25*P*
Lateral force* F_y	-	0.6*P*	0.36*P*
Lateral force** F_y	-	0.7*P*	0.42*P*

* non-guiding wheelset
** guiding wheelset
P = static vertical wheel load

However, wheel web could not be axisymmetric, for example due to the presence of holes (needed for wheel web mounted braking discs) and in this case the hypothesis of dominant radial stress could not be locally satisfied and therefore, multiaxial criterion (e.g. Crossland or Dan Vang [20]) should be used. Even if these criterions are prescribed by EN13979, they are not applied by wheels manufactures and the MPSM is used also for non-axisymmetric wheels.

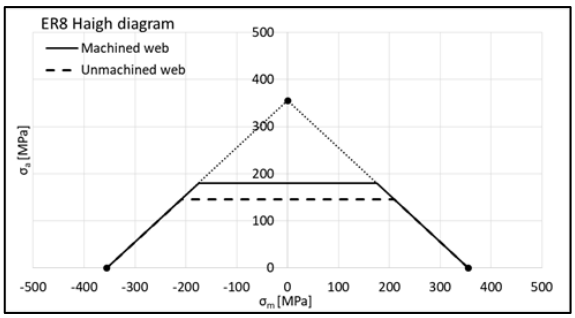

Figure 9. Haigh diagram used for the mechanical assessment of the solid wheels according to EN13979.

Finally, also casted wheels are considered by two EN technical specifications, but they are not included in the TSI. These documents are:

- CEN/TS 13979-2:2011 - Railway applications - Wheelsets and bogies - Monobloc wheels - Technical approval procedure - Part 2: Cast wheels.
- CEN/TS 15718:2011 - Railway applications - Wheelsets and bogies - Product requirements for cast wheels

They are applicable only for freight wagon wheels (up to 120 km/h) with chilled rim and only two steel grades are defined (C ER7 for tread braked wheels and C ER8). For these grades no major difference can be found respect to the previously described standards EN13979-1 and EN13262.

1.2.2. Standards for axles

Relevant standards for axle design are drafted by the Working Group 11 of the Technical Committee 256 of CEN and are mainly divided between standards for design methods and standards for product qualification:

- EN 13103-1:2017 - Railway applications - Wheelsets and bogies - Part 1: Design method for axles with external journals
- EN 13261:2009+A1:2010 - Railway applications - Wheelsets and bogies - Axles - Product requirements

The standards prescribe the material to be used for axle manufacturing. EN 13261 define three steel grades independently from the axle kind, i.e. powered (motor) or non-powered (trailer) and solid or hollow. These grades are defined in Table 5, together with the minimum values required from tensile and notch-impact at 20°C tests. Requirements for fracture mechanics are not prescribed, and crack propagation is considered sufficiently slow thanks to the extended plastic behaviour of the materials.

Table 5. Required tensile and impact mechanical properties defined in EN 13261. Values for impact tests are the average of three specimens and defined for room temperature.

Steel grades	R_{eH} [MPa]	R_m [MPa]	A_5 [%]	K_u [J] longitudinal	K_u [J] transverse
EA1N	320	550÷650	22	30	20
EA1T	350	550÷700	24	25	25
EA4T	420	650÷800	18	40	25

Measurements according to [14] performed by axles manufactures have shown values of K_{Ic} of 52 MPa√m for EA1N, 54 MPa√m for EA1T and 73 MPa√m for EA4T [21]. For the lower value considering a crack with a = 40 mm and an axle diameter of D = 160 mm, i.e. a/D = 0.25 corresponding to a Y= 0.67, the critical stress is σ = ± 226 MPa according to (2). This value is generally higher than the rotating bending stress to which an axle is subjected, as the maximum design fatigue limit is σ = ± 200/1.2 = ± 167 MPa (Table 6) for EA1N.

(2) $$\sigma = \frac{K_I}{Y(\sqrt{\pi a})}$$

However, under these conditions results of great importance the periodic control of the axle. In fact, even if the axles are designed for infinite life, i.e. the maximum alternating stress is lower than the fatigue limits shown in Table 6, during their service accidental damages could be generated due to impacts, paint detachment and corrosion, and grow to bigger cracks. The concept of *probability of detection* (POD) for non-destructive testing (NDT) is therefore crucial to arrange inspection intervals according to the predictive growth of certain defect and the minimum crack dimension a_i that can be detected, resulting in a *damage tolerance* approach [22].

Table 6. Fatigue limits for steel grades defined in EN13103. Values for EA1T are the same of EA1N. Safety coefficients apply respectively to: trailer axles, motor axles without press-fitted gears, motor axle with press-fitted gears.

Steel grades	Axle body [MPa]	Axle bore [MPa]		Wheel and brake discs fitting areas [MPa]		Bearing seats [MPa]		Safety coefficient to be applied for design [-]
	Solid and hollow	*Solid*	*Hollow*	*Solid*	*Hollow*	*Solid*	*Hollow*	*Solid and hollow*
EA1N	200	N/A	80	120	110	120	94	1.2; 1.3; 1.5
EA4T	240	N/A	96	145	132	145	113	1.33; 1.44; 1.66

As shown in Figure 10, only magnetic particles inspection (MT) reach a POD of 100% but its application can be done only dismounting the wheelset from the vehicle and it is not suitable for in-service inspection. Ultrasonic testing (UT), is therefore used for closer inspections using straight and angled probes applied on rotating holder applied to both ends of the axle, or roto-translating probes for hollow axles that let the inspection from only one side. One possible approach is to choose the initial crack dimension a_i as the one with the 50% of probability to be detected by UT. As shown in Figure 11, from this value it is possible to predict the crack growth and the number of cycles, i.e. mileage, needed to reach the maximum permissible dimension a_f. Then the inspection intervals are defined in such way at least two inspections are available to find the growing crack. It is therefore crucial the knowledge not only of the fracture toughness of the material, but also the crack growing rate, measured according to [23], and expressed according to the Paris' law (3), where C and m are material constants and ΔK is the stress intensity factor range $(K_{max}-K_{min})$.

(3) $$\frac{da}{dN} = C(\Delta K)^m$$

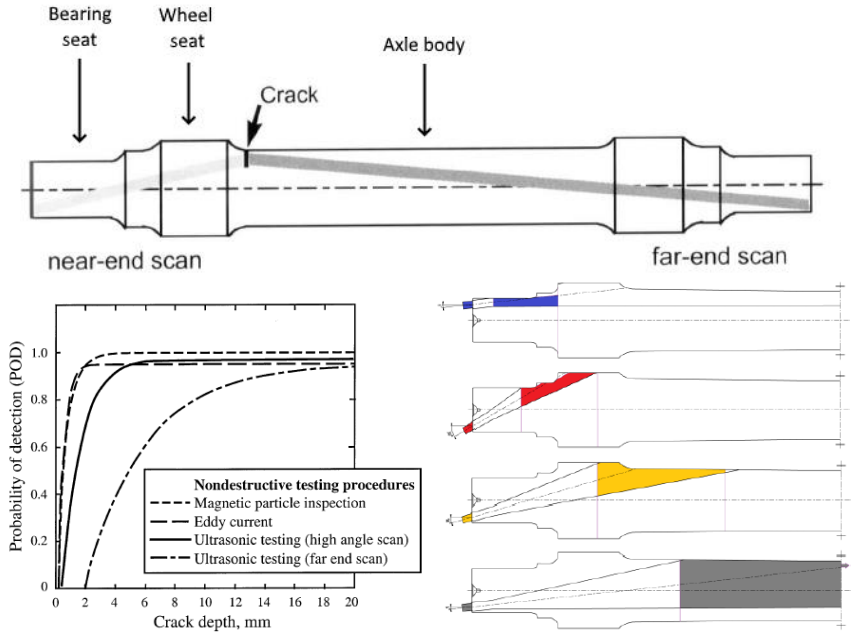

Figure 10. Geometry of an axle (above). Probability of detection as function of the crack size for different non-destructive testing methods (below, left) [22]. Example of inspection areas with a rotating probe applied at one end of the axle (below, right) [24].

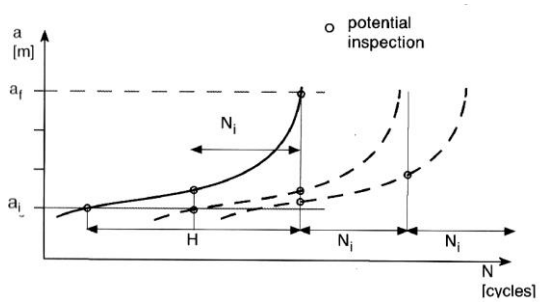

Figure 11. Example of inspection intervals definition in function of the initial crack dimension a_i e final crack dimension a_f [21].

For the approval according to EN 13261 specific rotating bending fatigue tests must be performed on reduced specimens for the material properties approval and on full-scale specimen for the product approval. The minimum required values are shown in Table 7. Values of F_1 and F_2 are the minimum stress level at which three full-scale specimens must be subjected for 10^7 cycles and survive without crack initiation, while R_{fL} and R_{fE} values are determined with a staircase method with fifteen reduced specimens after 10^7 cycles and a probability of survival of 50%.

Table 7. Fatigue limits for steel grades defined in EN13261. Values for EA1T are the same of EA1N.

	Reduced specimens		Full-scale specimens	
Steel grades	Un-notched R_{fL} [MPa]	Notched R_{fE} [MPa]	Axle body F_1 [MPa]	Axle bore (hollow axle) F_2 [MPa]
EA1N	250	170	200	80
EA4T	350	215	240	96

Design methods are defined in EN13103, in which loads to be applied are specified for the calculation of the resulting moment $MR = \sqrt{MX^2+MY^2+MZ^2}$ and the resulting nominal stress to be compared with the fatigue limits of Table 6.

1.2.3. Standards for bogies

For bogie frame design, the relevant standard is drafted by the Working Group 13 of the Technical Committee 256 of CEN and it is:

- EN 13749:2011 - Railway applications - Wheelsets and bogies - Method of specifying the structural requirements of bogie frames

Differently from the previously described standards, materials for manufacturing bogie frames are not prescribed by EN13749. This standard only specifies the general rules for the design and for the assessment, with the aim to reach a satisfactory design of bogie frames including bolsters and axleboxes.

The EN13749 can be applied to all kind of bogies (passenger or freight) and its general-purpose approach leave to the designer a quite high degree of freedom as the manufacturing process is not specifically described. Obviously, as in European countries welded bogies are historically used, the standard refers to [25] for the quality requirements of welds without however eliminating the possibility to use other kind of manufacturing processes. For example, axleboxes, dampers support, and brake caliper supports are often casted in ductile cast iron. Steel castings are also quite used welded at the main structure of bogie frames, which are usually made of S355 welded steel sheets (R_{eH}= 355 MPa; A_5 = 22%).

The assessment of a bogie frame is usually performed in four steps:

- FEA analysis with static and fatigue loads
- laboratory static test
- laboratory fatigue test
- on-track tests

About the first step, even if the standard suggests to use one method between the *endurance limit approach* and the *cumulative damage approach*, one of the most important open point is how to consider the multiaxiality of the stresses during the analysis [26]. There is not a shared approach as previously described for wheels design, and therefore each

manufacture can use their own methods. Moreover, there is not yet a European shared strategy for the assessment of the structural integrity of welds and often old design codes are used [27]. One of the most important guidelines used for welds assessment is the German code of practice DVS1612 [28], in which fatigue values for S355 and S235 steel sheets are given in terms of *MKJ* diagrams for base material and for several class of welded joints (Figure 12). The class of the joint, called *weld performance class*, is given by the combination of the stress category and the safety category related to each specific joint, according to [25].

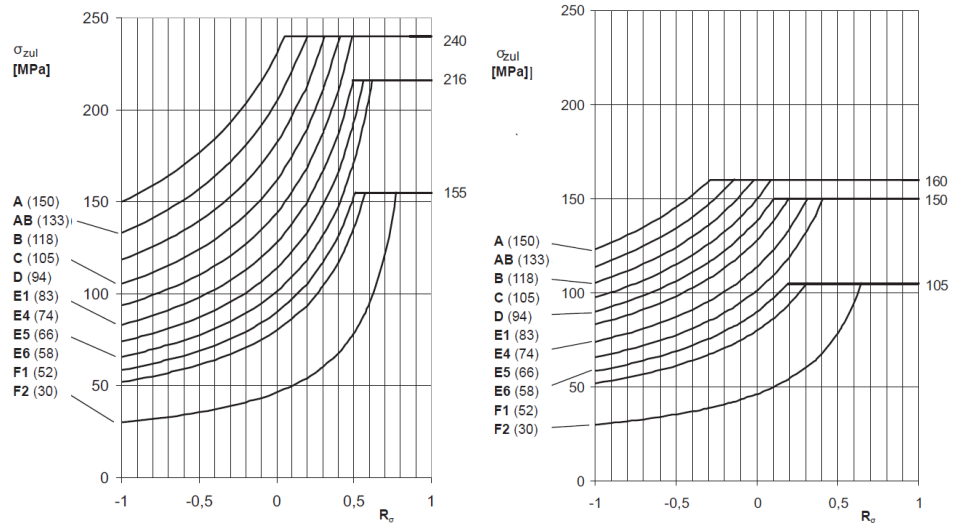

Figure 12. *MKJ* diagrams for S355 and S235 base material (A and AB) and welded joints (from B to F2) according to [28]. The maximum admissible stress σ_{zul} is given in function of stress ratio $R_\sigma = \sigma_{min} / \sigma_{max}$. The fatigue limit can be derived as $\sigma_a = \sigma_{zul}(1- R_\sigma)/2$.

Laboratory tests are performed under specific benches in which the whole bogie frame is under testing. The fatigue test is performed applying variable loads divided in three steps, in which the loads are applied considering the nominal values for $6x10^6$ cycles, then the nominal values plus 20% for $2x10^6$ cycles and finally the nominal values plus 40% for others $2x10^6$ cycles. The loads simulate the alternating inscription of the bogie to subsequent left and right curves, applying quasi-static lateral, vertical and torsional (due to twist) loads with superimpose dynamic cycles. These tests are therefore quite long and expensive, but their severity usually compensate for possible design uncertainties. The bogie design is therefore approved if no cracks are present at the end of the second step and only small cracks are generated during the last step.

1.3. Research and future trends in railway vehicles

Nowadays, the research on railway vehicles technology is aimed to improve the safety and the efficiency of transports. Considering the continuous growth in terms of commercial speeds, number of passengers and freight goods, these aspects are not trivial and their development involves a great number of people and processes, starting from the design and passing through the manufacturing, the testing, the approval and finally the maintenance.

As the service life of a railway vehicle is at least 30 years, maintenance plays a very important role on the *life cycle cost (LCC)* of a vehicle. For example, wheelsets overhaul due to wheels or axles replacement is today a complex matter, not only in terms of mechanical operations but also in terms of logistics flows. Therefore, one of the main research topics remains the study of the *wheel-rail contact* and its influencing parameters, in order to achieve a prediction of rail and wheel damages [29] or optimization of wheel profile [30]. The mechanism and the evolution of wear and tear at the wheel-rail contact are still today under investigations [31] and the wheels, that are design for a theoretical infinite life, can be scraped even after 300.000 km. Improvements to reduce their impact on maintenance costs are proposed in terms of managing the alloying elements in steels for wheels [32], optimal bogie curving inscription with active [33] or passive [34] steering systems, friction management in curves [35]. Moreover, condition monitoring of single components or vehicles behavior can be applied on-board [36] or wayside [37], improving safety and maintenance intervals. Phased array ultrasonic probes are today used to improve the detectability of defects in structural components such as wheels [38] and axles [39], with the aim to reach continuous in-service monitoring of their integrity [40].

A railway vehicle today must be also *track-friendly*, as several countries are adopting more complex computation of *Track Access Charges (TAC)*, to consider not only the static forces that a vehicle exert on the track, which can be optimized by lightweight solutions, but also the lateral and vertical dynamic forces depending on speed, curving inscription, acceleration, running over switches and crossings [41]. This approach let a more precise and fair allocation and prediction of the costs related to maintenance of track, and vehicle manufactures would be stimulated in developing novel solutions. A practical example of this process is the United Kingdom, where a wear-based *TAC* has been introduced since the separation between infrastructure and operators in 1994 and modern inboard bearings were consequently developed to reduce the bogie weight and to improve curving ability of vehicles [42]. A visual comparison between an inboard bearings bogie and a conventional outboard bearings bogie is shown in Figure 14 (left).

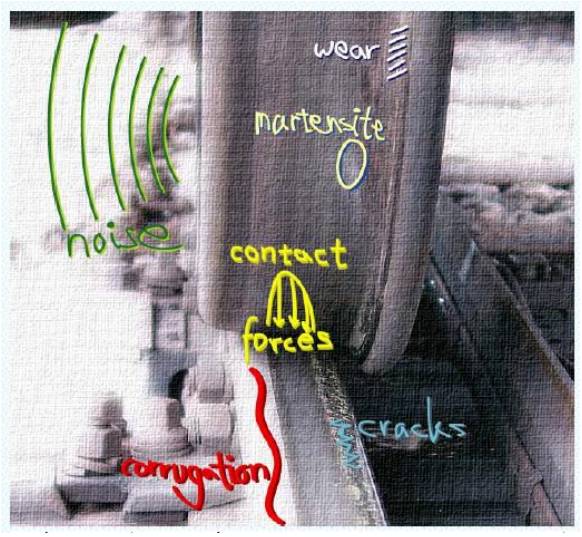

Figure 13. Representation of some phenomena related to the complex behaviour of the wheel-rail contact [43].

Bogie manufacturing with innovative materials is a popular strategy for consistent weight reduction of railway passenger vehicles. Bogie concepts in fiber composite material can be found since 1983 [44], but more recently prototypes have been produced and tested, such as glass fiber-reinforced plastic (GFRP) bogies [45] and carbon fiber-reinforced plastic (CFRP) bogies[3]. The efWING bogie from Kawasaki is shown in Figure 14 (right) and allows a mass reduction of about 40%.

Figure 14. *Left:* Class 220 multiple unit equipped with inboard bearings bogies (left) compared with class 221 multiple unit equipped with conventional outboard bearing bogies (right)[4]. *Right:* efWING bogie made of carbon fiber-reinforced plastic on testing[5].

[3] efWING bogie. http://global.kawasaki.com/en/mobility/rail/bogie/efwing.html (accessed 26.07.2019).
[4] Photo by Britishrailclass91 - Own work, 2008, CC BY-SA 4.0, https://commons.wikimedia.org/w/index.php?curid=3888438 (accessed 26.07.2019)
[5] Photo by Spaceaero2 - Own work, 2016, https://commons.wikimedia.org/wiki/File:JRshikoku_7200series_7303_S-TR67ef.jpg (accessed 26.07.2019).

Another important topic for environmental reasons is the *noise*. Great part of the noise emitted by a railway vehicle is due to wheel-rail contact, excited by both wheel and rail roughness. This noise source is called *rolling noise* which is the most important source in the speed range of 50÷250 km/h and for frequencies between 500 and 5 kHz [46]. Wheel vibration has a relevant role and damped wheels are therefore proposed [47]. Other noise sources such as *flanging noise* and *squeal noise* in curves affect vehicles with very low curving behavior (high angle of attack), especially for system with very low radius curves such as tramways, and the use of friction modifiers is the only possible solution for existing systems [48].

On the other side the rolling noise is a sensitive problem for freight wagons, which are still equipped with brake blocks. Cast iron blokes are traditionally used but will be no longer permitted in the following years, as they increase wheel roughness during high energy braking producing high rolling noise levels. Other kinds of blocks made of organic or sinter materials, such as LL (Low noise, Low friction) blocks or K blocks, have been development to replace cast iron, but introducing other difficulties such as thermal energy dissipation, wear and rolling contact fatigue [49]. Greater thermal input into the wheel could be very dangerous and special design are therefore needed, such as *thermostable solid wheels* [50]. These wheels are designed with a deep-curved web, to minimize the radial stiffness and at the same time limit the axial displacement of the rim during the braking application.

Figure 15. On the left, bottom view of the LEILA inboard bearings bogie, with cross-bracing used to improve steering and wheel web mounted brake discs to reduce noise. On the right, the TF25 bogie with primary vertical hydraulic damper and rubber-metal side bearers.

However, freight wagons design and operational management improvement is maybe the most challenging topic for the future. Even if the Y25 bogie has recently celebrated the 50th anniversary from its first development [51], it is still the most common freight bogie in Europe. The main reason can be found in the low manufacturing and maintenance costs, which have strongly reduced the possibility of the application of innovative solutions. However, the increase of the efficiency of goods transport by means of freight wagons is one of the main objectives for the next years and projects are dedicated to developing an innovative freight bogie with superior characteristics respect to current Y25 bogie [52] [53]. Several aspects must be involved in this process, with special attention to wagon design, monitoring and maintenance. As lower noise, greater load capacity, lower downtime and better ride quality are requested by railway companies, bogie designer must face very challenging problems. This is confirmed by considering that the state of the art of freight bogies [54], composed by improved design of Y25 (like the GB25RS or the TVP2007) or advanced new design (like the RC25NT, the DRRS25LD or the TF25), is not able to completely replace the classic design of Y25, even if greater performances could be guaranteed in terms of safety, speed and reliability. Inboard

bearings bogies have been designed also for freight vehicles. The most important example is the LEILA (*LEIchtes und LärmArmes*, i.e. light and low noise) bogie [55], shown in Figure 15 (left) and developed between 2000 and 2005, but due to commercial problems the testing phase was stopped during the homologation process. However, the first attempt to apply inboard bearings technology to freight bogies is dated back to 1984 as British Rail Research developed the LTF25 bogie in which hydraulic dampers and rubber spring elements were also used. Concerns about the design of a wheelset with internal journals and the necessity of on-board hotbox detection, led the manufactures to produce the bogie with more conventional external bearings, resulting in the TF25 bogie shown in Figure 15 (right), which has reached a considerable amount of manufacturing. Nowadays, EN standards cover both design of axles with internal journals [56] and on-board hotbox detection [57], which are compulsory for high-speed vehicles.

2. **Austempered Ductile Irons (ADIs)**

2.1. Cast Iron technology

Cast Iron, or more simply "iron", represents a wide range of materials with very different properties between each other. Their use in engineering applications is known since the *XVIII* century and for many years cast irons have been the cheapest way to realize finished products. The low melting temperatures together with the relatively insensibility to poor castings techniques led to a rapid spreading of this production process, with the main advantage that complex shapes were obtained with an accessible amount of energy. All these good properties can be summarized with the words from [58], in which the author describes cast irons as *nature's gift to the foundrymen*. Carbon *C* (2-4%) and silicon *Si* (1-3%) are the main alloying elements and the higher is their content, the higher is castability. Conventionally, as the chemical composition between various types of cast irons overlaps, the *carbon equivalent value* ($CEV = \%C + 1/3\% Si + 1/3\% P$) is used for classification.

However, cast iron technology is a complex matter and only in the second part of the *XX* century, thanks to the growth of Computer Aided Design (CAD) and numerical simulations, a deeper knowledge of the materials and a greater quality production have been provided [59]. In fact, the properties of cast irons mainly depend on the *form of carbon precipitation* (wear resistance, hardness, damping), and the *matrix structure* (mechanical properties).

Table 8. Property summary for various types of irons compared to cast steel with 0.3% of *C* content. Adapted from [59]. 1 = best; 5 = worst.

Property	**Spheroidal Iron**	**Malleable Iron**	**Flake Iron**	**White Iron**	**Cast Steel**
Castability	1	2	1	3	4
Machinability	2	2	1	-	3
Reliability	1	3	5	4	2
Vibration damping	2	2	1	4	4
Surface hardenability	1	1	1	-	3
Elastic modulus	1	2	3	-	1
Impact resistance	2	3	5	-	1
Wear resistance	2	4	3	1	5
Corrosion resistance	1	2	1	2	4
Strength/Weight ratio	1	4	5	-	3
Cost of manufacture	2	3	1	3	4

A schematic summary of the main properties of cast irons is given in Table 8 and compared to the reference properties of a cast steel. It is possible to see how only after the development of *spheroidal cast iron* (or ductile iron, for short DI) in 1948 the mechanical properties of those kinds of materials have reached a level comparable to those of steel, except for the impact resistance, which is still lower due to the brittle fracture behavior typical of cast irons. However, has been already said in the previous chapter that the impact resistance measured according to Charpy test is not a suitable method to understand the ability of a material to resist to crack growth and a deeper comparison will be given in the following paragraphs.

2.2. Ductile Iron and heat treatments

The main advantage of DI is that a good control on the composition and the cooling rate let to obtain a good quality material in terms of dimension and number of graphite spheroids and percentage of ferrite-perlite matrix structure, which allow to reach a good balance between strength and ductility, as shown in Figure 16. The classification and the main mechanical properties of DIs can be found in [60] or [61], in which thirteen grades are defined ranging from EN-GJS-350-22 (220 MPa of proof strength, 350MPa of tensile strength and 22% of elongation) to EN-GJS-900-2 (600 MPa of proof strength, 900 MPa of tensile strength and 2% of elongation).

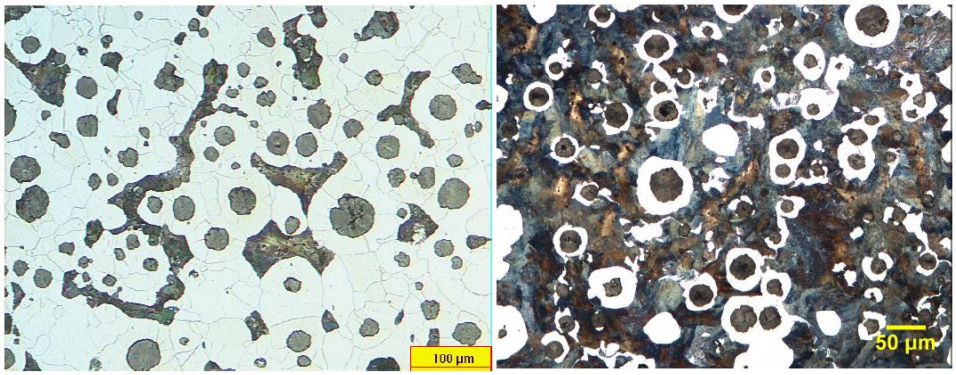

Figure 16. Microstructure of two different grades of Ductile Iron. EN-GJS-450-10 (proof strength of 310 MPa) with a prevalent ferritic matrix on the left and EN-GJS-600-3 (proof strength of 370 MPa) with a prevalent pearlitic (bullseye) matrix on the right. Images from [62].

If compared to the steel grades previously described for railway wheels and axles, it is clearly visible that to reach comparable tensile strength the elongation will be compromised. On the other hand, as the pearlite content increases, the hardness and the wear resistance increase. Therefore, lower grades of DI are usually preferred thanks to the higher toughness allowed by the prevalent ferritic matrix and used in low stressed components. For example, the grade EN-GJS-400-18 is commonly used in the production of casted axlebox for bogie frames, as shown in Figure 17. The designation is completed by LT, which stands for *Low Temperature* as it is specifically designed for low temperature application (-20°C), while the lowest grade EN-GJS-350-22-LT can be applied down to -40°C.

Figure 17. Typical railway axlebox casted in EN-GJS-400-18-LT, which houses the axle bearings and allows the axle-bogie connection supporting the primary suspension [63].

However, further grades of DI can be obtained by means of heat treatments, which allows to obtain different kinds of matrix structure. Figure 18 (left) shows improved mechanical properties for heat treated DIs, with outstanding results after the *austempering* heat treatment.

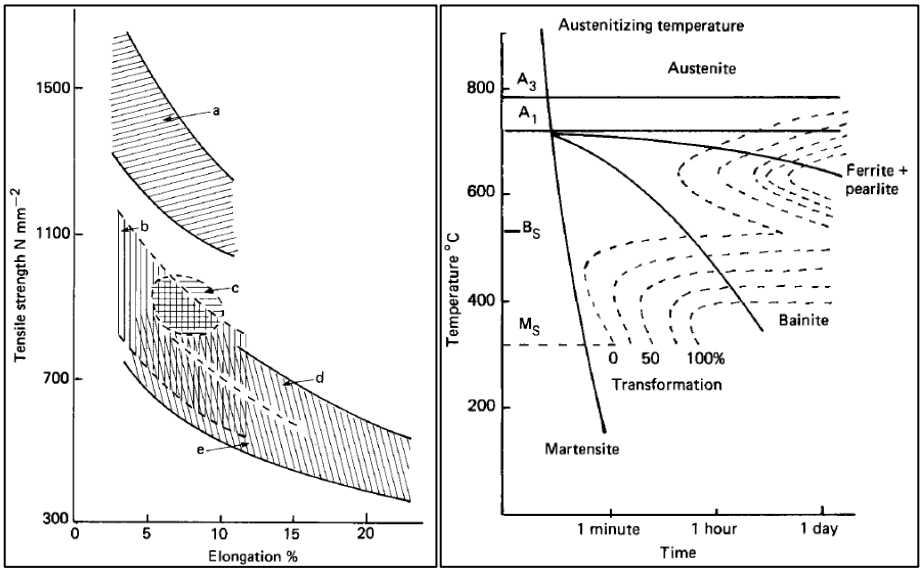

Figure 18. On the left mechanical properties of different kinds of Ductile Irons (a: austempered; b: quenched and tempered; c: normalized; d: as-cast bullseye; e: as-cast or annealed), on the right TTT diagram showing the transformation products that can be obtained with different cooling rates from the austenitizing temperature [59].

Except for stress relief purpose, heat treatments are performed heating the material over the critical temperature A_1 until all the structure is transformed in stable austenite. This temperature, differently from the eutectoid temperature of steels (A_1 = 727°C), can varies with the content of *Si*. However, an austenitizing temperature of 850 °C is usually enough. The material is then cooled at different rates to obtain a structure that can be made of austenite, ferrite, pearlite, bainite, martensite or a mixture of them (Figure 18 right). The temperature B_s at which bainite transformation starts is usually around 500°C, while M_s is the temperature at which martensite is produced and it is usually around 300°C. Heat treatments that can be applied to DI are mainly four:

- *Annealing:* it is used to generate a full ferritic matrix, softening the starting material. High ductility and toughness are therefore reached with slow furnace cooling.

- *Normalizing:* it is used to obtain a fine pearlitic matrix with improved strength and wear resistance and at the same time a reasonable machinability. The cooling rate must be high to reduce to ferrite formation and fan cooling may be needed.

- *Quenching and Tempering:* it is used to obtain the maximum strength and wear resistance without completely losing the toughness properties. Rapid oil cooling is needed to provide the transformation of austenite in martensite and then tempering is applied to reduce residual stresses and adjust mechanical properties.

- *Austempering:* it is a double stage heat treatment used to produce irons with the best mechanical properties in terms of both strength and toughness. *Austempered Ductile Iron* (ADI) has twice the strength of conventional DI with the same ductility. Quenching is stopped above the M_s temperature and maintained for few hours and then air cooling is applied before the starting of bainite generation. The matrix structure that is obtained is called “ausferritic”, due to the presence of ferrite and retained austenite. More details are given in the following paragraph.

Therefore, DIs offer a wide range of materials with different mechanical properties which give them a high versatility for industrial applications. Moreover, research on that field is active and nowadays several innovative types of DIs are available. Working on the composition chemistry of the alloy and the heat treatment cooling cycle gives the possibility to obtain peculiar characteristics for each application.

For example, without the use of heat treatments, improved properties can be achieved using the so-called *Solid Solution Strengthened Ferritic Ductile Iron* (*SSSF-DI*) with high *Si* content (about 4%) in a full ferritic matrix. Three grades are defined in [61]: the EN-GJS-450-18, the EN-GJS-500-14 and the EN-GJS-600-10. Even if these grades have an high proof strength/tensile strength ratio, with good elongation at fracture, some concerns about the high content of *Si* have been arise, especially for the effective ductility at high strain-rates when compared with an innovative DI called *Silicon Boron Durable* (*SiBoDur* for short), developed and patented by Georg Fischer Automotive AG [64]. *Isothermal Ductile Iron* (*IDI*) is an

innovative solution developed and patented by Zanardi Fonderie obtained by a heat treatment similar to austempering, with the difference that the first cooling is slower to cross the ferritic-pearlitic region of the isothermal diagram. A perferritic matrix with pearlite and ferrite interconnected is then obtained. A comprehensive comparison of these new materials can be found in [65], while the main properties are described in Table 9. Another Zanardi patented material is *ADI Wear* (*ADIWR*), a special ADI grade with enhanced wear resistance properties which shows comparable wear rates of white iron, with on the other hand higher toughness and machinability [66].

In Figure 19 the stress-strain curves from tensile tests of two ADI grades and one IDI grade are plotted. As typical of cast irons, the curves do not show any necking and the ultimate strength coincides with the failure strength due to a uniform plastic deformation stage. This kind of fracture is considered *brittle* respect to that of steels, where high deformations occur after the ultimate tensile strength and before failure (necking). However, this consideration is related only to a macroscopic comparison and could be misleading if used to compare different materials.

Table 9. Innovative ductile iron grades compared with the conventional ferritic-pearlitic EN-GJS-600-3

Material	Production	Matrix	E [GPa]	$R_{p0,2}$ [MPa]	R_m [MPa]	A_5 [%]	HB [-]
EN-GJS-600-3	As-cast	Ferritic-Pearlitic	174	370	600	3	190
EN-GJS-600-10	As-cast	Ferritic SSF	170	470	600	10	200
SiBoDur-700	As-cast	Ferritic-Pearlitic	175	440	700	8	-
IDI 800	Heat treated	Perferritic	155	480	800	6	250
EN-GJS-800-10	Heat treated	Ausferritic	170	500	800	10	250

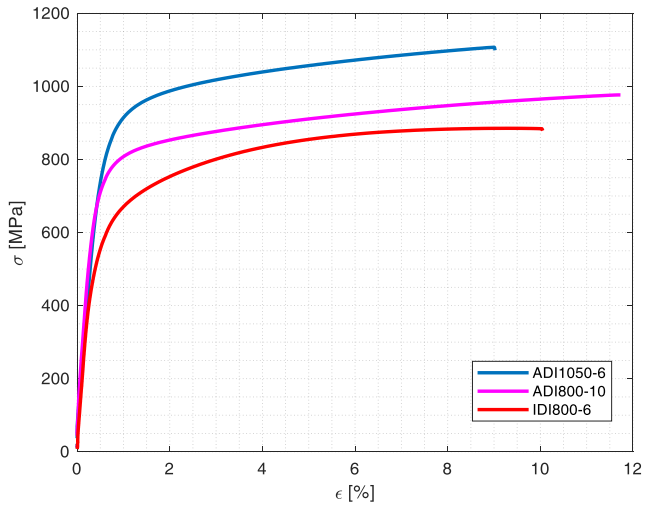

Figure 19. Stress-strain curves for two ADI grades (ADI1050-6 and ADI800-10) and one IDI grade (IDI800-6). The plastic phase consists in a uniform deformation and necking does not occur. Data supplied by Zanardi Fonderie.

Austempering heat treatment can be also applied to grey cast iron, obtaining AGI (Austempered Grey Iron) to improve hardness characteristics, while different solutions of austempering can be applied to spheroidal cast iron, such as LADI (Locally Austempered Ductile Iron) and CADI (Carbidric Austempered Ductile Iron) [67], which are both trademarks of Applied Process Inc.

2.3. ADI mechanical properties

2.3.1. General considerations

Thanks to the austempering heat treatment the mechanical properties of conventional DI are significantly improved in terms of both strength and ductility. The standards for this material, from [68] to [71] do not provide the chemical composition of the starting ferritic-pearlitic cast iron, as it strongly depends from the casting thickness and the characteristics that the final product must meet. Chemistry, austenitizing temperature and austempering temperature must be chosen properly in order to achieve the required parameters for certification without losing the machinability properties. For typical applications, *Cu*, *Ni* and *Mo* are usually added [62].

The heat treatment process consists in a two-stage cooling with an intermediate permanence at the austempering temperature T_{AUS}, which is defined above the martensite starting temperature. As shown in Figure 20, after the austenization (stage 1), the material is quenched up to T_{AUS} (stage 2), which is maintained (stage 3-I) enough time (few hours) to get stabilized austenite and stooped before the transformation in bainite is completed. Then, the material is cooled at room temperature without the formation of martesite. On the other side, continuing the isothermal transformation (stage 3-II) a full transformation of the retained austenite into ferrite and carbides occurs, obtaining a non-lamellar bainitic matrix. Differently than steel, this reaction is usually avoided as it determines a decrease in ductility and toughness [73]. Therefore, ADI final microstructure is composed by graphite nodules embedded in an ausferritic (ferrite and retained austenite) matrix.

Depending on the process parameters, several grades can be obtained. According to the EN classification (Table 10) five grades are defined by their mechanical properties while the last two are defined according to their hardness and used for applications where wear resistance is required. The minimum values of strength and elongation represent the normative values for product qualification and are related to machined specimens from samples casted apart from the main product casting and for relavant thickness lower than 30 mm. The higher is thickness the lower are the values. However, reference values for specimens machined from samples cut from actual product castings are given in Annex E of the same standard, while Annex G gives additional information about mechanical behavior as Young and shear modulus, fatigue limits, fracture toughness and so on. The most interesting grade for the comparison with steels commonly used in the railway field is the first grade (ADI 800) and in the following paragraph it will be described more in detail.

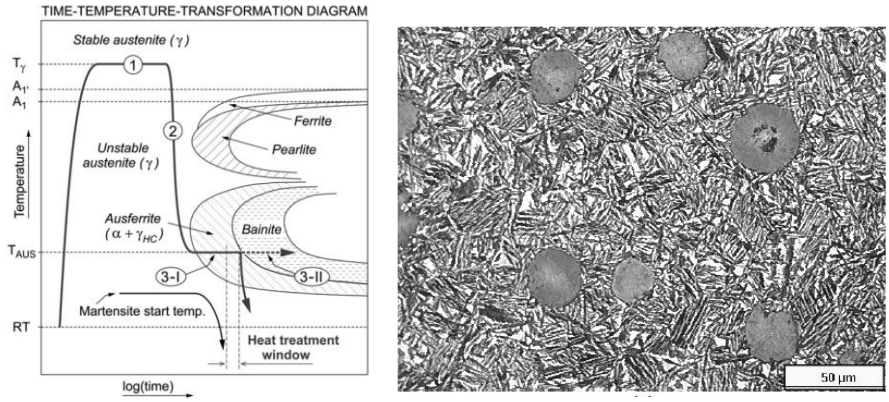

Figure 20. On the left a detailed TTT diagram with an austempering cycle superimposed (1: austenization at 850-900 °C; 2: quenching down to 250-450 °C; 3-I: holding at the austempering temperature and cooling at room temperature; 3-II: holding to obtain a complete bainitic matrix) [72]. On the right a typical ausferritic microstructure with graphite nodules, ferrite and retained austenite of 900-8 ADI grade [62].

Table 10. Main grades of Austempered Ductile Iron according to ISO standard [68]. Minimum values for material qualification are shown for a relevant casting thickness lower than 30 mm.

Short name	ISO designition	Ultimate strength [MPa]	Proof strength [MPa]	Elengation A_5 [%]	HB [-]
ADI 800	EN-GJS-800-10	800	500	10	250-310
ADI 900	EN-GJS-900-8	900	600	8	280-340
ADI 1050	EN-GJS-1050-6	1050	700	6	320-380
ADI 1200	EN-GJS-1200-3	1200	850	3	340-420
ADI 1400	EN-GJS-1400-1	1400	1100	1	380-480
ADI 1400	EN-GJS-HB400	1400	1100	1	400
ADI 1600	EN-GJS-HB450	1600	1300	–	450

2.3.2. The toughness misunderstanding

The ISO standard for ADI [68] prescribe values to be achieved for the notch-impact test only for ADI 800 grade. The minimum average value at room temperature is K_v = 10 J, which is only slightly lower if compared to the value defined for conventional ferritic ductile iron grades specifically designed to be tough even at low temperature (grade EN-GJS-400-18 has a minimum value of 14 J at room temperature). This is confirmed also by the results of impact tests applied to unnotched specimens shown in [74]. These values are much higher if compared to a fully pearlitic ductile iron with a similar strength of ADI800. Therefore, toughness is notably increased thanks to the austempering process. It should be noted that this conclusion can be draw also looking at the K_{IC} values. Reference values for ferritic and pearlitc grades can be found in the previous version of [61] (published in 2011) and they are confirmed by other works such [75] and [76]. In Table 11 elongation at fracture, impact strength or fracture toughness are compared for three different grades.

Table 11. Comparison of three iron grades in terms of elongation at fracture, notched and un-notched impact energy (at room temperature), stress-intensity factor.

Material grade	Elongation at fracture [%]	V-notch impact energy [J]	Un-notched impact energy [J]	Stress intensity factor [MPa/√m]
EN-GJS-400-18	18	14	160	82
EN-GJS-800-10	10	10	120	62
EN-GJS-700-2	2	2	30	30

Even if a certain relationship between these different parameters can be found, it is evident that the elongation at fracture and the un-notched impact energy are more related respect to the stress intensity factor because both are a measure of the total energy of fracture (initiation and propagation). Respect to fracture mechanics test, the impact test involves dynamic loadings that cannot be used to evaluate the crack propagation resistance and moreover, the specimen dimensions are not large enough to ensure plain-strain conditions. Therefore, impact energy could be a useful parameter to compare the elastic-plastic behavior of a material, but it is not suitable to compare the toughness of different material, such as steels and irons. Fracture mechanics tests according to [14] shall be used for crack propagation comparisons, while tests at high-strain rates with specific instrumentation like the *Split-Hopkison Pressure Bar* shall be used to compare the behavior under strikes and impacts. Also modified Charpy tests with pre-cracked specimens have been used to calculate a stress-intensity factor under dynamic conditions (K_{ID}), showing a superior fracture toughness of a good quality DI respect to cast steel [77]. Detailed evaluation of ADI crack propagation behavior can be found in [78] and [79].

Comparison between ADI and steel in terms of mechanical properties with special attention to toughness can be found in [80] and [81]. In both papers the properties of the steel grade 42CrMo4 quenched and tempered are used as benchmark. It is considered an alloyed steel with a very good strength ($R_{H,e}$ = 750 MPa; R_m= 1000÷1200 MPa) and tough at the same time (A_5= 11 % and K_v = 35 J). The stress-strain curve of this material is shown in Figure 21. Respect to ADI1050-6 the material shows an extended region with macroscopic deformation (necking) in the range 5÷14 % of elongation. This behavior is often considered as a measure of the higher ductility of steel respect to cast iron. However, in [81] the author performs a critical review of the different plastic behavior of the materials, comparing them by means of other tests such as three point bending test, torsion test and compression test. The results show that the ductility of the materials is nearly the same up to 5% of elongation (without considering necking) and differences can be related only to the lower elastic modulus of cast-iron (170 GPa) respect to steel (210 GPa).

Ductility under dynamic conditions (i.e. at high strain rates up to $d\varepsilon/dt$= 1200 s^{-1}) is evaluated for ADI in [82], [83] and [84], showing that the higher is the strain rate, the higher is the yield strength and the failure strain. Moreover, low temperatures have a limited effect in the reduction of failure strain while work hardening rate ($d\sigma/d\varepsilon$) is improved, showing a good ductility also in dynamic situation. Figure 22 shows the combined effects of lowering the temperature and increasing the strain rate.

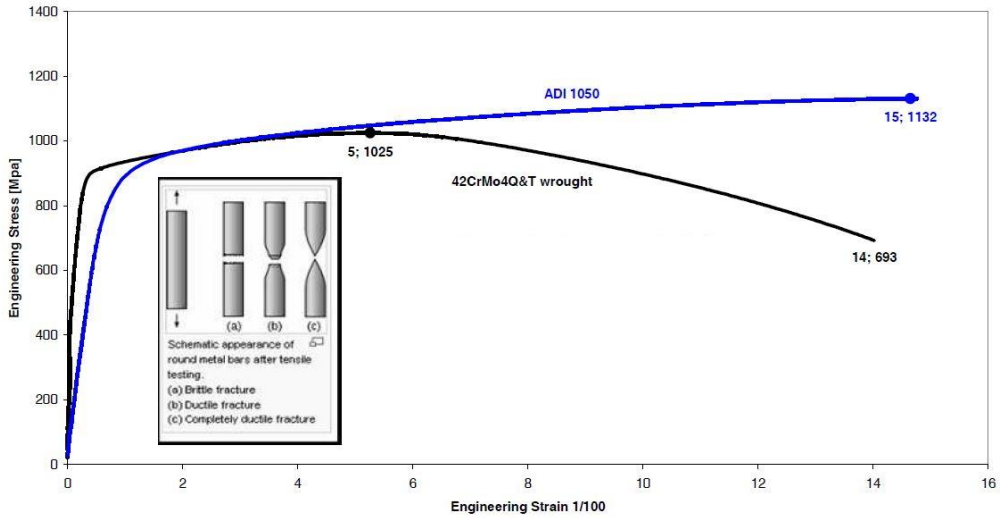

Figure 21. Stress-strain curve for 42CrMo4Q&T and ADI1050-6 [81]. Even if the fracture at a macroscopic level can be considered brittle for ADI and ductile for steel, the actual ductility comparison must be limited to the region of uniform plastic deformation (up to 5% of elongation for steel).

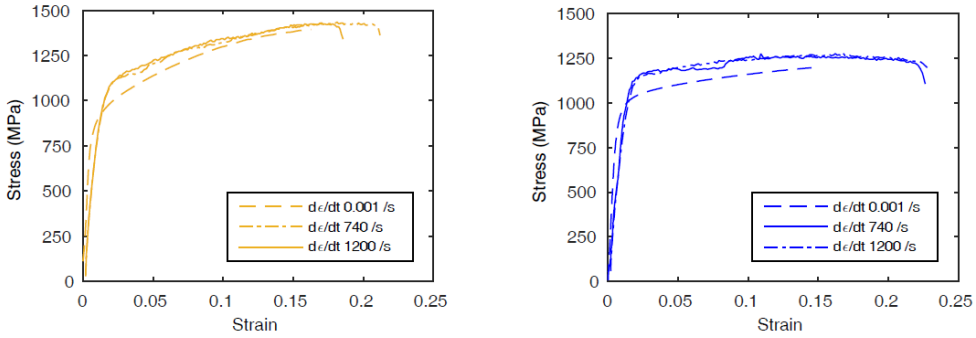

Figure 22. Effect of temperature (left -60°C and right 20°C) and strain rate on ADI1050-6 samples [84].

2.3.3. Fatigue behavior

In first approximation the fatigue limit can be calculated starting from the ultimate strength R_m according to Fuchs criterion $\sigma_a = 0.5\ R_m$ [85]. This general rule is also valid for cast iron family, but it is valid only for un-notched polished specimens, it does not consider the effect of the mean stress and it is usually referred to a 50% of survival probability. Its application is therefore limited. However, it is possible to understand that the fatigue limit of ADI grades is comparable with those of high strength steels. The standard [69] gives reference values for the endurance limit at $N = 2 \times 10^6$ cycles calculated in rotate bending loading conditions ($R_\sigma = \sigma_{min} / \sigma_{max} = -1$). Both un-notched and notched case are considered. These values are also show in Table 12. The ratio K_f between the un-notched and notched fatigue limits (fatigue notch factor) is also calculated. For ADI grades with high strength and hardness

(HB400 and HB450) the ausferritic matrix become more fragile and sensitive to the graphite nodules that behave like small internal notches. The fatigue limit therefore does not increase anymore and tends to the notched value (K_f tends to 1). The notched fatigue limits are obtained with a machined V-notch with an opening angle of 45° and a 0.25 mm of tip radius, as shown in Figure 23 (left). The notch dimension is not written in the standard, but usually the evaluation is made for specimens with D = 10.6 mm and a maximum stress concentration factor $K_t \leq 3$, which can be associated to a notch with $a \leq 0.5$ mm, as usually $K_t = 1+2\sqrt{(a/\rho)}$ [86].

Table 12. Fatigue limits of three ADI grades according to [69] considering a 50% of survival probability

Grade	σ_{a0} [MPa] Un-notched	σ_{aN} [MPa] Notched	$K_f = \sigma_{a0}/\sigma_{aN}$ [-]
ADI800	375	225	1.67
ADI900	400	240	1.67
ADI1050	430	265	1.74
ADI1200	450	280	1.61
ADI HB400	375	275	1.36
ADI HB450	300	270	1.11

Usually notch sensitivity is expressed in function of both K_f and K_t by means of the ratio $q = (K_f - 1) / (K_t - 1)$ and the fatigue limit tends to zero as the *notch sensitivity* increases (i.e. q tends to zero). However, q values are undefined for very small values of ρ and under a critical value of K_t the fatigue limit remains constant, as shown in Figure 23 (right). In that case notches can be considered as cracks or surface defects in general.

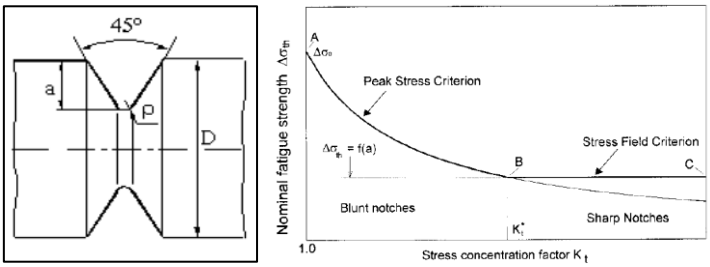

Figure 23. Circumferential V-notch used to evaluate the fatigue limit according to [69] (left). Fatigue strength in function of stress concentration factor [86] (right).

For cracks Kitagawa-Takahashi diagram is used to evaluate the effect of crack length on fatigue limit. As shown in Figure 24 (left) the diagram is based on the linear-elastic fracture mechanics (LEFM) considering that with certain crack dimension a, the fatigue limit decreases linearly (line B-C). The slope of the line is an indirect measure of the long-crack propagating threshold ΔK_{th}. Greater is this threshold, greater is the fatigue limit for a given crack dimension, which cannot grow further. For small cracks the fatigue limit is theoretically insensitive (line A-B), however experimental results have shown that the real trend is not linear, and the fatigue limit decreases gradually from the nominal un-cracked value $\Delta\sigma_0 = 2\sigma_a$ to the line B-C. The non-propagating maximum crack dimension a_0 is therefore only a theoretical value.

The value of ΔK_{th} is therefore the main parameter to assess the *crack/defect sensitivity* of a material. The most suitable method to calculate this parameter is using the crack grow rate curve (Figure 24 right) and considering the lower limit at grow rates equal to $da/dN = 1x10^{-10}$ m/cycle according to [88]. However, these values are obtained for $R = 0.1$, which are usually lower than those obtained in rotating bending due to the mean stress effect. Experimental results for different cast iron grades are shown in Table 13, where only the value of EN-GJS-400-18 is calculated by means of the direct method. ADI grades have fatigue limits in smooth condition equal or higher than pearlitic DI and at the same time propagating threshold like ferritic DI.

Table 13. Different cast iron grades compared according to their fatigue properties. Data from [75] and [89].

Grade	$\Delta\sigma_0 = 2\sigma_a$ [MPa]	ΔK_{th} [MPa√m]	a_0 [mm]
ADI800	800	16.8	0.140
ADI1050	848	17.5	0.135
ADI1200	774	13.0	0.089
EN-GJS-700-2	760	11.5	0.076
EN-GJS-400-18	362	14.3	0.496

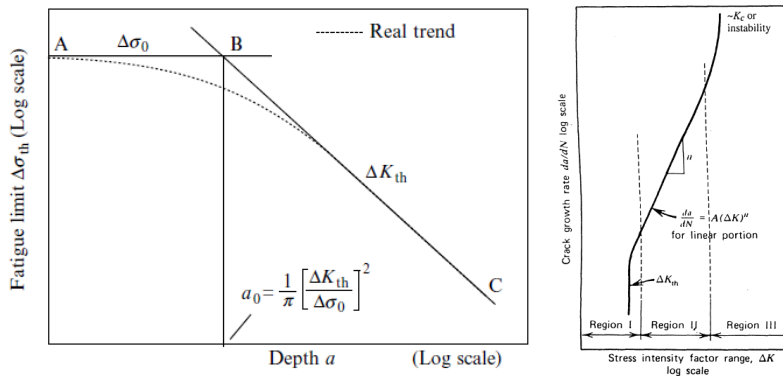

Figure 24. On the left, the Kitagawa-Takahashi diagram showing the effect of increasing crack depth a on the fatigue limit of the material [87]. The slope of the curve B-C is an indirect measure of ΔK_{th}. On the right the crack grow rate curve [85], which is the direct measure of ΔK_{th}.

The data from [89] are obtained by stair-case method in rotating bending condition using smooth and U-notched specimens. The applicability of notched specimens for the evaluation of the surface defect sensitivity has been demonstrated in [87] for several kind of steels. However, this not enough to understand the difference between machined and un-machined components. For casted components the surface quality strongly influences the fatigue properties of the material, especially for cast irons where green sand molds are used. In [89] the effect of the "as-cast" surface has been evaluated. The surface appears with an external *casted skin*, in contact with the mold, which suffers from high cooling rates and is affected by crystallographic defects, and a *transition layer* characterized by a ferritic structure in which small discontinues that usually are considered unavoidable. The "as-cast" surface has an average roughness of $R_a = 12.5$ μm.

The effect on fatigue properties can be considered with equation (4), developed from the results of an extensive work described in [90] and shown in Figure 25 for one grade od ADI. The value of this coefficient varies between 1.3 and 1.4 depending on the selected grade.

(4) $$K_L = \frac{182 + 0.26R_{p0,2}}{149 + 0.16R_{p0,2}}$$

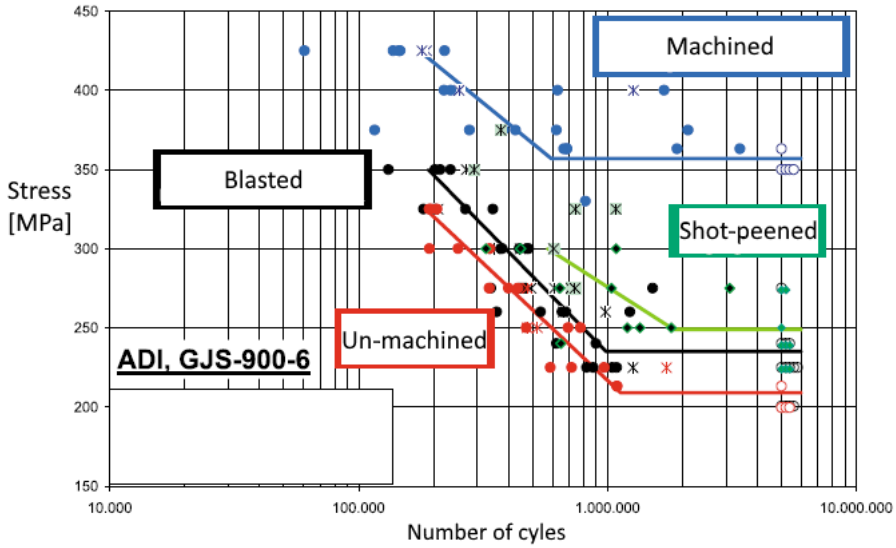

Figure 25. Wöhler diagram for ADI900 grade with different surface conditions. Modified and translated from [90].

Figure 25 shows that the fatigue limit can be increased also by blasting or shot-peening, but their effect is quite limited if compared with the costs of these operations, and therefore a machining is often more effective. However, all these coefficients are obtained by small specimens casted apart (*Lynchburg* samples) and the results are applicable to surfaces without considering the presence of defects. Larger castings can be affected by a certain number of defects due to sand inclusions or gas bubbles with dimension higher than the non-propagating crack. Typical defects can also reach 2x2 mm of surface and K_L must be increased in the range of 2.8÷3. During the design stage is therefore very important the visual inspection of prototypes according to [91], in which ranges of admissible defects are defined. However, although surface quality usually improves during the optimization of the manufacturing process, the more conservative coefficient is usually applied at a design stage.

Moreover, all the fatigue limits expressed so far are related to the values corresponding at the 50% of survival probability, but as shown in previous chapters this is often not sufficient in order to satisfy the standard requirements. Therefore, a further reduction coefficient must be applied to consider the statistical scatter or the experimental results, at least with a 97,5% of confidence.

2.3.4. Comparison with steels

In this paragraph a comparison between ADI mechanical properties and steels typically used for in railways structural components is performed. ADI800-10 is compared with steels for axles, wheels and bogies, considering mechanical properties provided by Zanardi Fonderie.

Two grades are chosen for axles: EA1N, which is the most common steel for axles manufacturing, and 30NiCrMoV12, which represents a special case which is not included in current standards, but it has been extensively used in Italy and it is still in service in the first high-speed fleet developed in '90s. This high-strength alloyed steel was used to manufacture lightweight hollow axles according to the Italian standard UNI6787:1971. Mechanical properties for these grades are taken from [92].

Two grades are shown also for wheels: ER7 previously described and another special steel developed in recent years by *Lucchini RS* with the aim to combine the strength of ER9 and the toughness of ER7 steels grade. The SUPERLOS® is not included in standards and it is used where European requirements are not mandatory. The values are provided for wheel rim, but for relevant wheel web parameters both values are provided. Values are taken from [93].

Table 14. Comparison of ADI800 with steels used in railway applications

	ADI800	EA1N	30NiCrMoV12	ER7*	SUPERLOS*
$R_{p0,2}$ [MPa]	670	370	860	560/380	640/500
R_m [MPa]	920	600	975	890/730	980/850
A_5 [%]	13	27	20	18/21	18/21
HB	250	/	/	265	290
K_u (20°C) [J]	/	55	70	27	24
K_v (20°C) [J]	10	/	/	11[a)]	9 [a)]
σ_a (50%) [MPa]	400	274	510	/	/
σ_a (90%) [MPa]	327	195[b)]	363 [b)]	315/260	370/320
K_f [-]	1.67	1.61	1.67	/	/
K_{IC} [MPa√m]	62	52	117	88	82
ΔK_{th} [MPa√m] (R = -1)	16.8	17	10	/	/
* Rim/Web a) Values for -20°C b) 95% survival probability c) 99.7% survival probability - = data not available					

From the previous comparison of the mechanical properties is therefore possible to conclude that ADI800 grade is a suitable material to replace steels in high stressed railway components. Static and fatigue properties are higher than the conventional steels EA1N and ER7, while only slightly lower than the upgraded grades of 30NiCrMoV12 and SUPERLOS®. At the same time, fracture mechanics values are higher than a commonly known "brittle" material. Moreover, it should be noted that all NDT procedures applied to steels can be applied in the same manner to all ADI grades.

2.4. Applications of ADI

Austempered Ductile Irons is one of the best materials for those applications where high strength, lightness and low wear are required such as hitches, suspension and powertrain components of off-highway vehicles. The combination of good mechanical properties (described in the previous paragraphs), the low density (ρ= 7100 ÷ 7200 g/m3) and a Young modulus similar to the one of steel (E=170 GPa), gives the opportunity to save more weight respect to low density material such as aluminium. Moreover, the fluidity of ADI leaves to the designer a high freedom for shape optimization, and there are many practical cases of welded steel structures replaced by only one casting with reduction of weight and manufacturing costs. Casted components can be machined after the austempering heat treatment, with few adjustments in cutting parameters, as described in Annex J of [69]. However, the austempering process does not lead to high distortions of the components and the machining can be performed completely before the heat treatment (ductile irons can be machined very easily) if high tolerances and high surface quality are not required, or roughly and then finish machining after the heat treatment. Examples and advices about ADI machining can be also found in [94].

Since many years automotive industry is very sensitive to the mass saving problem and for this reason ADI grades have been early used. Several examples of ADI applications on automotive components can be found in [95] and [96]. Gears, suspension components, transmissions and crankshafts are only some examples of applications and shown in Figure 26.

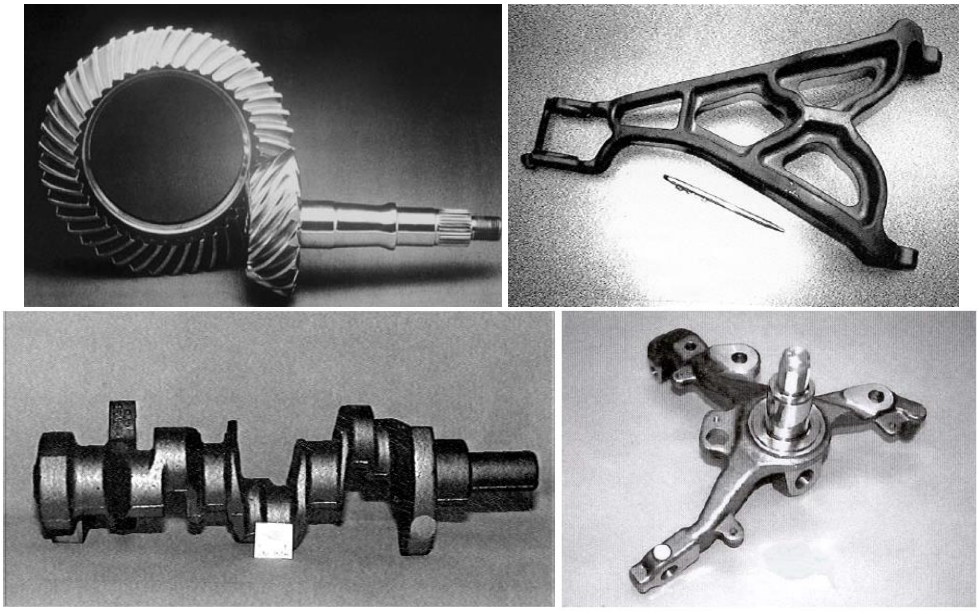

Figure 26. Examples of ADI applications from [95] and [96].

Gears manufacturing has been the first large application of ADI (hypoid gears developed by General Motors shown in Figure 26), but today only few data are available for

design purposes. Values of contact fatigue strength and root bending strength are available in [68] and [69], while experimental results can be found in [97].

An updated general view of current application of ADI can be found at Zanardi Fonderie website[6]. The production also includes special applications for railway freight bogies, consisting in the friction components (friction wedges and side bearers) of the suspension system of three pieces bogies, for which ADI1200-3 is used to improve friction stability, wear resistance and casting quality, respect to conventional iron or steel castings. Especially for the friction wedge, shown in detail in Figure 27, the design must be very accurate as its characteristic influences the ride quality of the bogie in longitudinal (warping), vertical and lateral directions [97].

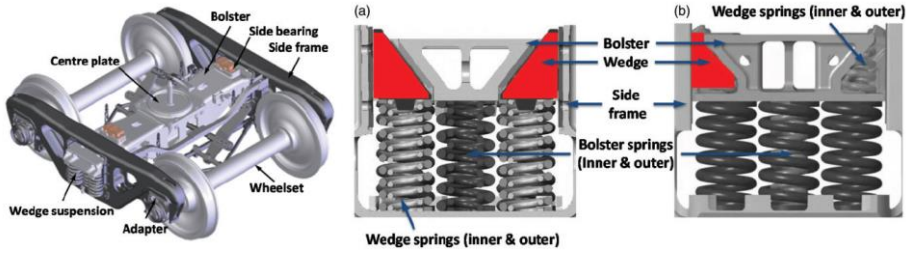

Figure 27. Left: Typical design of three-pieces bogie. Right: Two different arrangement of the suspension with *a)* variable "Barber" friction damping and *b)* constant "Ride control" friction damping.

Another application of ADI in railway vehicles can be found in FAG-Schaeffler catalogue of railway products[7], in which the casted ADI axlebox of Class 185 Locomotives is described. In this application ADI is used to produce a compact and light design increasing the strength by replacing conventional cast iron.

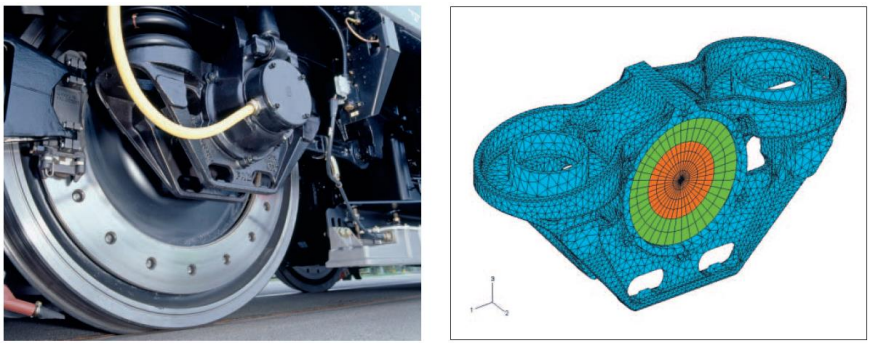

Figure 28. Casted ADI axlebox of Class 185 Locomotives from Bombardier, and its Finite Element model.

[6] https://zanardifonderie.com/en/products/portfolio/

[7] The catalogue "Product for railway application" is available at https://www.schaeffler.com/content.schaeffler.com/en/index.jsp (accessed on 26.09.2019)

More recently a monobloc wheel in ADI has been developed by Siemens within the Shift2Rail European project [99]. The wheel was displayed for the first time at the XXII InnoTrans trade fair in September 2018, but still today no information about the manufacturing and testing are available. As shown in Figure 29, the wheels are made of two ranks of spokes to reduce mass and the radiated noise emission, but the developers also claim other advantages such as lower wheel wear and lower polygonization problems due to the greater wear resistance of ADI respect to steel. However, how the wheel-rail contact is affected by iron wheels and steel rails is unknown. Full-scale tests with ADI monobloc wheels have been performed in the past, with apparently good results but no practical extensive application is followed to these tests.

Figure 29. Monobloc wheel in ADI EN-GJS-900-8 developed by Siemens. Left: the wheels on display at InnoTrans 2018. Right: A complete wheelset with monobloc ADI wheels [99].

According to [100], since 1976 a large research about wheel-rail wear has been conducted by Finnish Railways (VR), including wheels made of ADI (or KYMENITE as called in the paper). Both laboratory tests and field tests were performed concluding that both tread and flange wear of ADI wheels is lower than R8 steel, with a final 30% saving in life-cycle cost. Several ADI wheels were installed on real vehicles (track maintenance vehicles, coaches and metros) for a test period of about 15 years, but today none of these wheels is currently running on tracks, and no more results were published.

In the last years of 1990's studies about ADI wheels were performed also by German Railways (DB). In [101][8] rolling wear tests on samples to investigate the feasibility of ADI for railway wheels are described, resulting in very good behavior of ADI respect to steels. Moreover, tread failures due to faulty manufacturing were recognized as the main cause for stopping the previous research in Finland. Fracture mechanics assessment of ADI wheel by

[8] The paper was originally presented in German. A translated version can found at https://www.appliedprocess.com/document/263909_adi-an_alternative_mat_for_railcar_wheels_k_madler/ (accessed on 27/09/2019)

FEM simulations [103] were performed by DB to further evaluate the suitability of ADI as wheel material in terms of maintenance intervals, while full-scale roller-rig [102] was used to compare the wear performances of different materials, including ADI, with conventional ER7 steel. Wheels made of ADI did not show signs of damages or out-of-roundness even after 50000 km, with an increasing of about five times respect to ER7 and two times respect to Shinkansen steel. However, after these preliminary positive results, on-track tests were planned on double-deck coaches, but because of unpermitted indications found in the manufactured wheels (tread and rim) the experimentation was stopped.

Another evaluation of the suitability of ADI as wheel material to replace steel in wheel-rail contact can be found in [104][9], in which ADI has been compared with standard pearlitic steel used for tyres of trams. However, clear advantages have not been found after that analysis and ADI tyres have never been produced.

Even if other works about the suitability of ADI as wheel material are present in the literature [105], the advantages of the application of this material in the wheel-rail contact are not supported by enough field results. The state of the art is not enough to prove that the higher damping, the lower elastic modulus (which lead to a lower contact pressure) and the higher wear resistance found by laboratory tests are enough to guarantee the safety of the wheel-rail contact. Therefore, within this work it is not considered a possible straightforward application of ADI.

[9] The document is an internal report of Institute of Railway Technology of Monash University, provided by one of the authors by personal correspondence.

3. New applications for ADI

3.1. Survey of casted components in railway vehicles

In the previous chapters the current standards about running gears have been examined, but sometimes they don't cover the full range of components or manufacturing processes. Therefore, with the aim to introduce a new Ductile Iron in structural components of railway vehicles, a preliminary survey about casted components has been performed. The survey done during the XXI InnoTrans trade fair in September 2016 has been focused on both steel and cast-iron castings.

The results of the survey shown that only few components are made by casting and often they are related to pieces with small dimension and complex shape. An exception is the bogie frame. As already said, the standards for bogies do not impose the use of specific materials or manufacturing processes and castings are widely used especially for freight three-pieces bogies used in USA, Russia, South Africa and Australia. In Europe only few examples can be found as shown in Figure 30, which represent one of the two side frames of a passenger vehicle bogie.

Figure 30. Side frame for bogie, casted in steel A4 BS 3100 by SHB[10], mass of 435 kg. The A4 steel grade according to BS3100 standard is comparable to G17Mn5 of [106].

As shown in Figure 31, others smaller casted components for bogies are supports for brake calipers, bolster ends or yaw dampers brackets. Generally steel grades according to [106] are used, due to their good welding properties and their similar mechanical properties respect

[10] Stahl - und Hartgusswerk Bösdorf GmbH https://www.shb-guss.de/en/ (accessed on 07/10/2019)

to S355, leading to straightforward assessment and welding procedures. For example, the G20Mn5 quenched and tempered has 300 MPa of yield strength and an elongation of 22%.

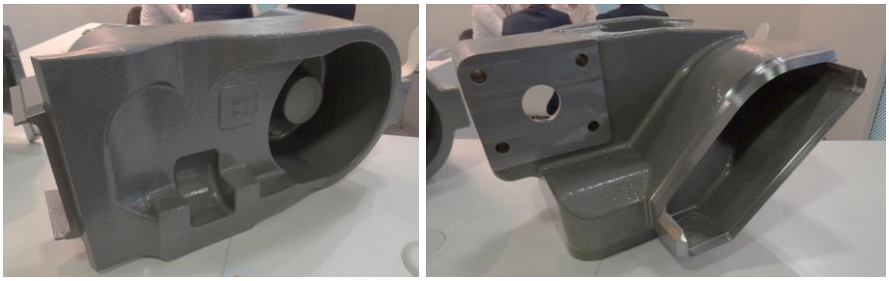

Figure 31. Steel castings from MLF[11] to be welded at the main structure of the bogie frame. On the left a bolster end in G20Mn5+QT (mass of 73.8 kg), on the right a brake support in G20Mn5V (mass of 75.1 kg).

Cast iron could be easily used for these parts, in order to save mass, but the connection with the main frame should be made by means of bolts or rivets, as welding could not be applied with enough reliability even if preliminary fatigue tests on dissimilar arc-welded joints, composed by ADI1050 and S355, have been experimentally investigated with good results [107]. The only parts of bogie frames that are made of cast-iron are axleboxes (Figure 17) and anti-yaw damper supports, shown in Figure 32.

Figure 32. Anti-yaw dampers with casted GJS400-18 LT supports attached to the coach.

Three-pieces freight bogies have already some cast-iron parts, which are also covered by ADI, while Y25 bogie have steel casted axleboxes made of two parts, the first housing the bearing and the second welded to the bogie frame. An example is shown in Figure 33. Other typical castings are brake discs, which could be made with both steel and cast-iron depending on the maximum speed of the vehicles. Usually grey cast-iron discs are applied for vehicles with speed lower than 160 km/h, and ADI cannot be applied due to the high temperature (over 300°C) that are reached during the braking phase.

[11] Maschinenfabrik Liezen und Gießerei GmbH https://www.mfl.at/en/foundry.html (accessed on 07/10/2019)

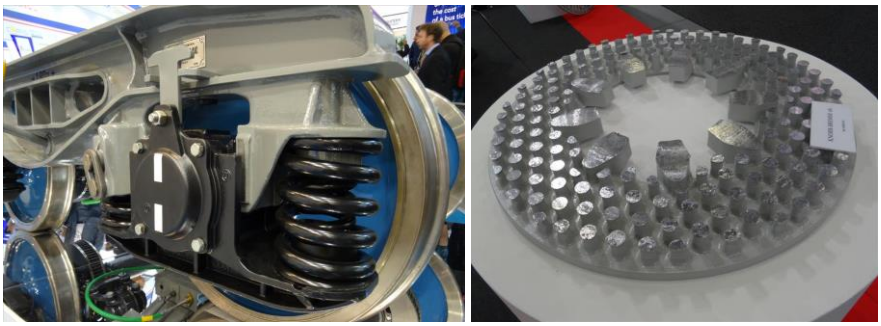

Figure 33. Left: Y25 axlebox and suspension support, casted in two parts the first housing the bearing (black component) and the second welded to the bogie frame (grey component). Right: Half section of steel brake disc.

Steel castings can be found in joints and couplers, which are mainly derived from the semi-automatic Janney coupler developed in the USA and shown in Figure 34. Today the Janney coupler is mainly used in heavy haul operations.

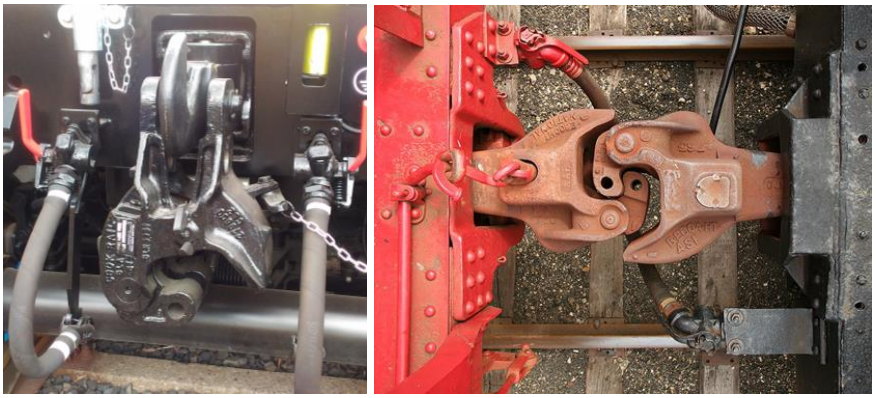

Figure 34. Left: steel casted coupler from William Cook[12] designed for a maintenance vehicle. Right: AAR Type E coupler developed in the USA as Janney coupler.

The last application found during this survey is the wheel centre for tyred wheel, shown in Figure 35. The practice of casted wheel centres comes mainly from steam locomotives, which had spokes to lubricate the inboard journal bearings. With the disappear of steam locomotives, also the inboard bearings solution disappeared in favor of external bearings and the spoked cast wheels were replaced by cast or rolled/forged axisymmetric wheel centres.

[12] https://www.william-cook.co.uk/ (accessed on 07/10/2019)

Figure 35. Spoked wheel centre for tyred wheel to be fitted on an electric locomotive wheelset, casted by Pleissner Gus GmbH[13] in G17CrMo55 (mass of 500 kg).

Considering that replacing conventional cast-iron with the more performant ADI is not interesting if strength is enough, and brake discs cannot be casted in ADI, the components chosen for the new application of ADI have been: wheel centre for tyred wheels, bogie frames and couplers.

3.2. Heavy Haul coupler

3.2.1. Design and failure analysis

Railway heavy haul couplers are large steel castings used for connecting wagons and locomotives, letting to transfer pulling and pushing forces (i.e. traction and braking forces) all along the train. The most common type of coupler over the world is the North American one, which is historically identified as the Janney coupler. Since its first development in 1873, this semi-automatic coupler has been further developed and different types of couplers are nowadays available. However, the basic concept has never changed and only some geometric features change from the different types, depending on the wagon to be applied.

The coupler is a critical component of railway freight vehicles, as it must guarantee high safety levels under severe working conditions with practically no maintenance. Moreover, to reach a very high freight transport capacity, heavier and longer trains are used. In this operating conditions, impact loads and low cycle fatigue, as well as defects in steel casting and insufficient dimension tolerances are the main causes of crack growth and failures of couplers. According to IHHA (International Heavy Haul Association) definition, a railway is considered as “heavy haul” if two of these requirements are satisfied:

- Operates unit or combined trains of at least 5000 gross tonnes

[13] https://www.pleissner-guss.de/ (accessed on 07/10/2019)

- Hauls at least 22 million gross tonnes per year or freight over a railway corridor of at least 150 km in length

- Regularly operates rolling stock with axle load of 27.5 tonnes or more

However, the capacity of heavy haul has grown in the last years leading to higher values of dynamic loads and higher resistance of the single components is required. A description of the current problems occurring to couplers in heavy haul operations can be found in [108].

As shown in Figure 36 the complete coupling system is usually composed by four main components:

- *the coupler* which is the steel casting that connect the two wagons and transfer the in-train forces between the wagons;

- *the draft gear* which let the reciprocal movement of the connected wagons buffering the in-train forces transmitted through the couplers and providing a shock adsorbing function in order to prevent that damages occur to the wagons or to the carried goods. The energy absorption method is usually made by springs and friction wedges (or rarely hydraulics);

- *the yoke* which is the steel casting that house the draft gear and transfer the forces from the coupler to the draft gear;

- *the striker* which is the steel casting which connect the draft arrangement to the center sill (and then to the wagon). It brings the lugs that are needed to compress the draft gear when it is moved by the coupler and the yoke.

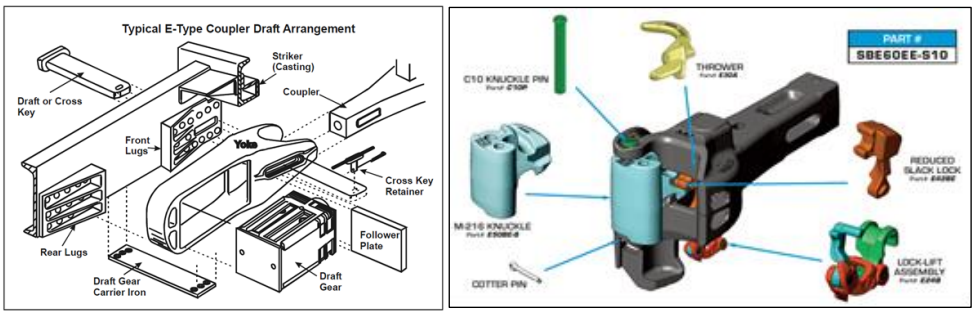

Figure 36. Left: Complete arrangement according to AAR E-type coupler[14]. Right: Details of the coupler, made by the body and the knuckle[15].

The mechanical coupling between wagons is performed by two part: the *coupler body* and the *knuckle*, which can rotate around a locating pin and therefore it is able to engage the

[14] https://www.wabtec.com/documents/6006/freight-car-draft-arrangements (accessed on 07/10/2019)

[15] www.stratoinc.com (accessed on 07/10/2019)

other knuckle. Then the knuckle is locked in its position and forces are transmitted to the coupler body thanks to complementary surfaces.

Grade E steel is the common material used for AAR couplers castings and it is defined in the standard M-201 of [109]. The material has a tensile strength of 830 MPa, a yield strength of 690 MPa and elongation of 14%. Depending on the type, the approximate mass of a complete coupler may be greater than 100 kg, mainly divided by the coupler body (70 – 80 kg) and the knuckle (20 – 30 kg).

The necessity of improvements to the current coupler design is proved by a recent work performed by TTCI (Transportation Technology Center, Inc.). In [110] the authors state that "between 2000 and 2011, an average of 230,000 knuckles and couplers were removed from service because they were either broken, cracked, or out of alignment. Although the exact age of each of these components is unknown, most of the removals occurred before the target life of the component was reached". This work on couplers by TTCI has involved FEM analysis, full-scale fatigue tests and load spectrum measurements, concluding that an increased draft load capacity for the knuckle/coupler system could be achieved through a combination of design changes and modifications to material properties.

Extensive work about this topic has been done also in Australia [111]. Failure analysis and FEM analysis were conducted in order to find the critical stress locations and to improve the coupler design. According to the author the fatigue life with the new design is increased of about 55%. The change in material was previously evaluated in [112], in which ADI Grade 1 (i.e. ADI900) has been compared with conventional steel for couplers manufacturing, in terms of toughness, fracture mechanics and wear, resulting in comparable mechanical properties. However, field results have not been reported after that evaluation. The ADI application in coupler castings has been also evaluated by the Michigan Technological University, in a research sponsored by NURail Center (National University Rail Center)[16]. However, it is a student project in which only some FEM analysis were performed but no clear results are available currently.

Therefore, the advantages of ADI application to coupling systems would not be so important and even if the change of material will let a mass reduction, this is not considered a critical point for heavy haul application if the fatigue life is not improved. ADI shows similar mechanical properties to the current steel grades with the additional problem that welding repair (which is allowed in heavy haul steel castings) is not possible.

[16] http://www.rail.mtu.edu/content/rail-car-coupler-redesign (accessed on 07/10/2019)

3.3. Bogie frame

As explained in paragraph 1.3, one of the main topics for the next years can be the development of a new bogie for freight wagons. In this field the manufacturing costs play a relevant role and they must be maintained as lowest as possible to compete with current standard freight bogies, i.e. Y25 in Europe and three-pieces bogie in the rest of the world. Castings are quite competitive in a large-scale production and it is confirmed by the fact the three-pieces bogies are all made by cast steel sideframes and bolsters. However, due to the poor quality of steel castings in-service failures could happen, and welded structures are often considered the best solution respect to steel castings [113]. Even if the application of cast iron could improve the casting quality in terms of defects, the problem of in-service repair by welding cannot be solved and therefore a direct replacement is not possible. This is especially true in USA, where research about "ultraweldable" steels have been performed to avoid post-weld heat treatment after repair welding [114]. Moreover, in the same research specific steel grades for temperature below -40°C were analyzed, as in this condition carbon steel could fail in brittle manner. However, both developments were stopped after a cost-benefit analysis showing that the increase of material purchasing would be too high if compared with the "small" number of derailments, i.e. 2.5% of the total equipment. This confirms the difficulties to introduce new materials in this field.

The possibilities offered by a new material such as ADI could be very interesting if applied to a new concept of freight bogie. Therefore, an innovative bogie arrangement has been developed as a replacement of Y25 bogie. The design includes a one-piece compact frame casted in ADI, as shown in Figure 37. The bogie is an inboard bearings bogie in which the primary suspension, made by only one horizontal coil spring with single-stage progressive stiffness, acts in longitudinal direction as done in the Wegmann-Kassel bogie, with the innovation that each spring connects the two swinging arms on one side and consequently the two wheelsets, replacing the eight springs used on each side of an Y25 bogie. Therefore, vertical movements of the wheelset and the bogie are transformed in horizontal movements by the swinging arm and energy is dissipated by friction (load dependent) in the cylindrical pin connection between the arm and the frame.

Structural verification has been performed according to the loads prescription of EN13749, including both static and fatigue assessment for a maximum axleload of 22.5 tones per axle. Even if the all stresses were below the limits for fatigue due to as-cast surface finish, the torsional stiffness of the one-piece casted frame was found too high for the application. In fact, due to the absence of the classical primary suspension the bogie cannot relies on the spring flexibility when a track twist occurs. Therefore, the structural flexibility of the frame, which is also shorter than a conventional one, become central in order to guarantee a good equalization of the wheel loads. This is usually evaluated by the wheel unloading parameter $\Delta Q/Q$ which must be lower than 0.6 to guarantee a safe running behaviour. Multibody simulations including a flexible body representing the bogie frame have shown that that parameter is not respected with the current design.

To overcome this problem a welded structure has been used to increase the flexibility of the frame. The description of this updated design lays outside the scope of this thesis and further references can be found in the list of published papers.

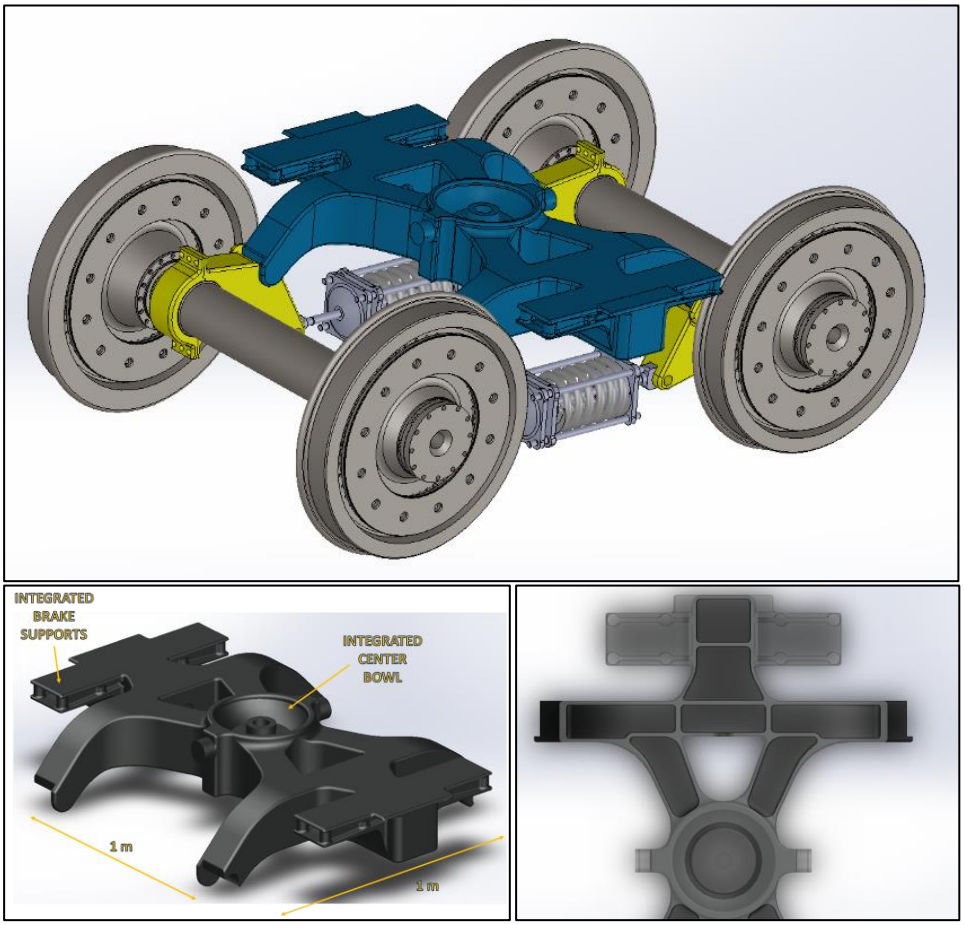

Figure 37. Above: innovative arrangement of freight bogie specifically designed as replacement of Y25. Below: the one-piece casted frame with integrated centre bowl and brake supports (left) and detail of internal view of the casting shape (right).

3.4. Tyred wheel

Even if tyred wheels have been the standard in all railway applications for more than 150 years, their success was obscured by monobloc wheels. They have several advantages in terms of safety and maintenance and their Life Cycle Cost is favourable compared to the standard manufacturing and maintenance process of tyred wheels. The design of tyred wheels has never changed during the years and optimization processes have never been applied to reach a competitive business with monobloc wheels. Therefore, a state of the art does not really exist, and tyred wheesl are not present anymore in the current standards. The only normative reference available today is about their maintenance, within the informative annex H of [115]. Here it is stated that "requirements for tyred wheels are specified in the following UIC leaflets: UIC 810-1, UIC 810-2, UIC 810-3, UIC 812-1, UIC 812-4, UIC 812-5 and UIC 813". These leaflets were published nearly 30 years ago (the most recent is UIC 810-1 that was re-released in 2003 with minor amendments from the 1981 edition) and therefore an updated design code for tyred wheels is missing.

The main problems dealing with the conventional design of tyred wheel are *the risk of losing the tyre* due to centrifugal actions in high-speed operation and thermal input during heavy continuous tread braking, and the *high maintenance costs* during tyre fitting and removal due to the high amount of manual work needed to overhaul tyred wheels.

3.4.1. Thermal capacity and structural behavior

As the risk of losing the tyre is an issue that deals with safety, nowadays tyred wheels are almost complety removed from freight wagons, and they will be no more allowed from 2020[17]. However, the heating problem was clear since 1968, when the ORE report [116] was delivered. Figure 38 shows the intrinsic limit of tyred wheels technology when applied to tread braked wheelsets. In the case of fully worn wheels (wheel 1, i.e. tyre thickness = 30 mm) tyre loosening always happens in less than ten minutes for braking power around 30 kW. It should be noted that for thermomechanical assessment of interoperable monobloc wheels, specifically designed for tread braking, the standard EN13979 prescribes a power input according to equation (5) maintained for 45 minutes.

$$P_a = m \times g \times \alpha \times v_a \tag{5}$$

Considering a mass m acting on the wheel equal to 10 tonnes, g equal to 9.81 m/s^2, v_a equal to 60 km/h and a slope α of 2.1%, the power results in about 35 kW. On bench tests the required power is 50 kW for 45 minutes applied for ten times consecutively. For these severe conditions, a big work about optimization of monobloc wheels for tread braking have been started, resulting in the development of thermostable wheels [50]. On the other side, Therefore, even with the evidence that the design of tyred wheels would not be suitable for heavy tread braking,

[17] Information from the "Final report on the results of the Joint Sector Group activities linked to the action plan defined under the Task Force Freight Wagon Maintenance", 17.12.2012, available on www.jsgrail.eu (accessed on 07/10/2019).

a re-design to consider them without thermal input (i.e. wheelset with disc brakes) has never been applied. Such tyre thickness between 30 and 70 mm (worn/new) and high interference values between the tyre and the wheel centre, which were required to maintain a minimum pressure during drag braking, can be strongly reduced obtaining advantages in terms of mass of the wheel.

Tyred wheels are in fact heavier respect to monobloc wheels. For example, the same wheel in the tyred version weight 420 kg, i.e. 80 kg more than the monobloc version (see Figure 1). Moreover, the wheel centre is highly stressed due to the compression loads during the tyre fitting. Except for the work described in [117] in which both circumferential and radial stresses on the external and internal surfaces of an S-shaped wheel centre were evaluated using strain gauges measurements, there are not recent studies about the effect of the tyre fitting process on the wheel centre. Steel grades used to manufacture wheel centres are characterized by high elongation at fracture and low yield strength and the resulting stresses due to tyre fitting are such that permanent deformation may occur, as shown in Figure 39, leading to an unpredictable behavior during service and during successive maintenance. Table 15 shows the steel grades that are defined by the leaflet UIC812-1, in which the technical specification for the supply of rolled and forged wheel centres are given.

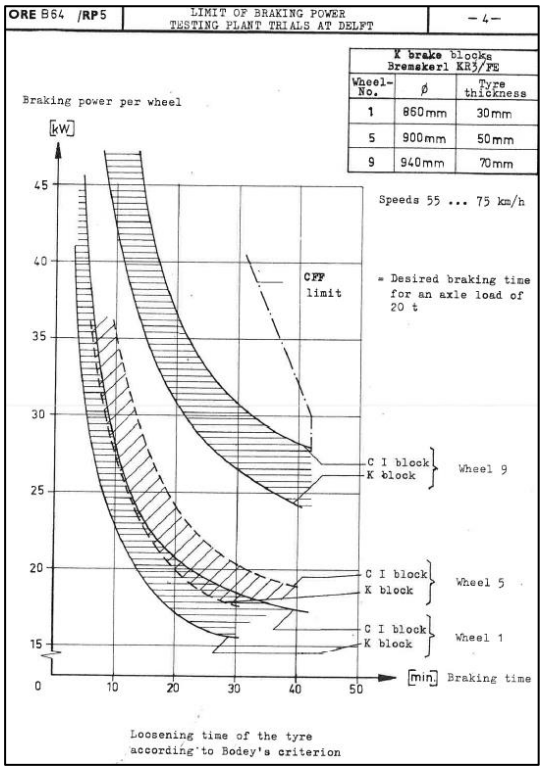

Figure 38. Time required to lose the tyre in function of the braking power for three tyred wheels with different tyre thickness (new=70 mm, half-worn=50 mm and fully worn= 30 mm) [116].

Table 15. Steel grades prescribed by UIC812-1 for wheel centre manufacturing. N=normalized, E=hardened and annealed

Leaflet code	Steel grade	Heat treatment	$R_{p0,2}$ [MPa]*	R_m [MPa]	A_5 [%]	K_u [-]**
C1	C22	N	240	410-490	27	35
C2	C35	N	300	500-650	20	25
C3	C45	N	340	650-760	16	15
C4	46MnSi4	E	450	750-850	20	20
* Yield strength is not provided by UIC812-1. Values are taken from EN10083-2:2006 ** Impact energy at room temperature						

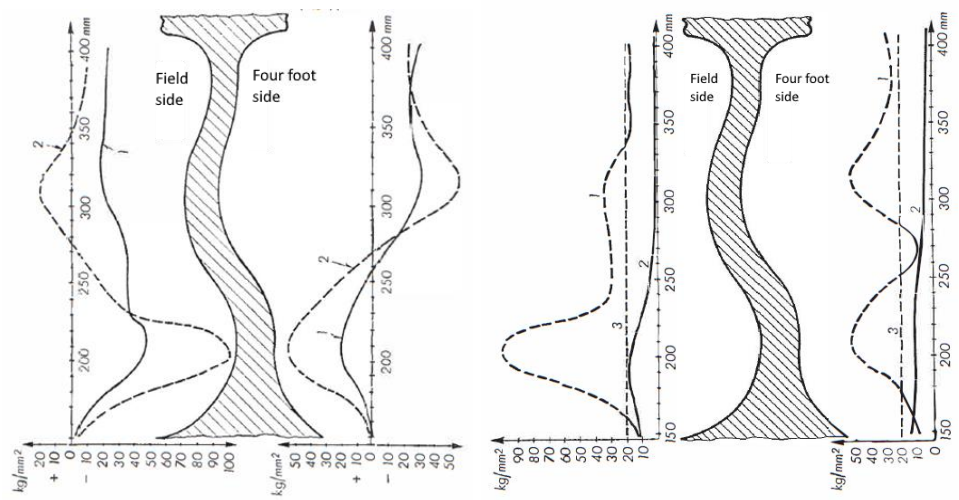

Figure 39. Left: circumferential (1) and radial (2) stresses during the fitting of the tyre on the wheel. Right: comparison of the von Mises equivalent stresses with the yield stress (3), for the axle + tyre fitting (1) and for the axle fitting only (2) [117].

The steel grades for tyre material are given in the leaflet UIC810-1, in which six grades are defined, as shown in Table 16. However, the most used one is the B5T grade.

Table 16. Steel grades for tyres defined in the leaflet UIC810-1. N=normalized, T=hardened and tempered

Leaflet code	Steel grade	Heat treatment	$R_{p0,2}$ [MPa]*	R_m [MPa]	A_5 [%]	K_u [-]**
B1	C50	N	355	600-720	18	15
B2	C55	N	370	700-820	14	10
B3	C60	N	380	750-880	12	10
B4	C70	N	420	800-940	10	10
B5	C60	T	580	800-920	14	15
B6	C65	T	620	920-1050	12	10
* Yield strength is not provided by UIC810-1. Values are taken from EN10083-2:2006 ** Impact energy at room temperature						

3.4.2. The maintenance problem

From the maintenance point of view, the advantage of having a removable tyre and therefore lower purchasing costs, is eliminated by the long and expensive maintenance procedures needed to change the tyre itself. In the "worst case", the following operations are traditionally performed, starting from the wheelset already removed from the bogie:

1. the wheelset is moved to a wheelset lathe where the retaining rings are machined and removed;
2. the wheelset is moved to the tyre cutting station, typically an alternating saw one;
3. the wheelset is moved to the tyre removal station, where the (nearly fully) cut tyres are pulled away from the wheel centre;
4. the wheelset is moved to the wheelset lathe where the wheel centres are machined to a new (smaller) diameter;
5. new tyres are moved to a vertical lathe and machined to the matching internal diameter to ensure the right interference;
6. new tyres are moved to the heating station;
7. both hot tyres and the wheelset are moved to the assembly station, where they are assembled with a manual procedure ("upside down");
8. retaining rings are installed manually;
9. after cooling, the completed wheelset is moved to a wheelset lathe where the wheels are reprofiled to the wanted profile and dimensions.

The weakest points of this process are:

- the presence of a retaining ring, which only acts to avoid the vertical displacement of the tyre when the mating pressure is totally recovered due to the thermal input;
- the removal of the tyre by means of cutting, which often lead to damage the wheel centre surface. However, this problem is avoided by heating the tyre for example with thermal induction;
- the purchasing of rough tyres to be machined twice, firstly on the inner diameter before the tyre fitting and then externally when the wheelset is assembled.

This final machining guarantees the respect of the wheelset tolerances such as internal gauge, radial and axial run-out according to EN13260, as shown in Figure 40 and Table 17. If the final dimension of wheelsets with tyred wheels are not respected and a further machining is needed, it means that during tyre cooling the displacements of the tyre is probably uncontrolled, with significant uncertainty of its final position. Such displacements could be the result of lateral and radial elasticity of the wheel centre, which is often design with a S-shape

web in order to recover the pressure even when the tyre is worn and the mating pressure between the tyre and the wheel centre would tend to decrease.

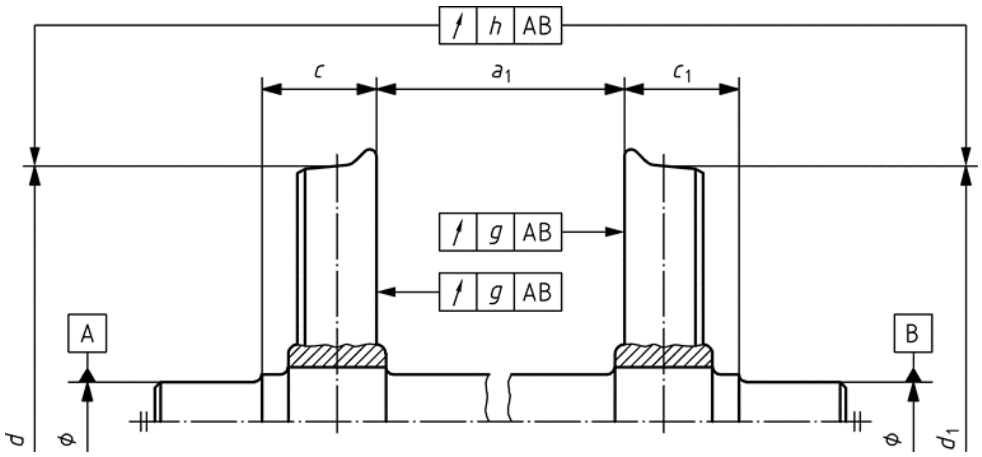

Figure 40. Sketch of a wheelset and main dimensions to be measured for assembly quality assessment.

Table 17. Values of tolerances to be respected after the wheelset assembly. Modified from EN13260.

Description	Symbol	Category of wheelset*		
		1	2a	2b
Distance between the internal wheel faces	a_1	+2 0	+2 0	+2 0
Difference in distances between the internal face of each wheel and the plane on the journal side defining the corresponding collar bearing surface	$c-c_1$	≤ 1	≤ 1	≤ 1
Difference in tread circle diameter	$d-d_1$	≤ 0.3	≤ 0.3	≤ 0.5
Radial run-out in tread circle	h	≤ 0.3	≤ 0.3	≤ 0.5
Axial run-out of the internal wheel face	g	≤ 0.3	≤ 0.5	≤ 0.8
*Category 1: vehicle with speed > 200 km/h Category 2a: vehicle with speed in the range 120÷200 km/h Category 2b: vehicle with speed < 120 km/h				

3.4.1.Multi-material wheels

More recently, tyred wheels with modified wheel centre have been developed. As the wheel centre material was aluminium while the tyre remains made of steel, these wheels were called multi-material wheels or hybrid wheels. The reasons behind their development were mainly lowering the noise emission [46] and mass reduction [118].

In the first case the wheel centre has been developed in order to increase lateral stiffness of the wheel, increasing the natural frequency of axial modes without increasing the mass. The web is four times (90 mm) thicker than the original web and the wheel was found 4.5 dB quieter than the original one. A version with tuned absorbers was also developed (Figure 41, left) with a further reduction of noise.

In the second case the wheel web was maintained to conventional values reducing the wheelset mass of about 25% (i.e. 263 kg lower than the reference wheelset). However, the new wheelsets included also an optimize axle in high strength steel (30NiCrMoV12, see Table 14) and the actual contribution of the wheels in mass reduction is not known. Aluminium grade used for wheel centre manufacturing was EN AW-6082T6, which has very poor mechanical properties. The authors describe the mechanical properties of the materal with the following values: yield strength of 300 MPa, ultimate strength of 340 MPa and elongation of 12%. Considering also that the Young modulus is three times lower then steel (70 GPa), these properties are not suitable to withstand the loads acting on a wheel, especially considering the high compressive stresses due to tyre fitting. The same authors show FEM simulation results indicating as the tyre fitting stresses reach -300 MPa, which are inadmissible values considering the strength of the material.

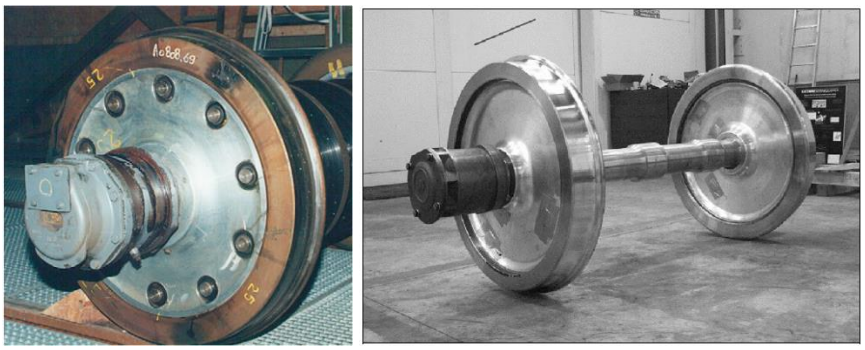

Figure 41. Multi-material wheels with aluminium wheel centre. Left: wheel with tuned absorbers developed to reduce noise emission. Wheel centre web is 90 mm thick but the mass is not increased. Right: wheel developed to reduce mass

Except for some prototypes these multi-material wheels has never been tested in service. Even if the use of a lightweight material for the wheel centre could help to reduce mass and noise, the maintenance weak points must be removed in order to consider again tyred wheel a competitor of monobloc wheel. Moreover, if the thermal loads are not present anymore, tyred wheels could be optimized. Starting from these considerations the tyred wheels have been considered as the best application for the ADI, as a new lightweight casted wheel centre together with a modified locking between the tyre and the wheel centre will let to improve maintenance of tyred wheels, with important saving on life cycle costs.

4. An optimized tyred wheel

4.1. Analysis of conventional tyred wheels

4.1.1. Stresses and strains of conventional wheel centres

Before strating with the design of a new tyred wheel with an optimize casted wheel centre, a preliminary analysis of the structural behavior of tyred wheels has been performed. As already said in the previous chapter, an updated review about the design of tyred wheel is not available and the only data are those from Sachs dated before 1973 [117].

Finite Element Analysis (FEA) is the tool used to estimate stress and strain fields obtained on the wheel centre deriving from both hub/axle shrink (or press) fitting and wheel centre/tyre shrink fitting. The input loads are imposed by means of the interference values calculated according to EN standards and UIC codes in force, considering their maximum and minimum values. As shown in Figure 42, the surfaces are modelled with their nominal dimension and the interferences are added at the contact definition as initial offset between the contact and target bodies of the wheel centre, the tyre and the axle. Non-linear frictional contacts with μ=0.3 have been used, while constrains are applied only to the axle in axial ad radial directions. Simulations were conducted for four tyred wheels:

1. a wheel for passenger trains (axleload 13 t/axle) with v≤200 km/h;
2. a wheel for freight trains (axleload 20 t/axle) v≤120 km/h;
3. a wheel for metro vehicle (axleload 12 t/axle) with v≤77 km/h;
4. a wheel for passenger trains (axleload 18.5 t/axle) based on a current monobloc wheel designed to run up to 360 km/h.

The main parameters of the wheels are described in Table 18. Three of these have an axisymmetric shape of the wheel web and therefore they have been modelled with 2D elements with axysimmetric behaviour, while for the last one 3D elements have been used considering a reduced model of 72° and a cyclic symmetry behaviour. A representation of the meshed models is given in Figure 43. For *wheel 4* the original wheel web shape and thickness were maintained, resulting in a straight wheel centre which is unconventional for a standard wheel

centres as it is believed to don't provide enough radial elasticity respect to S-shaped wheel centre (*wheel 1* and *wheel 2*). If the wheel centre has a good radial elasticity, it provides a recovering effect of the mating pressure during the tyre thickness reduction due to wear. However, this kind of design has been applied in the past to seek a constant pressure level in both new and worn tyre condition, in order to resist thermal input of tread braking, but experience has shown that it does not occur in practice, as shown in Figure 38. *Wheel 3* is designed for a metro vehicle equipped with brake discs, resulting in lower external diameter D and tyre fitting diameter D_e. The forged wheel centre of this wheel has a complex shape that was acquired with a 3D scanner. This shape, from which the wheel is called "corrugated wheel", was quite common in the past especially for small diameter wheels and gives a great resistance of the wheel to lateral load, resulting in a lower thickness and a lower mass of the wheel centre [119].

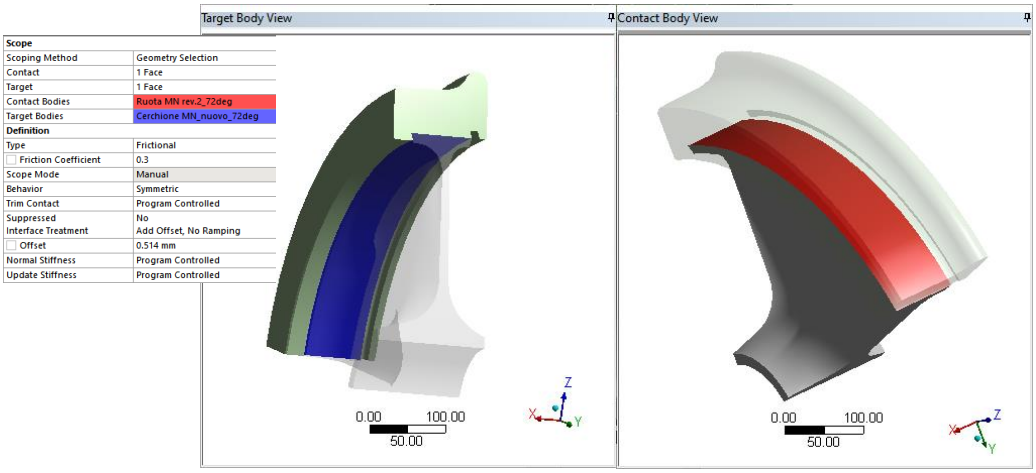

Figure 42. Example of non-linear frictional contact definition for *wheel 3*. Contact and target bodies are defined selecting the nominal surfaces of the wheel centre and the tyre respectively. In the normal direction the behavior is non-linear as the bodies cannot penetrating themselves, but their separation is allowed, while for the tangential behavior a friction coefficient is defined to model the lateral resistance of the couple. The same is applied to the hub/axle fitting, and for the other 2D models.

Table 18. Main parameters of the simulated tyred wheels

Wheel #	D [mm]	Wheel load *Pmax* [t/wheel]	*Vmax* [km/h]	Hub fitting diameter D_i [mm]	Tyre fitting diameter D_e [mm]	New tyre thickness S_n [mm]	Worn tyre thickness S_w [mm]	Shape of the wheel centre
1	940	6.5	200	190	790	75	40	S-shaped
2	920	10	120	185	790	65	40	S-shaped
3	840	6	77	160	718	61	31	Corrugated
4	920	9.25	360	220.5	790	65	30	Straight

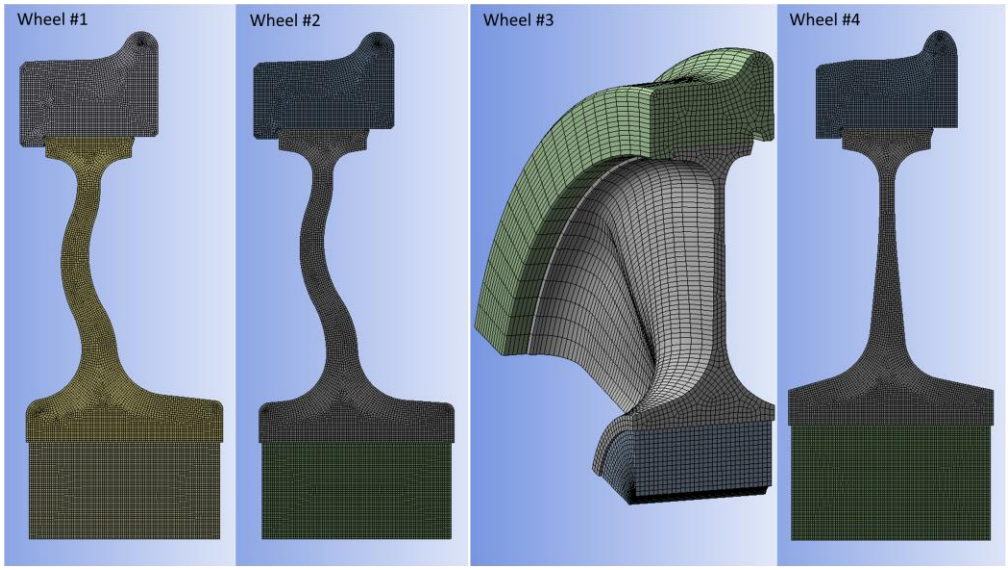

Figure 43. Meshed models of the tyred wheels chosen for the analysis. For *wheel 1*, *wheel 2* and *wheel 4* 2D elements with axisymmetric behavior are used, while cyclic symmetry with 3D elements are used for *wheel 3*.

According to the current maintenance procedures for tyred wheels in Italy, the interference value for the wheel centre and tyre shrink fitting was set according to equation (6), where D_e is the tyre fitting diameter in mm (typical value 790 mm), while the interference value for the wheel hub and wheel seat was set according to equation (7), where D_i is the hub fitting diameter in mm (typical value 200 mm).

$$i_e = \frac{1.3 \pm 0.1}{1000} * D_e \tag{6}$$

$$i_i = \frac{1.5}{1000} * D_i \tag{7}$$

The interference value i_e are in the order of 1 mm, and a temperature of 120 °C is enough to disengage the tyre from the wheel centre, while during the mounting process the tyres are usually heated between 200 °C and 250 °C and the maximum admitted by current regulation is 300°C.

For *wheel 2*, the radial and the circumferential stresses due to the application of tyre interference have been calculated and plotted in Figure 44 allowing a direct comparison with those of Figure 39 (left). Even if the simulated maximum values are slightly lower (the interference values used in [117] are higher than the ones used in the simulations and small geometry differences may influence the results), the trend of the stresses are almost equivalent. In addition, von Mises stresses were calculated and plotted in Figure 45 with the aim to compare the model to the results of Figure 39 (right). It is evident that the elastic limit is exceeded. A purely linear model of the material behavior is therefore unrealistic and an ideal elastic-plastic material model with a yield strength of 235 MPa was used. However, in the following the results are presented considering a linear elastic material model. Results can

therefore be evaluated regardless the different material properties (i.e. yield strength), but only considering the shape and the geometry parameters of the wheels

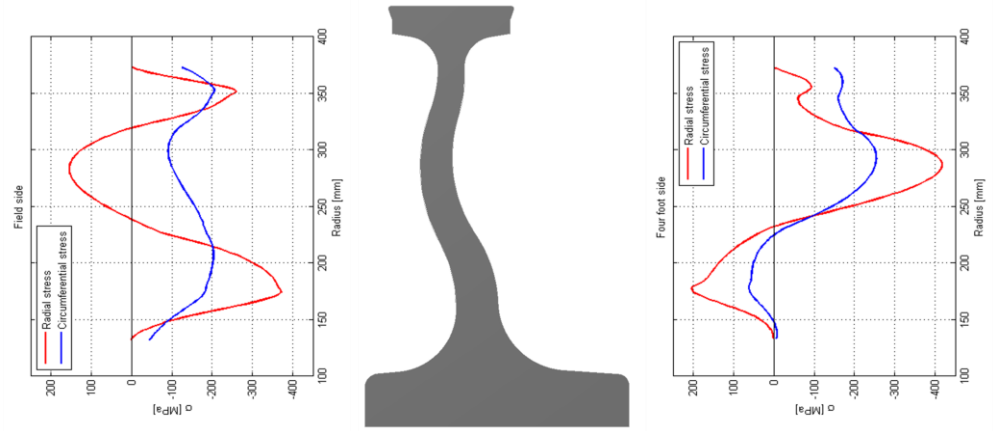

Figure 44. Radial and circumferential stresses in the case of tyre fitting only. Geometry of *wheel 2* is used.

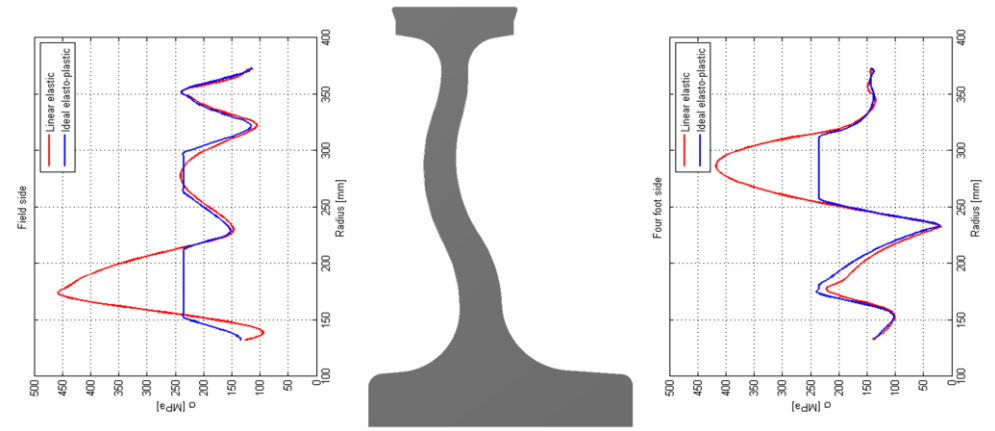

Figure 45. von Mises stresses for a linear elastic material model and an ideal elastic-plastic material model. Geometry of *wheel 2* is used.

The pressure distribution at the wheel centre/tyre interface is the parameter that guarantees the consistency of the tyred wheel assembly even in worn tyre conditions and with the minimum interference. These pressure values are strongly depending on the radial stiffness of the wheel centre and therefore it was chosen as representative parameter. The value of the radial stiffness was calculated applying a pressure of 1 MPa at the tyre/wheel centre interface and evaluating the radial displacement of the central node of the interface surface. The higher value of radial stiffness is obviously related to the straight web of *wheel 4*, while the others wheels have a more elastic wheel centre given by the S-shaped or corrugated web, which has the lower stiffness value As the radial stiffness of the straight web *wheel 4* is considered the highest practically reachable value, the other wheels are normalized to this reference value.

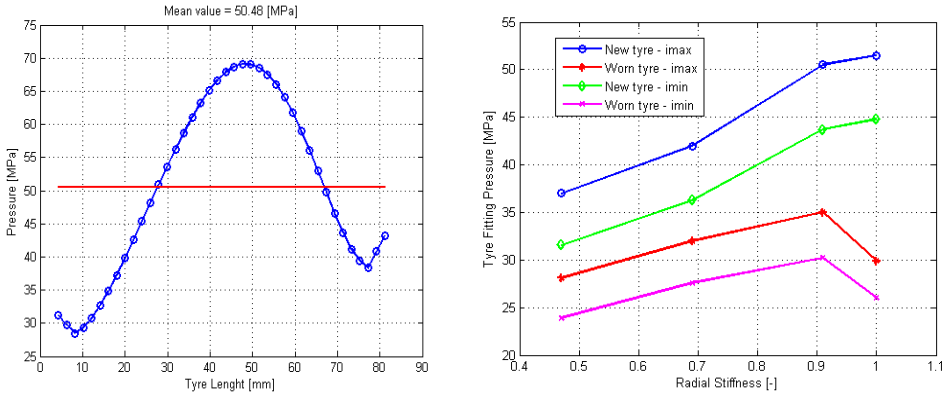

Figure 46. Left: Mating pressure between tyre and wheel centre for *wheel 1*. Right: mean pressure values plotted against the radial stiffness of the wheel centre for different combinations of tyre thickness and interference value.

Even if the straight wheel centres has a tyre pressure reduction of about 50% from the initial value, the minimum value is comparable to those of more elastic wheel centre and therefore the constraining action of the tyre on the wheel centre is guaranteed. Moreover, in all cases the maximum transmissible torque is greater than the ones obtained for the wheel/axle interface, even considering the worn tyre and the minimum interference.

Another important value to consider is the lateral displacement of the tyre after the fitting, which could modify the internal gauge of the wheelset, i.e. a_1 in Table 17. As shown in Figure 47, depending on the behavior of the wheel centre the lateral displacement can reach values up to 0.65 mm for *wheel 2*, i.e. an increase of internal gauge of 1.3 mm, while it is almost zero for *wheel 3* and *wheel 4* as the straight wheel centre deformation is mainly radial. However, all values are such that the internal gauge of the wheelset would respect allowable value (+2 mm). As the wheels are axysimmetric, axial run-out is not considered here except for *wheel 3*, but the oscillation around the mean value is negligible.

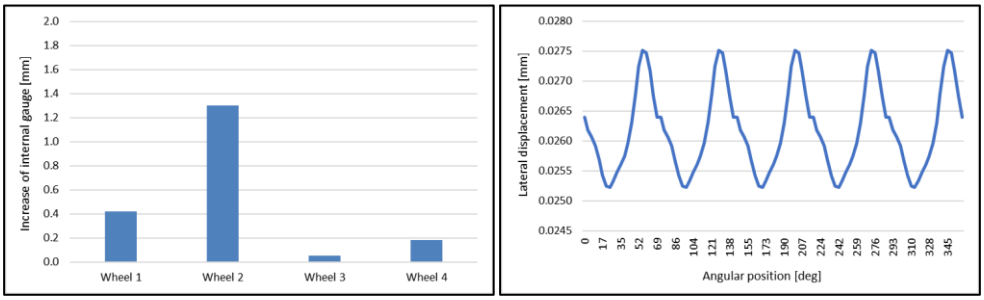

Figure 47. Left: Lateral displacement of the tyre plotted as increase of internal gauge for all the wheels. Right: Lateral oscillation of the tyre in function of its angular position for *wheel 3*.

A straight web is also interesting as the wheel centre is subjected only to compressive stresses, while the deformation of the other kinds of webs are such that high values of both tensile and compressive stresses are generated. This is shown in Figure 48 (left), in which the

minimum and maximum principal stresses on the wheel centre are plotted. On the other side as *wheel 4* has the maximum interference pressure, the tyre is subjected to the higher tensile circumferential stress, which increases as the thickness of the tyre reduces, i.e. the wear increases. The maximum value of these stresses occurs at the field side abutment, which have the minimum cross section, representing the structurally weakest point of the tyre.

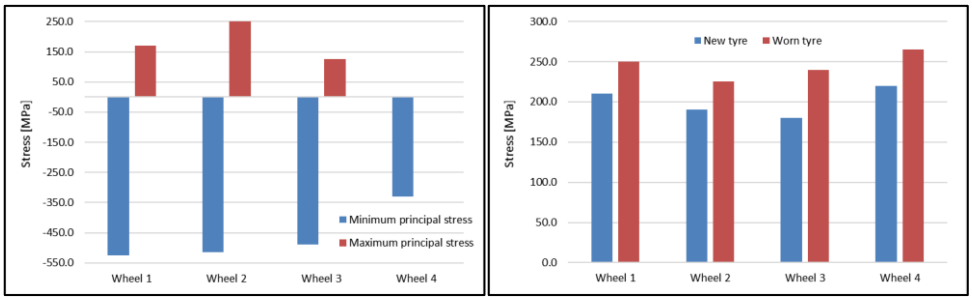

Figure 48. Left: Minimum and maximum principal stresses in the wheel centre. Right: Circumferential stress in the tyre for new and worn conditions.

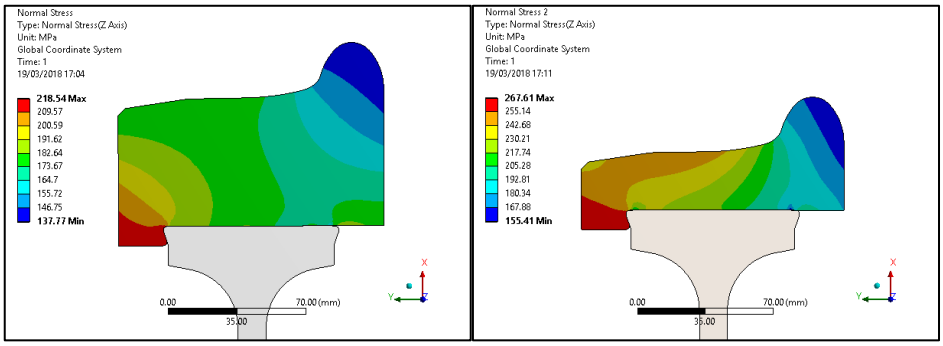

Figure 49. Circumferential stresses in the tyre in new (left) and worn (right) conditions for *wheel 4*.

4.1.2. Optimization without thermal input

The problem of tyre loosening and possible tyre/wheel centre relative rotation has always been central. One of the first study of slip of thin tyres fitted on wheels is [120], although only normal load (no traction or braking) is considered. Recently, the only contribution to the purely elastic problem when contact tangential forces are considered is [121], which defines the minimum friction coefficient between the tyre and the wheel centre to avoid spinning when no thermal inputs are involved and varying the mating pressure and tyre thickness. However, the authors conclude that the tyre thickness should be as great as possible to avoid fretting without giving practical and useful values. Moreover, the pressure and the thickness are considered independent, which is a wrong assumption as if the tyre thickness increases also the mating pressure between the tyre and the wheel centre increases.

The leaflet UIC510-2 *Trailing stock: wheels and wheelsets. Conditions concerning the use of wheels of various diameters* states the operating (fully worn) limits for tyre thickness.

Passenger coaches have a limit of 35 mm, but they can use tyred wheels only if their speed is $v \leq 160$ km/h, while for freight wagons it depends on maximum speed as follows:

- v > 120 km/h: tyred wheels are not permitted;
- v = 120 km/h: 35 mm;
- v = 100 km/h: 30 mm;
- v < 100 km/h: 25 mm.

However, the same leaflet explains that from 01.01.1989 only solid wheels (i.e. monobloc) are permitted on freight wagons, and the minimum tyre thickness has been increased in 2013[18] to 43 mm for all the freight wagons with speed greater than 80 km/h, until the complete stop of tyred wheels from 01.01.2020. All these limitations are clearly related to the unsuitability of tyred wheels to withstand thermal loads of tread braking, while the above limitations according to vehicle speed were not a solution to the thermal problem, to which only monobloc wheel could be effective. The effect of centrifugal force due to speed is small if compared with that of increasing the temperature, as shown in Figure 50, for a wheel with straight wheel centre web and for different speeds. In fact, the centrifugal actions are able not to produce enough radial deformation to recover the interference and when the tyre is worn, the mass is so small that the effected is nearly zero.

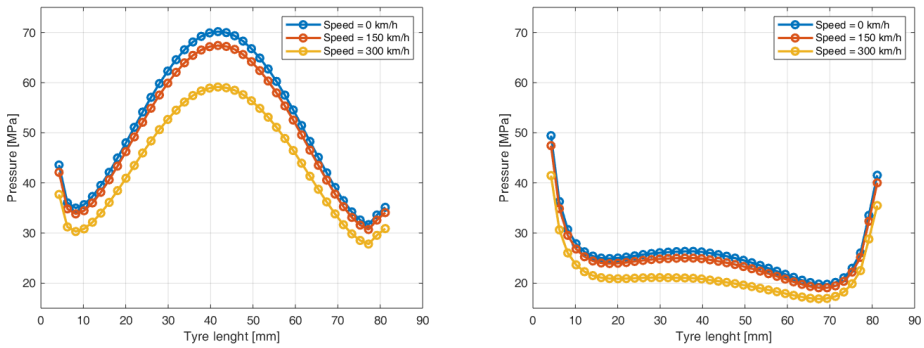

Figure 50. Effect of the centrifugal force on the mating pressure between tyre and wheel centre. A certain effect is only relevant in new tyre condition (left), in which mean values pass from 51.5 MPa to 43.9 MPa. In worn condition (right) the tyre mass is low and the pressure reduction is minimum even if the starting value is lower.

To understand the possibility given by the absence of tread braking on designing tyred wheels, it is needed to evaluate the behavior when the maximum tractive force is applied. About starting torque, a limiting value of μ=0.33 was adopted according to the classical equation by Curtius & Kniffler. However, it is worth to highlight that depending on the kind of vehicle different traction problems could occur. On coupled axles locomotives of heavy

[18] Joint Sector Group, Use of tyred wheels in tread braked freight wagons with v_{max} > 80 km/h, 2011, available at http://jsgrail.eu/doc_list.asp?cat_id=15 (accessed on 11/10/2019).

diesel locomotives for examples, chatter phenomena (a.k.a. broutage) may lead temporarily to extra loads on the transmissions. In this case it is prudent to adopt a conventional wheel-rail friction coefficient of μ=0.6; while electric locomotives may suffer from short circuit at the motors, of limited duration but significantly higher torque. It is usual in this case to adopt a conventional wheel-rail friction coefficient of μ=0.8.

Considering a sufficiently short portion of the tyre of thickness t as a sort of "third body" inserted between the tyre and the rail, as shown in Figure 51, to transmit any given torque T' at the wheel centre-tyre contact purely by the fitting, a pressure p'_{fit} acting on the surface A is needed according to equation (8), while a pressure p'_{fit_N} according to equation (9) is needed when a vertical load N is present.

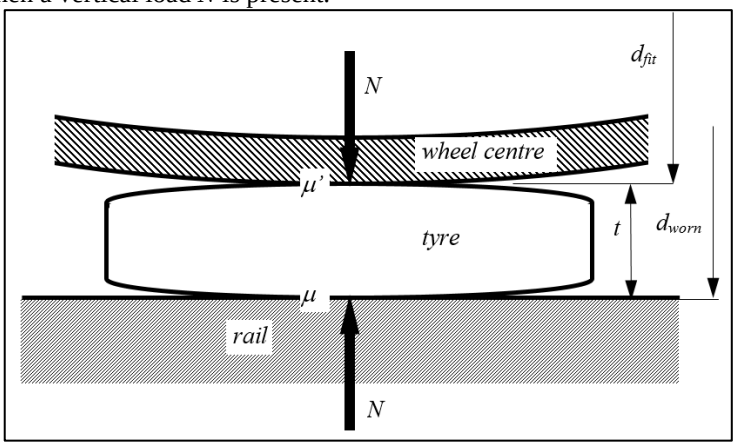

Figure 51. Schematic representation of the wheel centre-tyre-rail contact.

(8) $$T' = \mu' p'_{fit} A \frac{d_{fit}}{2}$$

(9) $$T' = \mu'(N + p'_{fit\_N} A) \frac{d_{fit}}{2}$$

It is possible to conclude that $p'_{fit\_N} = p'_{fit} - N/A$, resulting in a beneficial effect of the vertical load. If $T = \mu N(d_{worn}/2)$ is the torque to be transmitted at the wheel-rail contact it must be that $T'=T$, from which it is possible to find the pressure as a function of the friction coefficients, according to equation (10), with the possibility to reach almost zero pressure when $\mu/\mu'=1$.

(10) $$p'_{fit\_N} = \frac{N}{A}\left(\frac{\mu}{\mu'}\frac{d_{worn}}{d_{fit}} - 1\right)$$

It results that even in conservative conditions the pressure needed to transmit the torque is very low, as shown in Table 19. Obviously, such small mating pressure lower than 1 MPa are not manageable, but the tyred wheel design is strongly over-dimensioned respect to the need of transmitting torque. Even if centrifugal forces are considered it is impossible to reach

the pressure values found in Figure 46 and therefore an optimization in terms of tyre thickness and mating interference can be performed, if thermal input on the tyre is not applied. Varying the values of interference from 0.4 to 1.4 mm and the mating diameter from 790 to 810 mm the pressure has been calculated considering a wheel with external diameter of 920 mm in new tyre condition and 830 in worn tyre condition. The results are mapped in Figure 52, in which the pressure due to different combinations of thickness/interference is given. The minimum value obtained is 11.6 MPa, becoming 5.6 MPa in the worn conditions, which could be suitable considering the previous considerations. The mass of tyre would be 30 kg lower than the current one and the maximum tyre stress would lower than 100 MPa due to the lower interference.

Table 19. Minimum pressure needed to transmit the torque of four different vehicles ideally equipped with tyred wheels.

Tyred wheel geometric properties				Wheel load	Friction coefficients and ratio			Tangential force	Required pressure
D_{worn} [mm]	w_{fit} [mm]	d_{fit} [mm]	A_{fit} [mm^2]	N [N]	μ [-]	μ' [-]	μ / μ' [-]	$N(\mu - \mu')$ [N]	p_{min} [MPa]
840	90	780	220540	53955	0.33	0.3	1.10	1619	0.045
920	90	860	243159	98100	0.6	0.3	2.00	29430	0.460
960	90	900	254469	84170	0.8	0.3	2.67	42085	0.610
1170	90	1110	313845	103005	0.8	0.3	2.67	51503	0.594

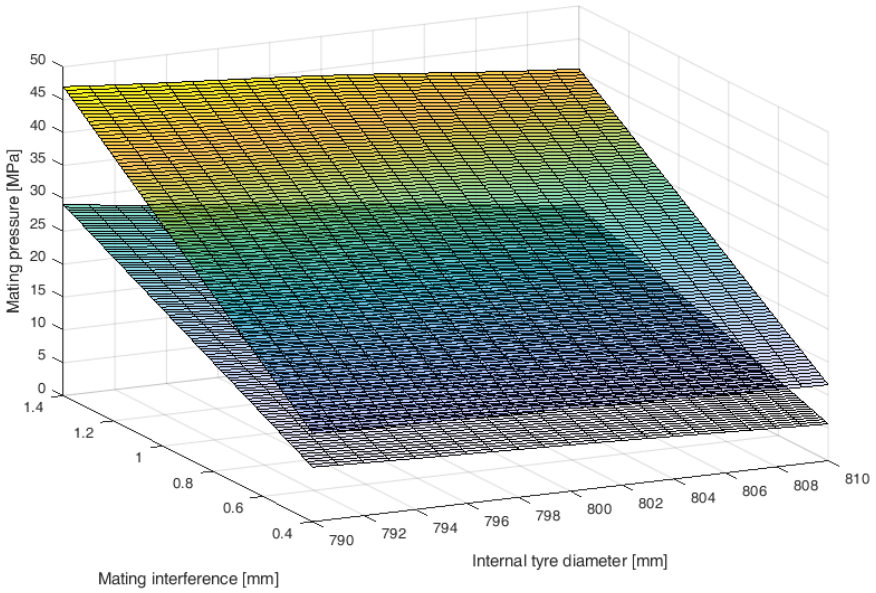

Figure 52. Pressure map in new tyre condition (upper level) and in worn tyre condition (lower level) as function of mating interference and internal tyre diameter. Values are given for a fixed external diameter of 920 mm (new tyre) and 830 mm (worn tyre).

4.2. The reference wheels

4.2.1. ANM metro wheel

The first attempt of optimization of a tyred wheel has been performed on the wheel of a vehicle running on Line 1 of Naples metro (managed by ANM[19]), i.e. *wheel 3* in Figure 43. The complete wheelset is shown Figure 53. This wheel has been chosen to evaluate the feasibility of a casted ADI wheel centre, comparing it with the original one which although designed in 1990 it was already optimized thanks to the forged and corrugated wheel centre.

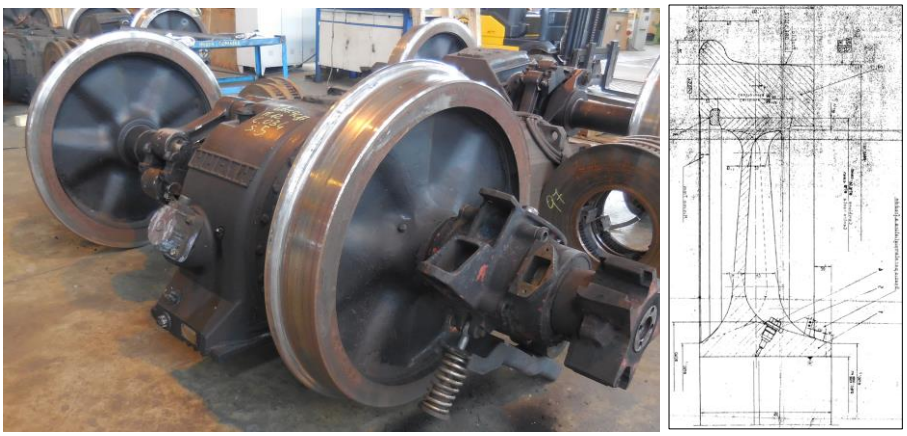

Figure 53. Left: Wheelset of the metro vehicle with tyred wheels in Piscinola workshop. Due to the presence of traction motor inside the wheels, the disc brakes are mounted externally. Right: original drawing of the wheel dated 1990.

With a wheel web of 10 mm the wheel centre mass is only 88 kg. However, after several design review a proper shape for a casted wheel centre was found, with a mass saving of 8 kg. The new design is shown Figure 54, together with the original model reconstructed according to the drawing starting from the real 3D scanned geometry. It is worth to highlight that the mass saving contribution is due to the lower density of cast-iron respect to steel. However, the casted wheel centre would have other advantages as the easiness to cast complex shapes. The arrangement with two opposite and inclined ranks of spokes would be very difficult to produce with casted steel. The shape is shown in detail in Figure 55 (left) and let to reproduce a triangular link that reacts to external forces without bending. The feasibility of the shape has been verified by Zanardi Fonderie, by means of the simulation software MAGMA, which let to evaluate the cooling time and the thermal modulus of the various part of the casting. According to Chvorinov's rule [122], the equivalent thermal modulus can be calculated from the geometric modulus $m = V / A$ and the cooling time $t = Bm^2$, in which V is the volume of

[19] ANM (Azienda Napoletana Mobilità) is the primary provider of urban public transportation in the city of Naples, Italy. In addition to the network of tram, trolleybus and motorbus, ANM operates the Metro line system and four urban funiculars.

the casting, *A* is the emitting surface area and *B* is the mould constant depending on the material and the mould characteristics such as density and thermal conductivity. The main scope of the simulation is to verify that all the possible shrinkages are localized outside the main casting areas. As shown in Figure 55 (right), the hot spots located on the hub and on the external diameter can be managed by the use of proper feeders, while the zones below the bifurcation of spokes are difficult to reach and they could be the most critical points of the casting.

The shape with spokes would also be advantageous in terms of sound emission, as the total lateral surface of the wheel is 50% lower than the starting one. Finally, the use of casting let the purchasing of this component easier respect buying it from standard wheelset manufactures, which are no more interested in developing new wheel centres, especially for small fleets of old vehicles, such the one in this case. In fact, as the wheel manufacture closed in 2003, currently the mobility company ANM is relying only in the spare parts remained from the original supply.

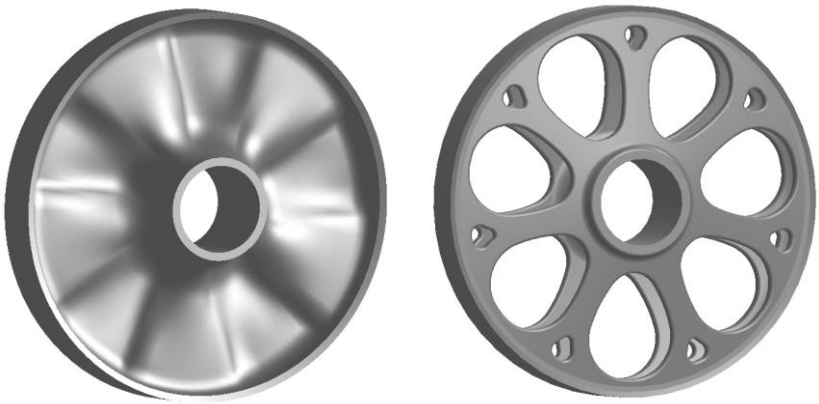

Figure 54. Left: Model of the original wheel centre, with external diameter of 718 mm and mass of 88 kg. Right: Model of the new wheel centre to be casted in ADI with two rank of spokes. Final mass saving is 8 kg, thanks to the lower density of the material.

Due to the optimized shape, the spoked wheel centre is more elastic respect the original one. This is shown in Figure 56 (left), in which the radial stiffness of the corrugated wheel centre is compared with the spoked one made of the same material, i.e. steel, and made of cast iron. The lower radial stiffness gives lower stresses in the tyre, which are plotted in Figure 56 (right) in the worst case of worn tyre condition and maximum interference. On the other side, with the minimum interference the low stiffness and the worn tyre give the lowest mating pressure. The mean value is in fact equal to 22 MPa, which is only 2 MPa lower than the minimum value for the corrugated tyred wheel (see Figure 46 right), and therefore still compatible with the application. In the axial direction, the spoked wheel is instead stiffer even considering the lower elastic modulus of cast iron, as shown in Figure 57, helping to reduce the bending elastic strain, and therefore the stress, at the hub of the wheel centre.

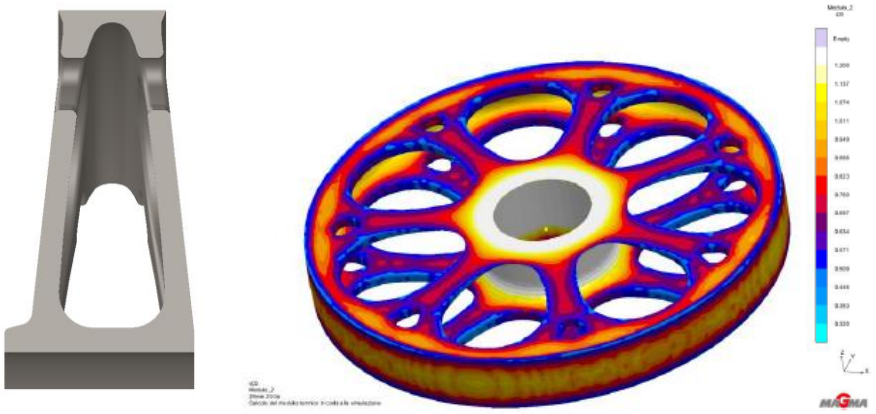

Figure 55. Left: Section view of the casted wheel centre with two ranks of spoke. Right: thermal modulus simulated by dedicated simulation software to verify the feasibility of the shape.

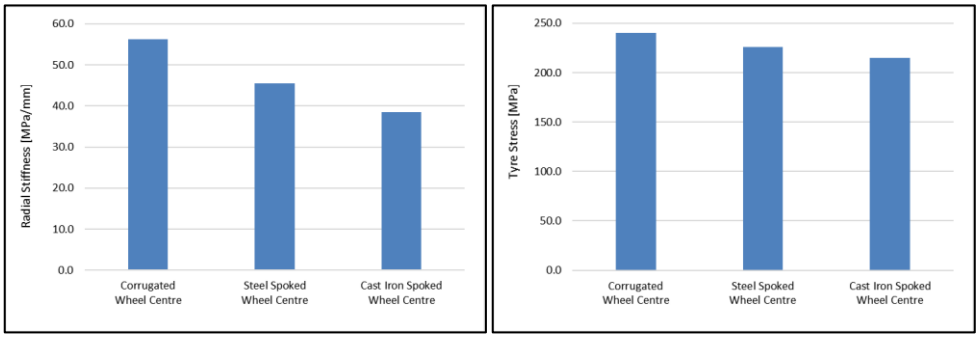

Figure 56. Radial stiffness (left) and circumferential tyre stress (right) comparison between the corrugated original wheel centre and the spoked one. To evaluate the effect of the optimized shape the spoked one has been considered made of both steel and cast iron.

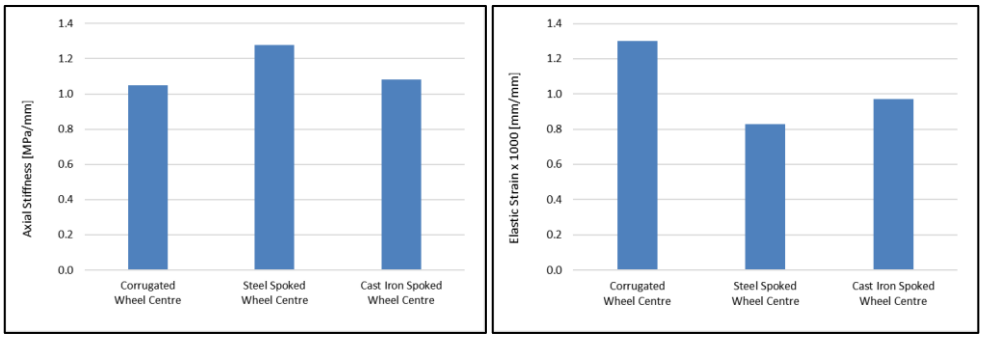

Figure 57. Axial stiffness (left) and wheel centre elastic strain (right) comparison between the corrugated original wheel centre and the spoked one. To evaluate the effect of the optimized shape the spoked one has been considered made of both steel and cast iron.

As the two ranks of spokes are designed to be symmetric respect to the fitting surface, their deformation is almost radial, and the lateral displacement is only 0.04 mm with nearly zero oscillation around the mean value. The structural behavior of the wheel has been assessed by FEM analysis, considering static and dynamic loads according to EN13979 and the standard values of interference between tyre and wheel centre. The configuration of the FEM model is shown in Figure 58. In this case the wheel centre is mostly stressed by the compression due to the tyre fitting. The material chosen for the evaluation is the ADI800 grade, i.e. EN GJS 800-10, whose mechanical properties are described in Table 14. With a minimum yield strength of 500 MPa, no permanent deformation can occur. The von Mises stresses due to the tyre and hub fitting are plotted in Figure 59 (left) with the maximum stress equal to 400 MPa in new tyre condition in the zone of the bifurcation opening. This is confirmed by the fatigue analysis, which at this stage has been performed with a simplified method. Considering the load application described in Table 4, case #2 was found the most stressing one, as shown in Figure 59 (right), and applying this case at two opposite angular position, i.e. 0° (on the spoke) and 180° (between two spokes) simulating the wheel rotation, the maximum stress variation has been calculated by the combination of the two solutions. The Soderberg criterion is used for the mean stress correction, which has different formulations if the mean stress is positive or negative, i.e. tensile or compressive. Therefore, in order to highlight the presence of compressive mean stresses, a "signed" von Mises stress has been evaluated, as it gives to the von Mises stress the sign of the largest principal stress. Finally, an equivalent alternating stress S is found to be compared with the fatigue limit of S-N curve at R= -1. Even if this method is clearly affected by some limitations, it is considered suitable for the feasibility analysis, as:

- the radial deformation of the spokes due to tyre fitting gives a pre-compression stress field to the wheel centre and the external loads are not able to recover these stresses and bring to positive maximum principal stresses even in worn tyre condition. This is shown in Figure 60 (left) in which principal vectors are plotted. It is known that fatigue life is not affected in the same way for tensile mean stress or compressive mean stress, and cracks in a notched component subjected to compressive mean stress cannot grow further until an external load introduces either a tensile stresses such that the initial compressive stress is totally recovered or further compressive stresses result in a total stress that exceeds the yielding point of the material [123]. Soderberg criterion results therefore in a conservative evaluation of the compressive mean stress, as $S_e = \sigma_a \veebar \sigma_m < 0$.

- the use of the signed von Mises indicator to consider the multiaxiality of the stress field is usually a not suitable simplification for wheel design and the MPS method is defined in the EN13979. However, the pre-compressed wheel centre represents a special case respect to monobloc wheels and also for tyred wheels, as previously seen. Stress fields can be classified by means of the biaxiality index a (or principal stress ratio), defined as the ratio of the smaller principal stress and the larger principal stress for each node. If a = 0 the stress is uniaxial, if a = 1 the stress is equibiaxial and if a = -1 the stress is pure shear. In this case the spokes are mainly subjected to monoaxial compressive stress as shown in Figure 60 (right), in which the biaxility index is plotted. As the wheel centre is designed to work mainly in compression, most of the parts of the wheel centre have a biaxiality index near zero even if external loads are applied, especially for the central part and base of the spokes, which are the most stressed areas.

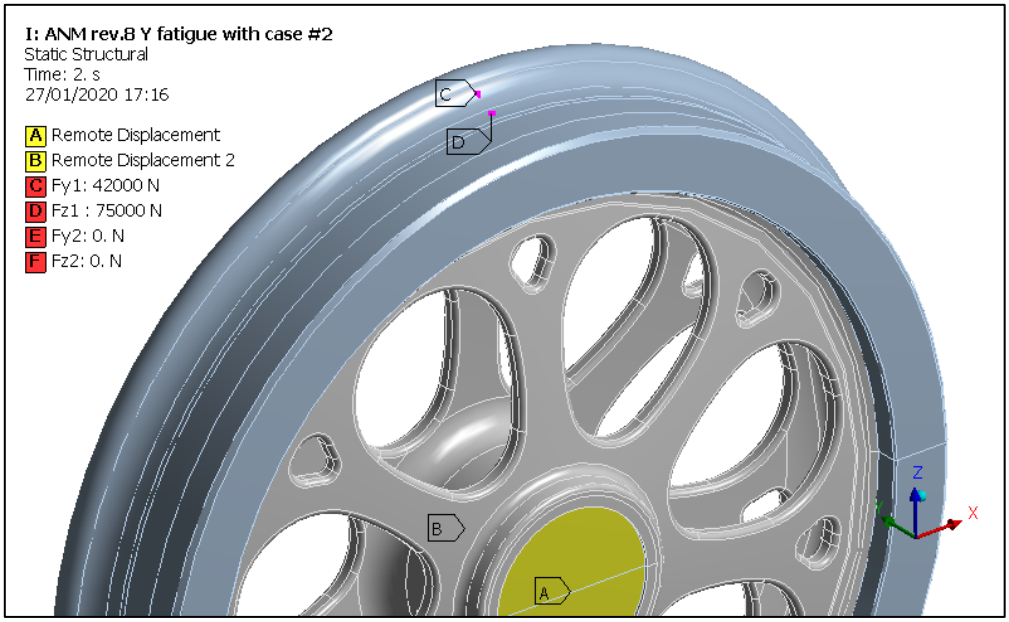

Figure 58. Set-up of the structural analysis at the second time-step. The wheel centre is fitted on a sample axle, which is fixed at its ends (labels A and B). Labels C and D are the application nodes on the tyre of lateral and vertical forces, while labels E and F are located at the opposite angular position respect to C and D, and they are active only at the third time-step. Contacts are modelled as shown in Figure 42 and the interference loads are applied during the first time-step. Values of loads are calculated for case #2 (i.e. running in curves) of EN13979.

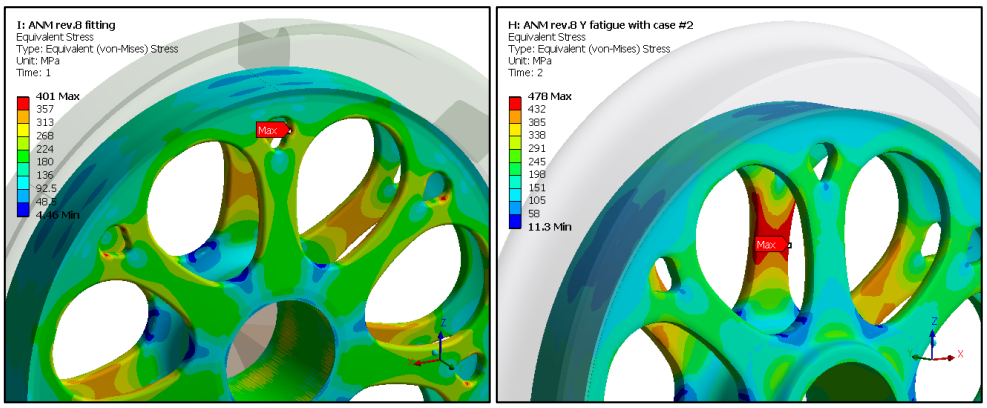

Figure 59. Left: von Mises stresses due to the tyre fitting. Right: von Mises stresses due to tyre fitting and vertical and lateral load at the wheel rail contact.

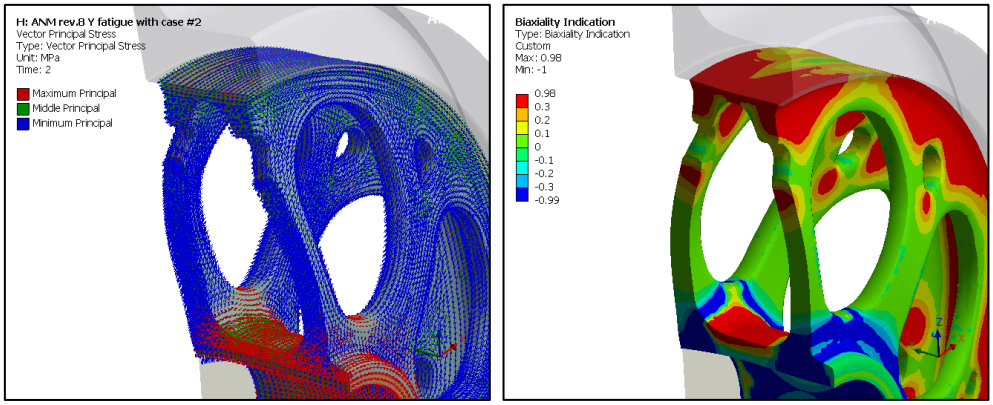

Figure 60. Left: Vectors of principal stresses due to tyre fitting and loads of case #2 of EN13979. Deformations are amplified of a factor 80, showing that the front spoke is extended, and the rear spoke is further compressed, but compressive mean stress is not recovered. Right: Biaxiality index showing that spokes are subjected to monoaxial compressive stress, i.e. $a \approx 0$.

All the considerations explained in paragraph 2.3.3 about the fatigue behavior have been used to calculate the fatigue limit and compare the alternating stresses derived from the fatigue analysis, starting from the experimental data provided by Zanardi Fonderie. All the parameters are shown in Table 20 including the reduction coefficients that consider small surface defects (surface quality *L1*) and large surface defects (surface quality *L2*). This kind of quality and the corresponding reduction coefficient are used for the calculation of fatigue limit shown in Table 20, i.e. $S_e = 87$ MPa. To increase the fatigue limit a better surface quality can be considered obtaining a value of $S_e = 153$ MPa. Shot-peening is not considered as large costs would be rewarded by only a 30% increase of fatigue life (from 87 MPa to 114 MPa), while machining, which brings the value to $S_e = 245$ MPa, would be very difficult to perform. Equivalent alternating stresses obtained in this analysis are plotted in Figure 61, in which fatigue limit S_e is exceeded in the zone of the bifurcation opening.

Table 20. Left: Corrected fatigue limits for machined and un-machined samples using reduction coefficients due to casted skin, machining and increased probability of survival. Right: Values of the reduction coefficients. $S_e = 87$ MPa is obtained for casted skin quality *L2* and for 99.7% of probability of survival. The same for machined material considering a fine machining.

	Thickness [mm]		
	0-25	26-50	51-75
Ultimate strenght [MPa]	920	860	820
Yield Strenght [MPa]	670	620	590
Elongation [%]	13	11	10
Nominal fatigue limit [MPa] - PS 50%	400	376	360
Corrected fatigue limit for un-machined material [MPa]	87	82	79
Corrected fatigue limit for machined material [MPa]	245	230	220

Coefficients		
	L1	**L2**
As-cast skin	0.625	0.357
Shot-peening	1.3	
Machining $R_a = 0.4$	1	
Machining $R_a = 3.2$	0.88	
90 % Probability of survival	0.82	
99.7 % Probability of survival	0.61	

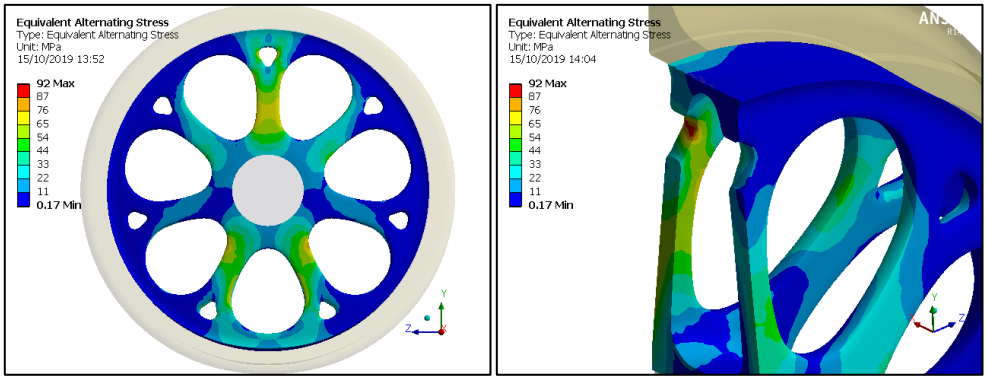

Figure 61. Equivalent alternating stresses due to the application of lateral and vertical loads in opposite angular positions, in worn tyre conditions. Fatigue limit S_e is exceeded in the zone of the bifurcation opening.

4.2.2. TRENORD ALn668 wheel

The tyred wheel of ALn668, a Diesel Multiple Unit (DMU) developed in Italy since 1950 by FIAT Ferroviaria and still operating in several non-electrified lines, has been chosen to study the influence of maintenance on the service life of tyred wheel and to test a solution able to eliminate the maintenance problems described in paragraph 3.4.2. About twenty vehicles of this type are present in the rolling stock fleet of TRENORD[20], mainly operating on the line Brescia-Edolo. The wheel, whose original drawing shown in Figure 62 (left) is dated 1957, has a rolled S-shape wheel centre with external diameter of 790 mm and a 65 mm thick tyre in new condition. Due to the low mass of the vehicle, 37 tons in empty condition and maximum 54 tons in laden condition, the requested braking power is low and tread brake applied on the tyre, as shown in Figure 62 (right), do not represent a critical problem such the ones described for freight wagons. Moreover, the maximum admissible speed is 90 km/h. The four wheelsets of one of these vehicles, has been therefore used to analyze the maintenance procedure and to implement a modification of the locking system between tyre and wheel centre.

Recalling the weak points described in paragraph 3.4.2, the presence of a third component, i.e. the retaining ring, is critical for the mounting and dismounting the tyre. However, the aim of the retaining ring is to avoid the tyre loosening in the case that the mating pressure on the cylindrical coupling is lost, but it does not prevent the lateral displacement of the tyre respect to the wheel centre. Moreover, the ring is manually forced in the tyre groove during the assembly of the wheel and it could happen to lose it. It was then proposed to machine on the mating parts a dovetail self-locking shape capable to eliminate the need of the retaining ring. The schematic representation of this kind of locking is shown in Figure 63 for a hypothetic internal tyre diameter of 800 mm. Today, all machine tools are equipped with a CNC (continuous numerical

[20] TRENORD is a railway company responsible for the operation of regional passenger trains in north-west of Italy, especially in Lombardy region. The company was established by Trenitalia and Ferrovie Nord Milano (FNM) in 2009.

control) and the availability of CMM (coordinate measuring machines) is common in nearly all workshops. This lets an easy machining of difficult shapes, including of course conical surfaces. To calculate the interference ISO tolerances are used instead of the empirical equations function of the fitting diameter, i.e. equation (6), and adding 0.4 mm (0.8 mm on the diameter) of conicity. A temperature of 300°C (maximum heating temperature prescribed by UIC812-4) is sufficient to mount the tyre on the wheel centre.

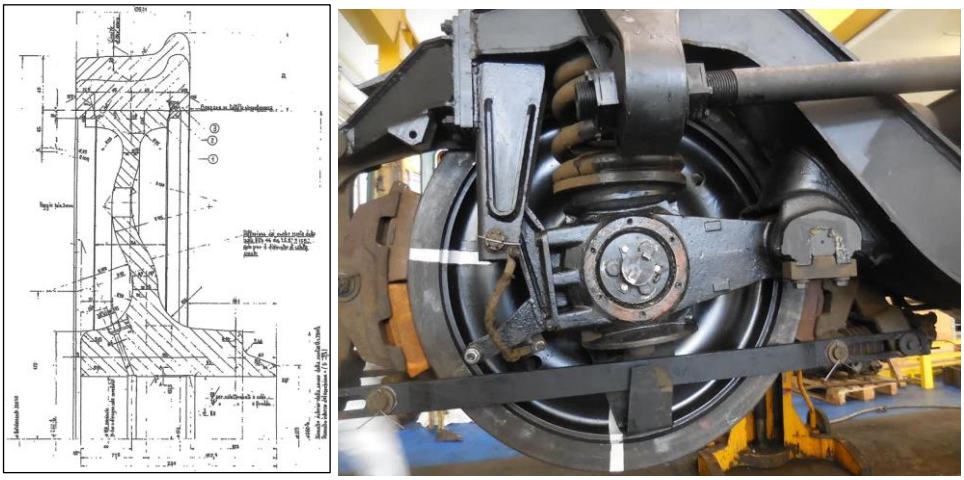

Figure 62. Left: Orginal drawing of the tyred wheel for ALn668 dated 1957. Right: Side view of the wheelset mounted on the bogie at the depot of Iseo.

Before machining new tyres and new wheel centres with the modified shape, four wheelsets have been disassembled and measured. The results are shown in Figure 64, in which the diameter and the length of the mating surfaces are reported and compared to the nominal values, i.e. 790 mm for the diameter and 90 mm for the length of the mating surface. The values are always lower than the nominal dimension, showing an important variability also between left and right side of the same wheelset. This confirm the artisanal way to perform maintenance on tyred wheels, as the wheel centre on the mating surface is often machined after the mechanical removal of the tyre and a fully finish new tyre cannot be used, adapting its internal diameter to the current dimension of the wheel centre.

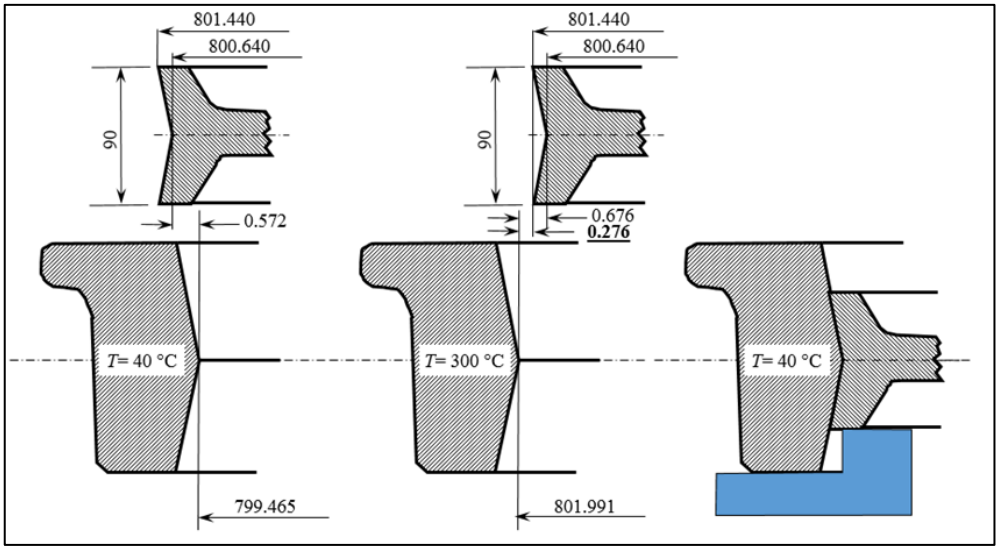

Figure 63. Relative position of coaxial wheel centre and tyre with 800 t7/S8 coupling in cold (right) and hot (centre) conditions. Enough radial play for mounting of 0.276 mm is obtained even with the maximum radial interference of 0.572 mm. Right: simple tool to guarantee the respect of geometrical tolerances after fitting.

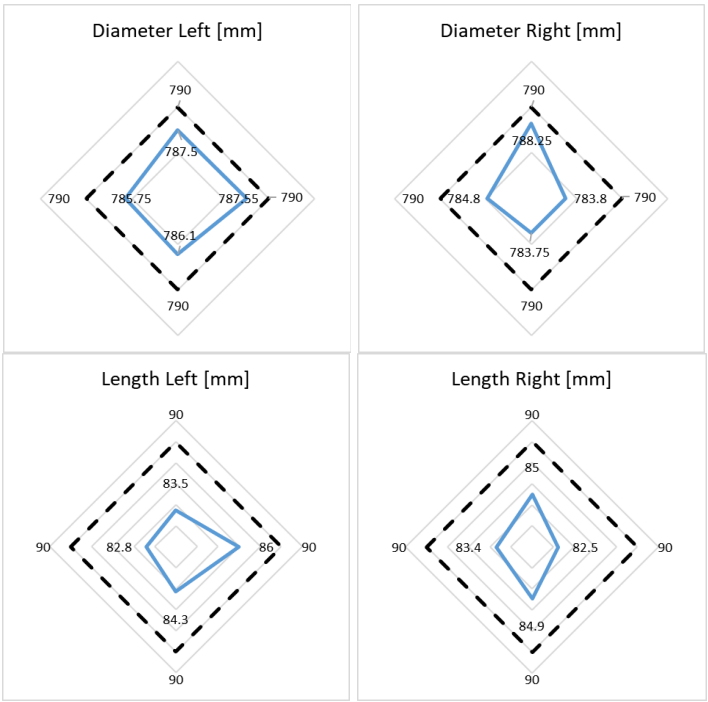

Figure 64. Results of the measurement performed on four disassembled tyred wheels. Both the diameter (above) and the length (below) of the mating surface are lower than the nominal values (dashed lines).

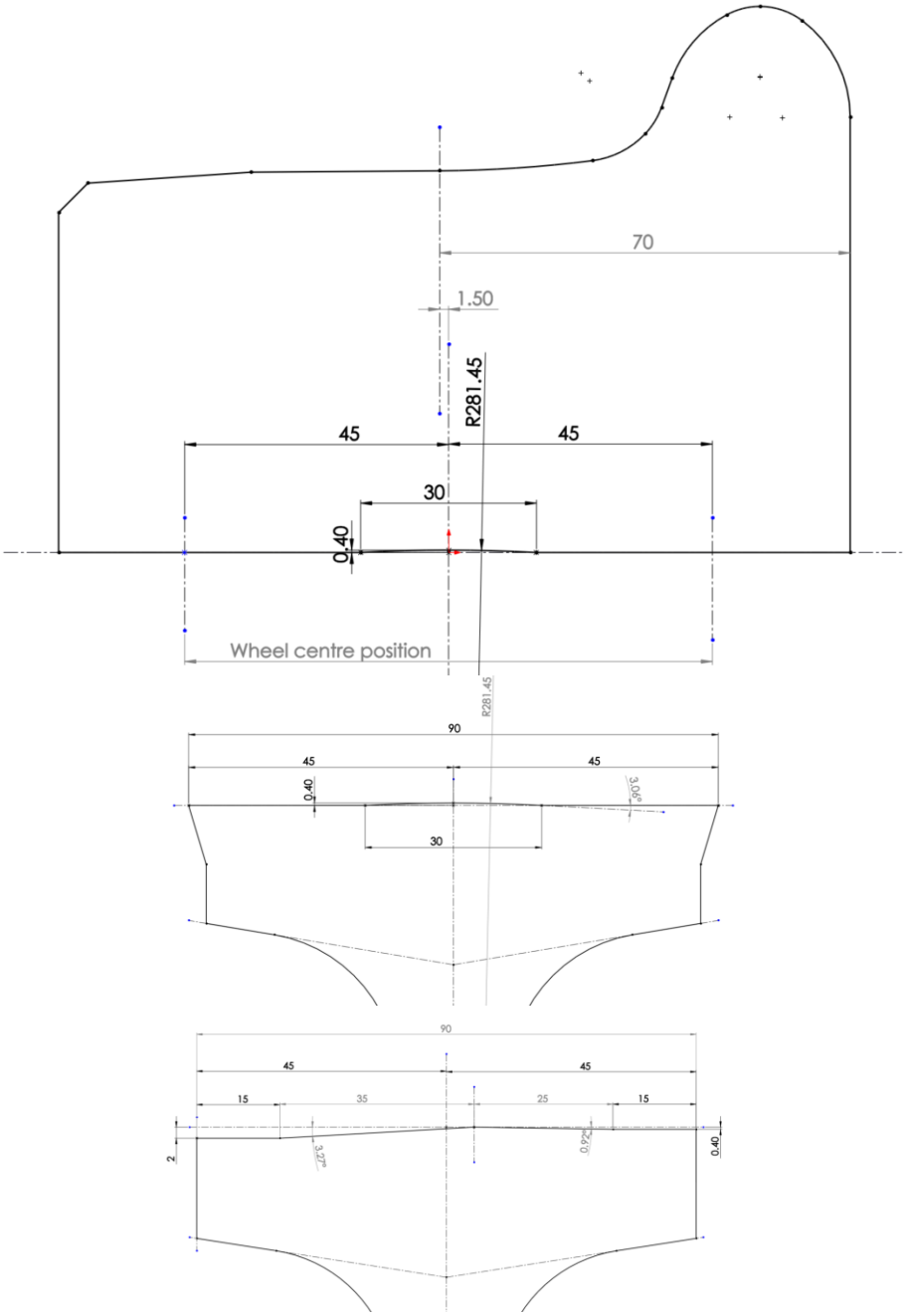

Figure 65. Mating shapes of the new locking type between tyre and wheel centre. Above the tyre with toroidal groove. In the middle the corresponding toroidal abutiment in the wheel centre. Below the asymmetric dovetail on the wheel centre (the corresponding tyre is not shown for space reasons).

The machining of the new coupling has been performed by Nuova Comafer [21], according to two different drawings shown in Figure 65, in which the dovetail concept shown in Figure 63 has been modified. That kind of symmetric solution with the groove on the wheel centre side was discarded as FEM calculations in the elastic-plastic domain suggested to reverse male / female combination. The abutment is then located at middle of the mating surface, in which the radial stiffness of the wheel centre is greater than the lateral border of the surface. Moreover, the toroidal shape let to have a greater slope with the same abutment, while the asymmetric shape let to increase the abutment on the field side (2 mm), which must withstand greater lateral forces.

According to Table 4, considering a wheel load of P= 66 kN, i.e. an axleload of 13.5 tons, the maximum lateral force acting on a driving wheel is Y_g= 0.7P= 46.4 kN towards the gauge side and Y_f=0.42P = 27.8 kN towards the field side. To check the ability to withstand axial forces, FEM simulations were performed applying a force that is ten times the maximum lateral force at the wheel rail contact, i.e. F_{proof}= 0.46 MN, uniformly distributed around the tyre. This kind of load application is clearly unrealistic as the in-service loads acting on wheels are located at the contact point between tyre and rail, as shown in Table 4 and Figure 58, but it can be easily applied to evaluate the upper limits of the lateral strength of the new kind of coupling[22]. It also allows the use of 2D elements with axisymmetric behaviour and a finer modelling of the coupling area, without large increase of the computational time. An elements size of 0.5 mm has been set for the coupling surfaces of the tyre and the wheel centre and non-linear frictional contacts with μ=0.3 have been used. An example of FEM results in the elastic-plastic domain is shown in Figure 66. It is worth to highlight that the wheel center steel has a lower yield strength if compared to the one used for tyres, and therefore plastic deformations primarily occur on it. According to Italian standard UNI 7175:1973 the steel for wheel centres is an Fe42, corresponding to a C22 of Table 15, while according to UNI 6102:1990 the steel grade for tyres is Fe740, corresponding to a C55 of Table 16. These materials have been modeled with a bilinear model considering constant isotropic hardening between the yield strength and the ultimate strength.

Although the approach originally proposed was intended to be applied only to disc braked wheels, the ALn668 is a tread braked vehicle and therefore, the original interference and tyre size were kept unchanged. Moreover, a check was performed also supposing that the interference is fully recovered during a drag braking (zero mating pressure). Safety coefficients F_{max}/Y_g or F_{max}/Y_f are described in Table 21, and in most cases the coupling is able to fully transmit the proof load, i.e. F_{max}= F_{proof}, also in the case of no pressure on the surface. In this case, in fact, the positive coupling is enough to prevent the fully lateral shift of the tyre. Only in one case (asymmetric dovetail with force to the field side) the coupling cannot completely withstand the load, nevertheless, the safety coefficient remains >> 1, considering 3 mm as the highest admissible lateral shift of the tyre.

[21] Nuova Comafer S.r.l. is a manufacturing company of railway components founded in 2004 and based in Naples. It is specialized for bogie manufacturing, wheelset maintenance and vehicles revamping.

[22] This load condition simulates a back-pressure test, which is used to assess the strength of shrink-fitted wheels on the axle, according to EN13260.

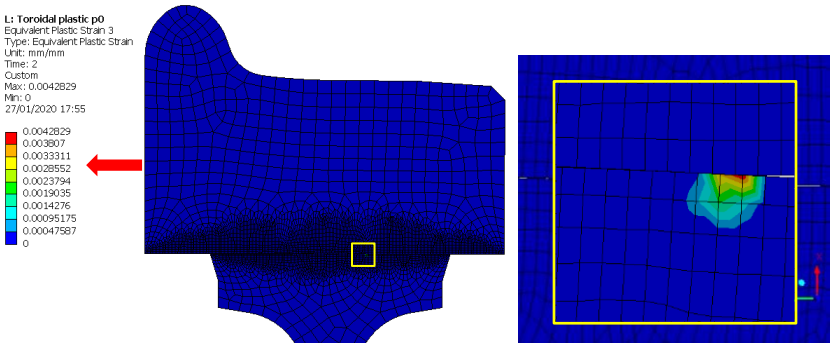

Figure 66. Equivalent plastic strain at the toroidal mating surface between tyre and wheel centre, due to the application of an axial equal to 0.46MN (red arrow) and without interference (zero mating pressure). The resulting lateral displacement between the tyre and the wheel centre is 2.8 mm.

Before mounting the wheel, a lateral tyre displacement of 0.4 mm has been estimated by FEM simulation, as shown in Figure 67 (left). The wheels have been then assembled with fully finished tyres, as shown in Figure 67 (right) and measured to verify the final dimensions of the wheelsets are within the limits provided in Table 17. All the values were correctly within tolerances, with a maximum lateral displacement of the wheel between 0.25÷0.5 mm, i.e. an increase of internal gauge a_1 in the range of 0.5÷1 mm (< 2 mm). Also, the other parameters were found in line with the standards, as axial run-out was 0.3 (<0.8) and radial run-out 0.2 mm (< 0.5). Therefore, no further machining has been needed.

Table 21. Safety coefficients (S.C.) obtained by the application of 0.46 MN axial load on the tyre.

Kind of coupling	Max slope [%]	S.C. with minimum interference [-]	S.C. and shift without interference [-]
Toroidal *Gauge side*	5.35	$F_{max}/Y_g > 10$	$F_{max}/Y_g >10$ (Δx=2.2 mm)
Toroidal *Field side*	5.35	$F_{max}/Y_f > 16.7$	$F_{max}/Y_f > 16.7$ (Δx =2.8 mm)
Asymmetric Dovetail *Gauge side*	5.71	$F_{max}/Y_g > 10$	$F_{max}/Y_g > 10$ (Δx =1.7 mm)
Asymmetric Dovetail *Field side*	1.6	$F_{max}/Y_f > 16.7$	$F_{max}/Y_f = 6.7$ (Δx =3.0 mm)

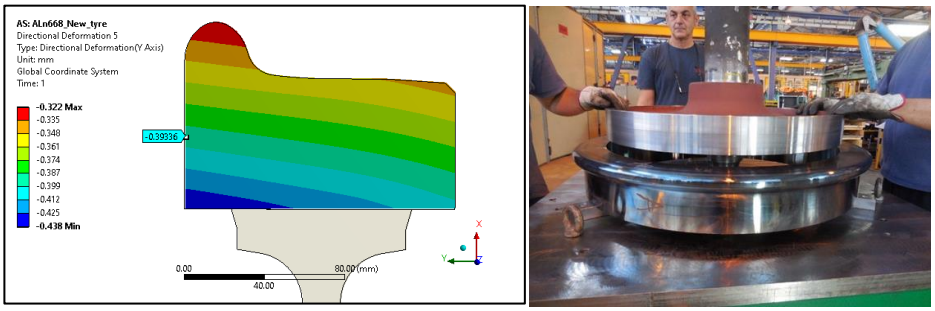

Figure 67. Left: Lowering a trailed wheelset on a hot tyre. Due to the absence of lateral abutment, the tyre is resting on the specifically designed mounting jig with calibrated shims. Right: FEM estimation of the lateral wheel displacement during fitting.

Finally, the new coupling has been tested on track. The DMU ALn668.1036 was equipped with the four wheelsets in the Iseo depot and then tested on 21 and 22 November 2018. Routes included both flat tracks run at the maximum vehicle speed (90 km/h) as well as steep sections (*i*=26‰). A thermal camera FLIR One Pro was used during the tests to observe the temperature reached by brake blocks and tyres. A particularly meaningful test was the application of 7 (seven) consecutive emergency stop brakings from the maximum line speed (70 km/h) while running downhill on an around *i*=22‰ line stretch. Figure 68 shows the mounting location of the thermal camera and an example of a thermal image recorded during the last emergency braking. Wheel centre and tyre always remained below 100°C, with similar temperatures. This shows that the safety margin against tyre dismounting was largely in excess on this application. It is worth to remind that tyre thickness and interference indicated in UIC codes apply for any type of rolling stock (locomotives, freight wagons, passenger cars, etc.), any speed and any axleload, confirming that old standards were largely oversized for a light DMU. No tyre spinning and no tyre axial displacement were observed, confirming that the concept was reliable enough even under non-realistic conditions.

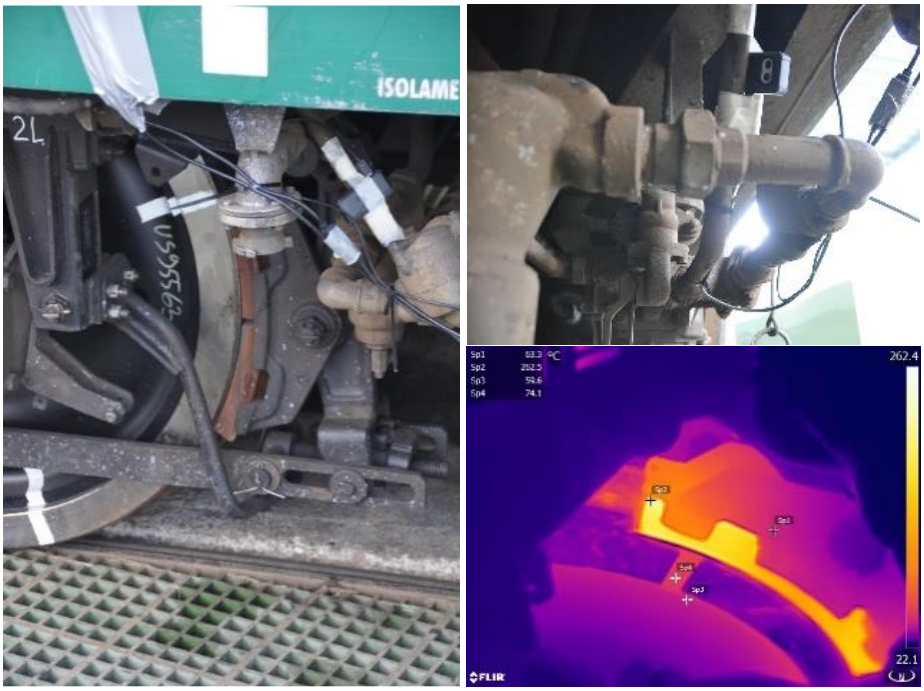

Figure 68. Thermal camera framing one wheel and a thermal image shot during the last of seven consecutive emergency braking.

With this experimentation is possible to conclude that the maintenance of tyred wheel can be strongly improved with simple modifications and with a proper use of tools like FE or CNC. Moreover, the obtained results let presume that the method can be applied also on other vehicles with higher speeds, with even better values if a modern wheel centre is used.

5. The Liberty Wheel

From the analysis and the experience described in the previous chapter, a new tyred wheel has been developed, which includes an optimize ADI casted wheel centre and a modified tyre locking in order to improve maintenance. The wheel, which has been designed, manufactured and tested, is called *Liberty Wheel*, mainly due to the freedom that the railway operator would have in terms of wheelset purchasing and maintenance adopting this solution. The development has been performed based on the ALn668 tyred wheel, but the concept can be obviously extended to other wheels, also monobloc wheels, with important advantages for regional trains, EMU or DMU, urban trains, metros and trams.

5.1. Maintenance optimization

Nowadays, almost all smaller railway enterprises sign full-service contract with vehicle suppliers or with external workshops to keep their wheelsets in good shape and to safely operate their fleets. Only larger railway enterprises still have their own second level workshops, where wheels are replaced, axles are machined and checked and so on. Moreover, the current maintenance is often contradictory respect the two basic concept that both the axle and the wheels are designed for infinite life, i.e. they do not fail if properly operated in service whatever long they serve under a vehicle. However, both wheels and rails suffer of many kinds of defects, which often are unavoidable problems and soon or last wheel tread will wear, and the nominal profile must be periodically restored machining it by means of underfloor lathe. This reprofiling process can be applied a limited number of times, until the wheel tread must be changed with a new one. If the wheel is monobloc the whole components must be scrapped. Replacing a monobloc wheels may also damage the wheel seats, i.e. those portions of the axles that interface (with interference) with the wheels. Consequently, axles need to be machined. After a few cycles, the axles need to be replaced, and this once again contradicts the assumption that axles should last forever.

In paragraph 4.2.2, has been demonstrated how maintenance of tyred wheels can be strongly improved with minor modifications and a proper design of the wheel centre. The easiness of replacing tyres has been therefore demonstrated and adopting this solution every railway operator can be free to perform the maintenance of the wheelset by their own, changing tyres by only a heater (for example an induction heater) to dismount the worn tyres and to mount the new ones. A dedicated workshop will be unnecessary and a warehouse with only fully finish tyres is needed. However, the dovetail solution has the disadvantage that wheelsets

can assembled only vertically with special shims calibrated in order to find the correct position between tyre and wheel centre. For this reason, the drawing was changed to restore the abutment, which can be used as mechanical reference for axial position. In this way a simple conical shape will be enough to prevent any possible lateral movement toward the field side and removing the retaining ring. In this case the value of conicity has been increased from 0.4 mm to 0.6 mm, i.e. 1:75 (1.33%) considering the 90 mm of length, as shown in Figure 76, and the abutment has been downsized respect to conventional tyre, in the way to reduce the circumferential stresses in this zone.

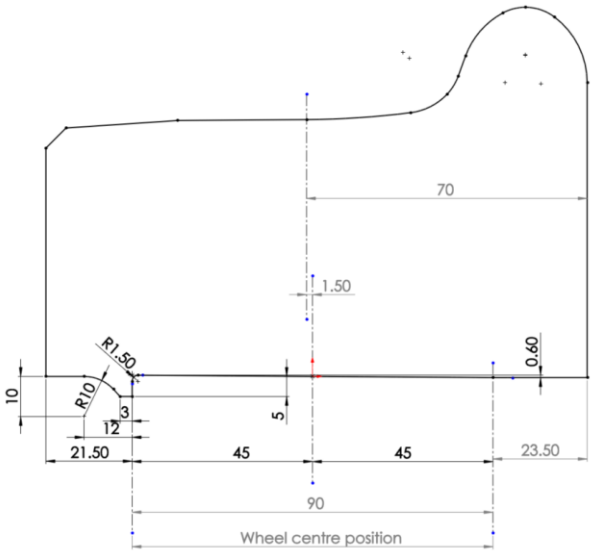

Figure 69. Drawing of the final solution adopted for the locking of the tyre on the Liberty Wheel.

To stress the concept of how this simple modification can impact the way of maintenance of railway vehicles, a simulation of fully automatized workshop has been performed using RobotStudio[23] software, in which two robots (one for each side of the vehicle) are able to remove the worn tyres and to mount the new ones automatically. Heating of new tyres can be performed with induction heaters, while heating of worn tyres to be removed can be made by LASER heating directly with underfloor automatic trolleys. The warehouse can be automatized too, with activation due to the signals arriving from a Wayside Profile Monitoring System (WPMS). The application of this kind of automation will be optimal for inboard bearings bogies.

[23] RobotStudio is a software provided by ABB Robotics, which let to perform offline programming of robots. https://new.abb.com/products/robotics/robotstudio (accessed on 17/10/2019)

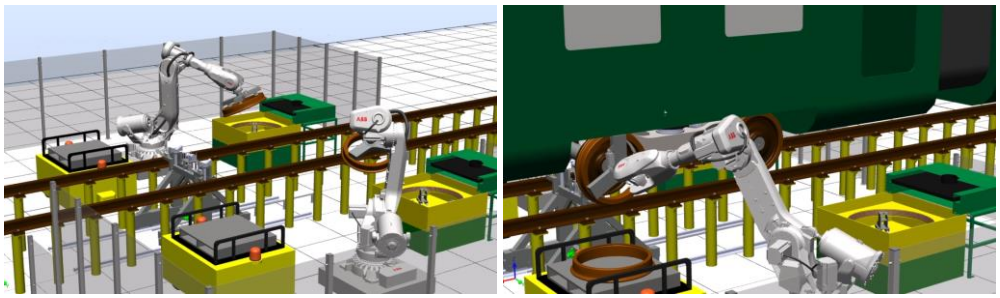

Figure 70. Screenshots of the video[24] that shows the modelling of a fully automatized workshop. On the left frame the two robots are picking the tyres from the AGV (Automated Guided Vehicles) and placing on the induction heaters. On the right frame the robot has just removed the worn tyre and it is now mounting the new one.

The internal diameter of the tyre equal to D_{fit}= 792 mm with tolerance based on t7/S8 coupling, gives a range of interference of 0.94÷1.145 mm which is in line with the empirical equation depending on the diameter. Even if the value of conicity has been increased respect to the previous experimentation, the maximum total interference of i_{max}= 2.345 mm to be recovered during tyre mounting is still compatible with the tyre heating temperature of 300°C, according to equation (11), in which T_f is the final heating temperature, T_i is ambient temperature and α is the steel coefficient of linear thermal expansion, i.e $1.2x10^{-5}$ $°C^{-1}$. Considering a T_i = 40°C, a final temperature of 287 °C is needed and a sufficient mounting play is guaranteed when the 300°C are reached.

(11) $$T_f = T_i + \frac{i_{max}}{\alpha D_{fit}}$$

5.2. Casted ADI wheel centre

The second innovation of the Liberty Wheel is an optimized casted wheel centre based on the philosophy of two inclined rows of spokes, described in paragraph 4.2.1. That kind of geometry has been therefore adapted and properly modified to be a replacement of the rolled and forged steel wheel centre of ALn668. The final shape is shown in Figure 71 compared with the current one and in section view in Figure 72. The new wheel centre lets a mass reduction of 50 kg.

[24] Full video available at https://www.youtube.com/watch?v=xS-rDXDP3gE (accessed on 19/10/2019.

Figure 71. Comparison of the current wheel centre (left) with casted new one (right). A mass saving of about 50 kg is achievable with a final mass of the wheel centre equal to 130 kg.

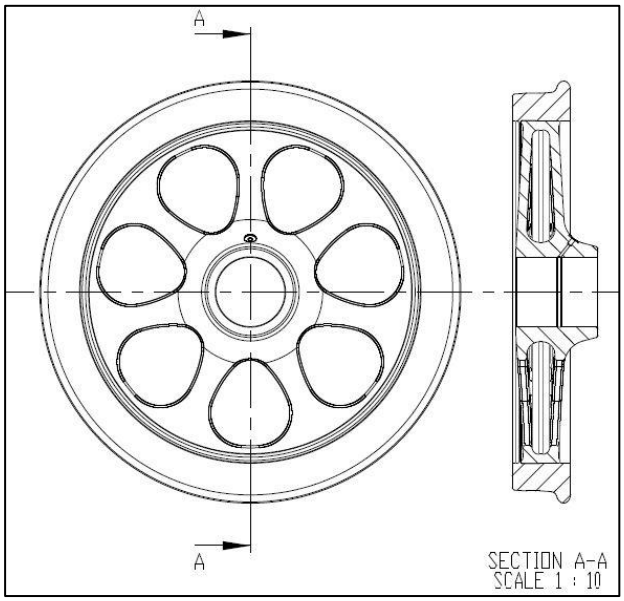

Figure 72. New tyred wheel with ADI casted wheel centre and steel tyre designed as replacement the ALn668 DMU original wheel. Even if the spokes are symmetric, they are shifted respect to the centre of the hub.

To remove the critical points found in the previous analysis, the opening at the top of the spokes has been removed, with advantages of lower stress concentrations and better casting quality. In this case, Fonderia Baraldi[25] took care of the computer aided design of the mould, verifying that a good quality casting can be reached without internal porosity. The results of simulations are shown in Figure 73, and no internal defects has been found after the mould

[25] Fonderia Baraldi Sivano S.r.L. is a foundry specialized in small to medium size cast iron castings. The factory is based in Montagnana near the city of Padua.

optimization with two filling points (located at the external diameter) and one feeder point at the hub. Chillers in some specific position were also considered.

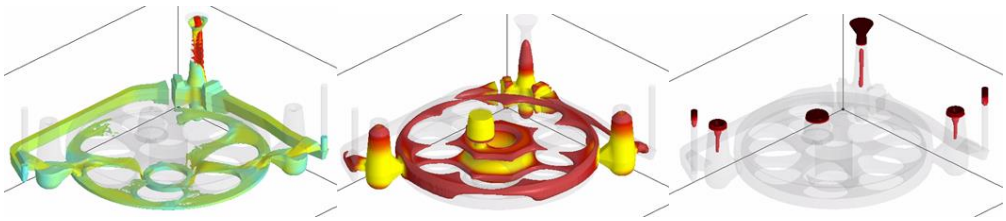

Figure 73. Results of simulations performed to verify the casting quality in terms of: velocity of filling (left), solidification time (middle) and shrinkage (right).

Static and high-cycle fatigue validation of the geometry has been performed also in this case, starting from the fitting loads due to the mechanical interference with the tyre and the load cases described in the standard EN13979. The von Mises stresses due to tyre fitting are lower than the minimum yield strength, as shown in Figure 74 (left), while Figure 74 (right) shows the detail of a spoke, in which the vectors representing the principal stresses are plotted for each node and it is possible to see that the minimum principal stress (compression) is dominant over the other components.

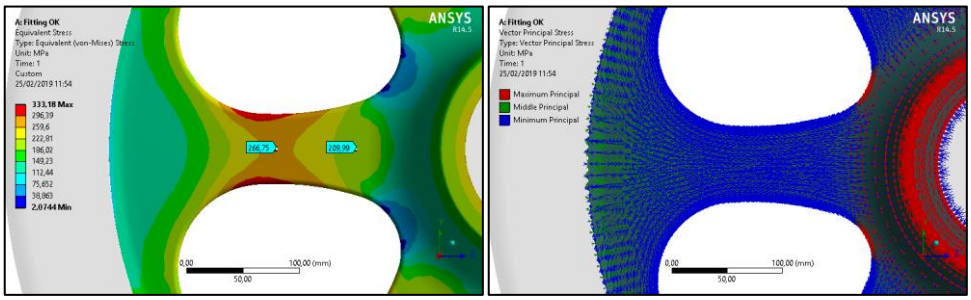

Figure 74. Left: Equivalent Von Mises stresses due to the tyre fitting process, to be compared with the yield limit of the material. Right: Plot of the vector principal stress of each node. Except for the fitting zones, minimum principal stress is dominant on the other stress components.

The curved track load case, superimposed to the fitting load case, is the most critical one due to the greater lateral forces towards the inner part of the wheel. However, the initial compression stress is not totally recovered on the external spoke of the wheel centre, as shown in Figure 75 (left).

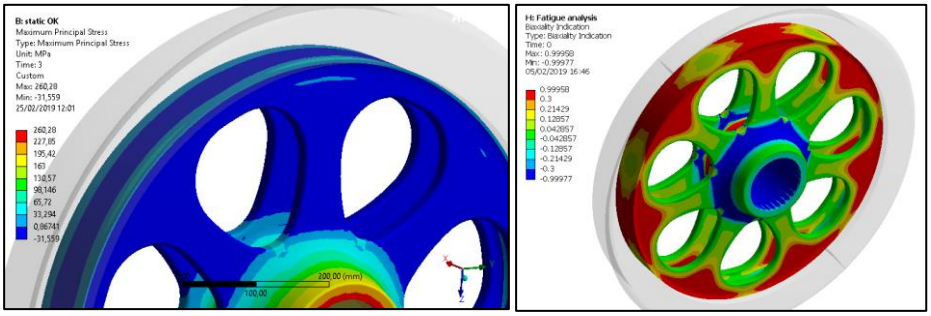

Figure 75. Left: Maximum principal stresses after the application of external loads derived from case 2. The initial compression state is not fully recovered. Right: Biaxiality index for the ADI wheel centre with fitting loads and external loads (case 2). Values near zero corresponds to uniaxial stresses.

As described in paragraph 4.2.1, fatigue limits can be very low if a poor casting surface is considered. However, the effect of mean stress on fatigue life of mechanical components is usually important for notched parts, where high stress concentrations may occur [124]. These may be the reason why the assessment of monobloc wheels is usually done comparing the alternating stress with the alternating fatigue limit independently from the mean stress value (see Figure 9). Even if this method could be questionable, it is used since many years and proved to be reliable for the steel grades ER7 or ER8 commonly used for monobloc wheels. In this specific case a large increase of fatigue life can be instead achieved considering that any cyclic stress such $-R_{p0,2} \leq \sigma(t) \leq S_e$ leads to no crack propagation. The Haigh diagram derived from this hypothesis is shown in Figure 76.

Moreover, as for the new wheel centre the main stress state is the radial compression of the spokes, it is reasonable to apply the MPSM even if the wheel is not axisymmetric. Large part of the spoke is already subjected to uniaxial stress and the application of the criterion is straightforward. Each load case is applied at 6° interval along the circumference of the wheel for both new tyre and worn tyre. To investigate if the external forces can recover the initial compression of the spokes, the worn case is evaluated considering the minimum tyre fitting interference. In the resulting Haigh diagram, shown in Figure 77, the couple of mean and alternating stress are plotted. As the method is conceived to find the principal stresses independently from their directions, projection 33 represents the state stress for all those nodes that are always in compression, i.e. $\sigma_m + \sigma_a \leq 0$, while projection 11 is the state stress for the nodes that show a tensile maximum principal stress, i.e. $\sigma_m + \sigma_a > 0$. It appears that all stress pairs fall into the "safe region" with reasonably high safety margins, paving the way to further lightening of the wheel centre or, similarly, to the possibility of bearing higher axle loads.

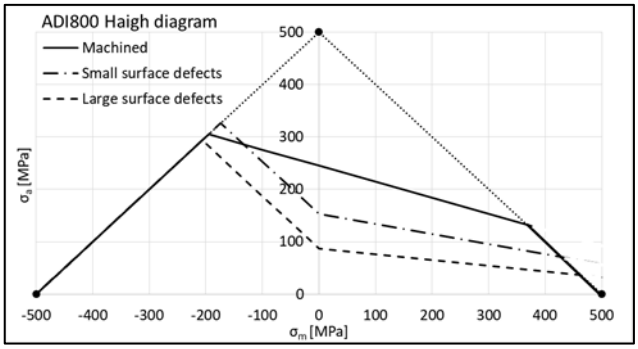

Figure 76. Haigh diagrams for ADI800-10 used for the casted wheel centre.

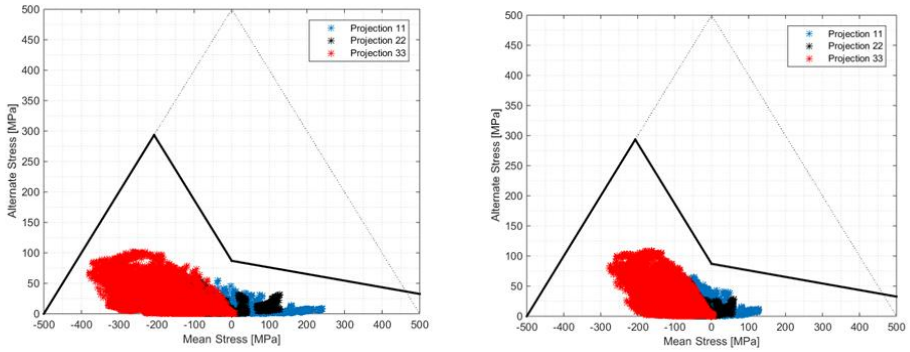

Figure 77. Haigh diagrams resulting from the fatigue analysis in new tyre condition (left) and in worn tyre condition (right).

Tyre stress due to fitting, i.e. circumferential stresses, are estimated in 195 MPa in new condition and 220 MPa in worn condition with 30 mm of residual tyre thickness. These values are compatible with the value usually found in conventional tyres, as previously shown in Figure 48 (right). In fact, the wheel centre radial stiffness is quite low, i.e. 54 MPa/mm considering a medium value between the zones over the spokes (stiffer) and the zones between the spokes. Due to the good elasticity of the wheel centre the difference of the mating pressure between the new condition with maximum interference and the worn condition with minimum interreference is only 9 MPa, passing from 36 MPa to 27 MPa. Moreover, maximum pressure is located at the border of the mating surface, helping to reduce contamination and therefore the possibility of fretting. The deformation during fitting is not perfectly radial as the maximum lateral displacement of the tyre is estimated in 0.3 mm due to the not fully symmetry of the spokes respect to the hub center, as shown in the section of Figure 72.

Also in this case the coupling strength has been simulated as previously described in paragraph 4.2.2, applying a uniform lateral load along the tyre and considering both cases of maximum mating pressure and zero mating pressure. Due to the non-axisymmetric shape of the wheel centre, a cyclic symmetry has been selected to reduce the computational time and to allow a finer mesh in the contact zone. As shown in Figure 78 (left), in the first case the coupling can withstand the full applied lateral force, i.e. $F_{max}= F_{proof}= 0.46$ MN, resulting in a safety coefficient $F_{max}/Y_f > 16.7$ towards the field side, while it decreases to $F_{max}/Y_f = 4$ in the

extreme case, shown in Figure 78 (right), with p=0. In this case a maximum lateral displacement of 3 mm between the tyre and the wheel centre has been considered, resulting in an F_{max}= 0.11 MN.

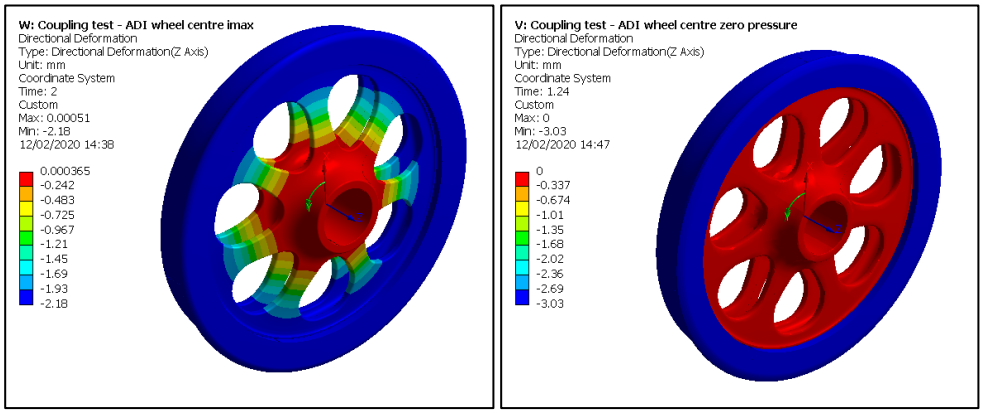

Figure 78. Left: verification of the lateral strength of the conical mating with nominal pressure conditions, which is able to withstand the full applied force of 0.46 MN. Right: verification of the lateral strength of the conical mating with zero pressure conditions, at the simulation time which gives a lateral displacement of 3 mm. In these conditions the lateral resistance of the coupling is 0.11 MN.

5.3. Liberty Wheel manufacturing

After the design stage, the wheel centres were manufactured in a single batch of twelve units, with the following results: one was defective (sand dragging), one was used untreated for acoustical tests, one was cut to get samples for destructive tests and nine were austempered and machined. The sequence of the manufacturing process is shown in Figure 79. The upper and the lower part of the sand mould were created after the production of a split wooden model, and then the final "negative" shape is obtained inserting one chromite core for the hub hole and a polymerized sand core for the internal cavity between the spokes. Chillers are properly inserted in the mould in order to drive the solidification. After cooling, castings were removed from the mould and sand blasted. All wheels were visually checked after sand blasting. One wheel in the batch was radiographed according to ASME B16.34-2017 (RT 100% full coverage). The casting resulted conforming to acceptance criteria ASTM E446 level 3. One hundred percent of the wheels were UT tested according to EN 12680-3 and resulted conforming to acceptance criteria CL.3. The austempering has been performed by Zanardi Fonderie, together with the destructive tests of samples in order to assess the material according to the standards.

Tensile stresses, elongation, and hardness were tested on samples according to EN ISO 6892-1:2009 (tensile) and EN ISO 6506-1:2014 (hardness). In Table 22 all results of mechanical properties are shown and compared with the minimum values according to [68]. Only the values for specimens casted apart (*Lynchburg* samples) are normative for the standard, while the other derived from the real casting are only informative. However, all values were largely in excess, with a yield stress at least 20% higher than the value used during the design and elongations are particularly high compared to spheroidal cast iron with similar tensile strength.

Machining of the wheel centres has been performed by Nuova Comafer after the heat treatment. As shown in Figure 80 only the hub and the external diameter, i.e. the mating surfaces with the axle and the tyre, were machined with the correct interferences. A conical external surface has been created to fit the tyre according to the drawing in Figure 69. Machining of tyre is shown in Figure 82. The wheel centres were then fitted on an axle by shrink fitting, measuring the radial, axial run-out and unbalancing. All these parameters were found within the limits, without additional machining. Figure 81 shows the assembled wheel centres, ready for the tyre mounting.

Figure 79. Sequence of wheel centre manufacturing stages. From top-left angle: 1) machining of the wooden model 2) painted model with chillers 3) the "negative" sand mould 4) the same with inserted cores 5) molten cast-iron inside the mould 6) final casting after sanding 7) cut wheel centre to check internal integrity of the spokes 8) visual checking of the casted surface 9) cut austempered wheel centre to obtain specimens for destructive tests.

Table 22. Mechanical properties of the samples derived from the cutted wheel centre. Minimum values according to [68] are also shown.

Part	Reference thickness [mm]	R_m [MPa]	Min value	$R_{p0.2}$ [MPa]	Min value	A_5 [%]	Min value	HBW [-]	Min value
Specimen casted apart	< 30	997	800	674	500	12.7	10.0	292	250-310
Hub	30÷60	821	740	598		5.8	5.0	292	
Spoke	< 30	951	790	654		10.8	8.0	298	
Rim		918		617		11.0		285	
Hub face	-	-	-	-	-	-	-	296	

Figure 80. Machining the wheel centre performed by Nuova Comafer workshop in Piscinola (Naples) on a horizontal CNC lathe.

Figure 81. Left: wheel centres machined and mounted on an axle. Right: detail of the indication of the axial (0.04 mm) and radial (0.1 mm) run outs.

The fully machined tyre were then heated at 300°C and mounted vertically, as shown in Figure 83. After the complete cooling the final wheelset dimensions has been measured, showing all the quotes within the tolerances, with a lateral displacement of the tyre of about 0.4 mm. Two wheelsets have been assembled and to verify the wheelset integrity a back-pressure tests has been performed according to EN13260, by which the wheelset shall withstand a lateral force F for thirty second without showing any displacement between the components. The lateral force, measured in MN, is considered empirically equal to the 4‰ of hub diameter. In this case, d= 160 mm and F= 0.64 MN, which has been applied with success to both wheelsets.

Figure 82. Machining of tyres with conical mating performed by Nuova Comafer workshop in Piscinola (Naples) on a horizontal CNC lathe.

Figure 83. Left: Hot tyre resting horizontally during wheelset final assembly. Right: First wheelset assembled with Liberty Wheels.

5.4. Design assessment and testing

As described in the previous paragraph, two full wheelsets have been assembled with the Liberty Wheels and mounted on a bogie of ALn668 from TRENORD. The scope is to perform other on-track tests as described in paragraph 4.2.2. Pass-by noise measurement were also planned during these tests, to compare the noise emission of two different bogies, one equipped with conventional wheels and on equipped with the Liberty Wheels. Parallel to this activity one of the austempered wheel centre has been instrumented with strain gauges with the aim to perform full-scale fatigue tests on a complete Liberty Wheel. Other laboratory tests have been performed to compare the vibrational behaviour of free wheel centres.

5.4.1. Laboratory tests

To understand the dynamic behavior of the new wheel centre respect to the axisymmetric one, some laboratory tests have been performed with accelerometers and instrumented hammer. Firstly, the natural frequencies of both wheel centres, shown in Figure 84, were measured and compared with the results of a modal FEM analysis. In Figure 85 the results of the comparison are reported, showing a good agreement between the model and the real component.

Figure 84. The original wheel centre (left) and the casted wheel centre (right) of ALn668 during the frequency response test at the University of Florence laboratories.

	Numerical		Experimental	
N°	f [Hz]	Description	Axial measurment	Radial measurment
1	446	Axial	460	
2	520	Bending 4 nodes	537	
3	520	As 2 orthogonal		
4	970	Hub/Bending		
5	970	As 4 orthogonal	1007	
6	1041	Bending 6 nodes	1064	
7	1041	As 6 orthogonal		
8	1623	Mixed (hub resting)	1672	
9	1623	As 8 orthogonal		
10	1683	Radial - Polygonal 4 lobes		1664

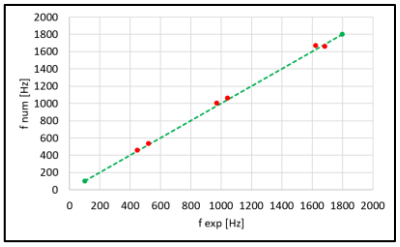

Figure 85. Left: List of the free-free natural frequencies of the casted wheel centre estimated by numerical and experimental analysis. Right: comparison of the two kind of results as validation of the FEM model.

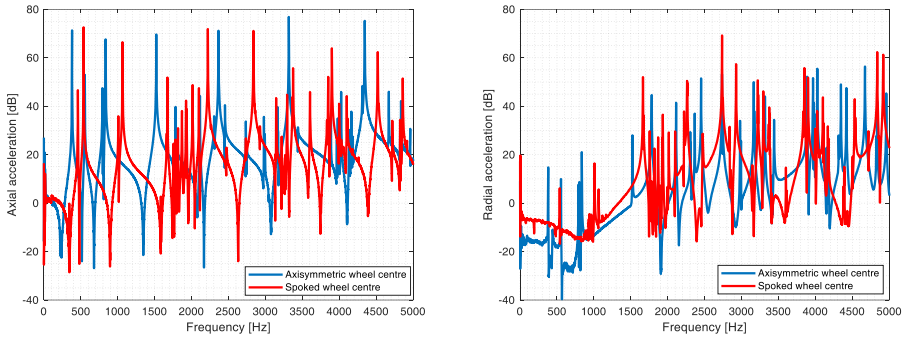

Figure 86. Frequency response of the cast iron (spoked wheel centre) and steel (axisymmetric wheel centre) wheel centres in axial direction (left) and radial direction (right).

The first mode (axial mode) of the casted wheel centre is at 460 Hz, higher than the first mode of the steel wheel centre, which is a bending mode with four nodes at 370 Hz, while its first axial mode appear at 540 Hz. These frequencies were used to evaluate the damping properties of the two materials, using the Hilbert Transform, which return a vector with a real part (the original signal) and an imaginary part (the signal shifted ¼ of wavelength). The original signal is therefore filtered to obtain only the interested component f_0, and then computed with the Hilbert Transform. The magnitude of the modified signal gives the decay rate of the signal in that frequency over the time, and damping can be computed considering the time needed for a decay of 8.7 dB. From this value, named *time constant* τ, the damping ratio can be obtained according to equation (12).

$$\zeta = \frac{1}{2\pi f_0 \tau} \tag{12}$$

In Figure 87 (left) the signal decay for the axial mode of both wheel centres is plotted against the time with nearly the same results. In fact, damping ratio can be estimated equal to $6.5\text{x}10^{-4}$ for cast iron and $5.0\text{x}10^{-4}$ for steel. All the other modes have a lower damping, in the range of $1\div2\text{x}10^{-4}$, excepted for the hub bending modes which is $7.95\text{x}10^{-4}$ for cast iron and $8.2\text{x}10^{-4}$ for steel.

Therefore, the common experience of the greater damping properties of cast iron respect to steel seems to be not respected. However, these results can be applied to perform a proper FEM analysis including damping properties and using these results to numerically compute the sound power emission according to ISO 3744:2010. A comparison between the estimated FEM frequency response and the measured one for cast iron wheel centre is shown in Figure 87 (right). As shown in Figure 88, the FEM frequency response has been evaluated using the *mode superposition method* and applying an harmonic force $\{F\}=\{F_x;F_y;F_z\}=\{1;1;1\}$ on a node of the external surface of the free wheel centre, while the modal damping ratio of the first nine modes has been inserted with the *MDAMP* command.

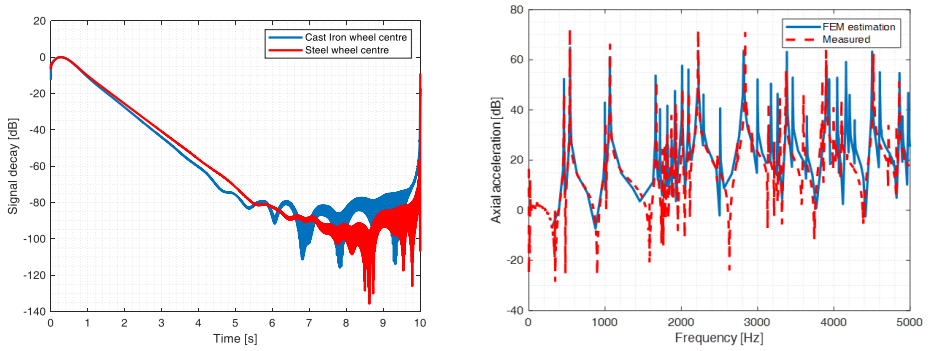

Figure 87. Left: Decay rate computed with Hilbert Transform for the frequency of axial mode of both wheel centres. Right: comparison between the numerical (including damping) and experimental frequency response of cast iron wheel centre.

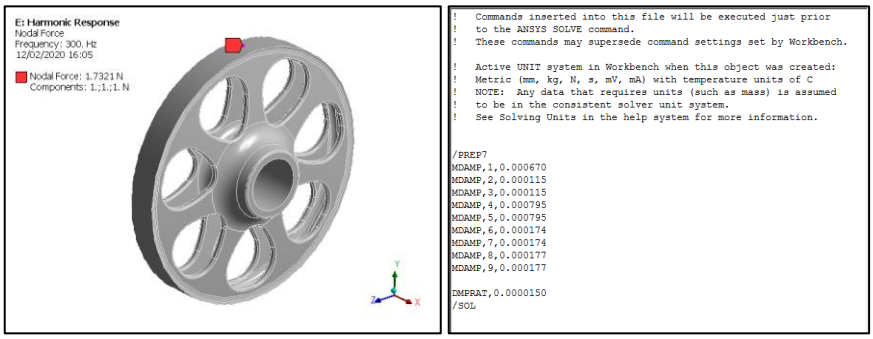

Figure 88. FEM model set-up for the FRF estimation of the spoked wheel centre. The input (nodal force application) and the output (acceleration response measurement) are both positioned in a node of the external surface of the free wheel centre (left). Damping for each mode has been added to a constant damping ratio (*DMPRAT* command) with the *MDAMP* command (right).

5.4.2. Structural verification

A full-scale test was planned at the fatigue test bench available at railway laboratories in Florence, Italy. The test bench owned by RFI[26]. and managed by Italcertifer[27], fulfil the requirements described in EN13262 for wheels qualification. The UIC code [19] describes in detail the procedure to perform the tests and process the results in order to find the design fatigue limits. Allowable stresses for ER7 steel grade are given for machined and un-machined wheel webs, and it appears clear that several full-scale fatigue tests and the long experience of railway operators were needed to statistically determine the S-N curve according to the

[26] RFI S.p.A. (Rete Ferroviaria Italiana) is the main infrastructure manager of railway network in Italy.

[27] Italcertifer S.p.A. is the main Notified Body for certification of railway systems in Italy. Their facilities include test benches for homologation of railway vehicles.

Bastenaire method [125]. With this bench, shown in Figure 89, it is possible to analyse the fatigue behaviour also in non-purely alternating conditions, i.e. R≠ -1, which reflects the in-service condition where the lateral load towards the gauge side is higher than the load towards the field side.

Axial loads induce radial stresses in the wheel web and therefore the fatigue limit obtained is related to uniaxial stress state. This is the reason why the whole process, given by the combination of MPSM method for design and the fatigue test for the assessment, is defined reliable only for axisymmetric wheels, as in these cases the radial stresses due to in-service external loads is higher than circumferential stresses. Even if the new wheel centre is not axisymmetric, the main stress in the spokes is almost radial (uniaxial) as the preload given by tyre mounting generates compression in the spokes that is not fully recovered by external loads.

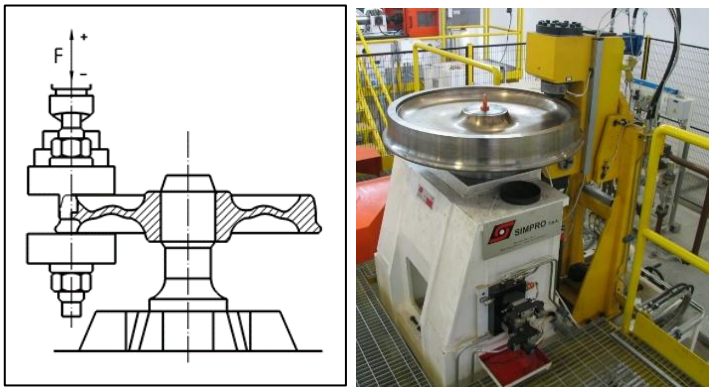

Figure 89. Left: Schematic representation of the fatigue test bench according to. Right: Photo of the bench in Florence with an axisymmetric wheel mounted.

However, the main difference with a monobloc wheel is that the tyred wheel has non-negligible mean stresses. Therefore, it was decided to measure this kind of stresses during the fitting of the tyre, in order to validate the FEM model and to understand the initial stress. Strain gauges were applied on a wheel centre on both the internal side and the external side. Three couples of spokes has been therefore instrumented for a total of sixteen strain gauges applied, which was the maximum number of channels of the acquisition hardware. Wheel centre has been firstly press-fitted on the "dummy axle" needed to mount the wheel on the test bench, then the tyre has been heated and fitted on the wheel centre. In Figure 90 the wheel centre with six instrumented spokes is shown, before (up-left) and during the tyre fitting (up-right).

It is worth to highlight how in the first minutes of cooling of the tyre, the wheel centre is not in contact yet and therefore it deforms radially toward the external. This is confirmed by the fact that the strain gauges measure a positive deformation that can be translated in about 125 MPa for the middle strain gauge after 20 minutes. Then the tyre starts compress the wheel centre and the strain gauges measure negative deformations which reach a stable value after about 3 hours. Figure 91 (left) shows the time history during cooling. The final values confirm that all the spokes are in compression with good agreement with the estimated FEM values, which are within the 10% of the measured values. Stresses on the internal spoke are quite higher than the external one, confirming that the deformation of the wheel centre is not perfectly symmetric.

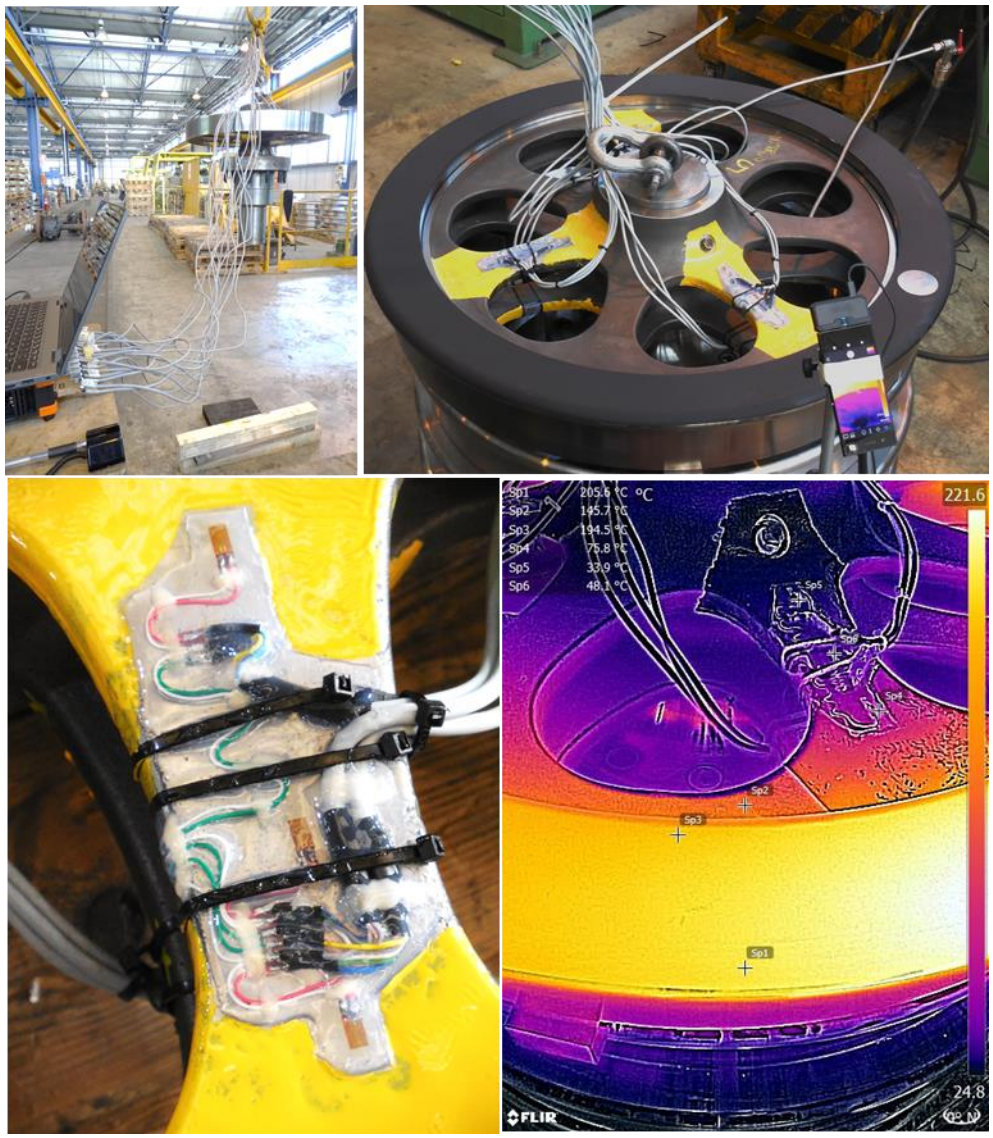

Figure 90. Up-left: instrumented wheel centre (connected to the acquisition device) mounted on the "dummy axle" and ready to be fitted. Up-right: instrumented wheel centre during tyre fitting. A thermal camera is used to control the wheel centre temperature. Below-left: detail of one instrumented spoke with three strain gauges. Below-right: Temperature 25 minutes after fitting, showing the maximum temperature reached on the wheel centre.

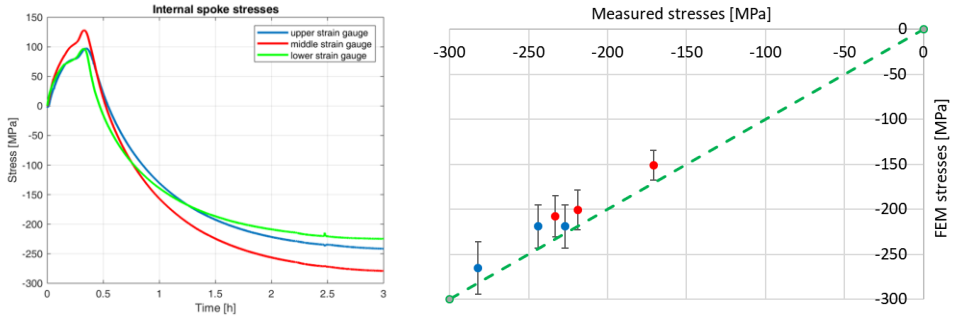

Figure 91. Left: time history of the stresses derived from the strain gauges applied on one of the internal spokes. Right: Comparison between the measured and FEM estimated stresses, within an error of 10%. Blue dots are related to the internal side and red dots are related to the external side.

The tyred wheel is then mounted on the test bench. The fatigue test planning has been done considering that only one sample was available and the fatigue limit for the specific application in nearly unknown. An extensive test campaign, such as a stair-case method, was therefore not possible and a constant amplitude method, such the one described in EN13262, cannot be applied. Therefore, to find a fatigue limit in the particular condition of the preloaded wheel centre, and therefore to verify the hypotheses made for the definition of the Haigh diagram of Figure 76, an accelerated test method, called Locati method [126], was used. In this method the load is increased by a certain number of steps T, in order to induce an increasing stress and each load step i is maintained for a number of cyle n_i. As the method is based on damage accumulation, it is necessary to define j S-N curves, with different endurance limits. The curves were created by defining three possible limits at 10^6 cycles, and then calculating the coefficients of the Basquin equation $S = AN^b$. Thus, for each load step i is possible to calculate the number of cycles until failure N_{ij} and then cumulate the damage D_j according to equation (13).

$$D_j = \sum_{i=1}^{T} \frac{n_i}{N_{ij}} \tag{13}$$

Nine steps were defined, starting from a lower bound of 100 MPa and an upper bound of 300 MPa. The forces needed to induce this kind of stress in the wheel centre were preliminary found by FEM simulations. Figure 92 shows an example of the effect of an alternating force of ±120 kN in terms of alternating stress (the effect of the mean stress is discarded by the subtraction of the two opposite results). This force value is enough to generate a stress state higher than the maximum supposed. The three values D_I, D_{II}, D_{III} are finally plotted against the supposed endurance limits S_I, S_{II}, S_{III}, in order to obtain an interpolated curve by which is possible to define the exact fatigue limit when the curve reach D= 1.

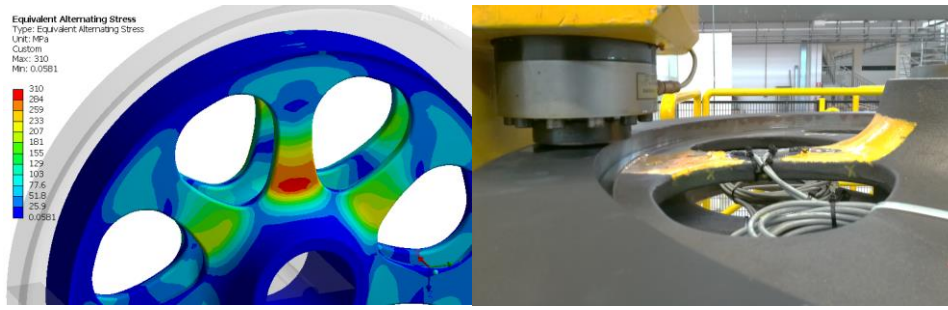

Figure 92. Left: Alternating stress of the simulated fatigue tests obtained with an axial force of ±120 kN. The maximum stress of 310 MPa is reached at the base of internal spoke. Right: Wheel mounted on the bench.

The actual relationship between the force applied and the measured stress has been found before starting the tests. In Figure 93 the relations for the most stressed points, i.e. the bases of the internal spoke (left) and the external spoke (right), are shown. These values are then used to translate the force recorded by the bench in stresses, which are shown in Figure 94, considering nine days, i.e. one day for each step, with 50000 cycles each.

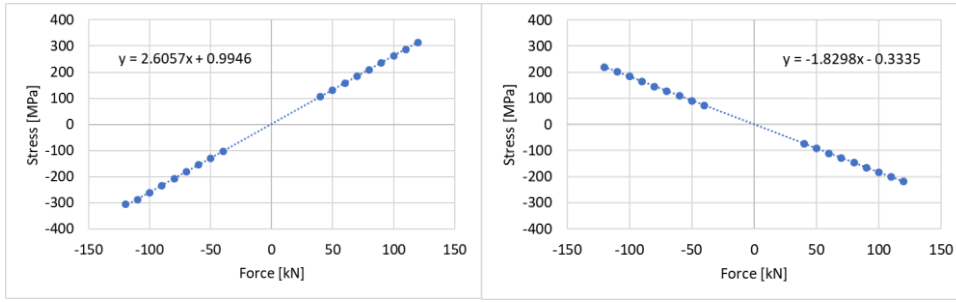

Figure 93. Relation between the applied axial force of the bench and the resulting stresses measured by strain gauges at the base of internal (left) and external (right) spokes.

At the end of these steps non cracks were found, and the test continued at the maximum stress level up to three million cycles. No failures were found even at this stage, and the maximum dynamic force of the bench, i.e. ±150 kN corresponding to a maximum stress of ±385 MPa, has been then applied. However, after only 31386 cycles the test has been stopped due to a relevant increase of the axial displacement. The full time-history of the applied stress and the result rainflow analysis are shown in Figure 95. Penetrant Testing has been therefore performed on the spokes without success because the crack was found on the "dummy axle" on which the wheel is fitted and held to the bench. Figure 97 shows the position of this failure. Even if the stress in that position is unknown, it worth to highlight that the axle is made of 31NiCrMo12 with high mechanical properties.

Even if the total damage can be calculated, as the failure did not appear the application of a method based on damage accumulation is not significant for the estimation of the fatigue limit. However, as shown in Figure 96, the maximum alternating stresses applied during the tests are higher than the fatigue limit used for the verification of the wheel centre. Considering the Haigh diagram developed in Figure 76 with an endurance limit for R= -1 equal to 87 MPa,

the total damage at the end of the test would be 2.5, which is clearly incompatible with the observation that no cracks occur. Even if a clear fatigue limit cannot be stated for the present application, the fatigue test has demonstrated the high safety margin that has been considered during the design phase and at the same time the impressive mechanical properties of the material. Therefore, with a proper campaign of full-scale fatigue tests, considering also the worn tyre condition, a further optimization of the shape of the wheel centre is possible.

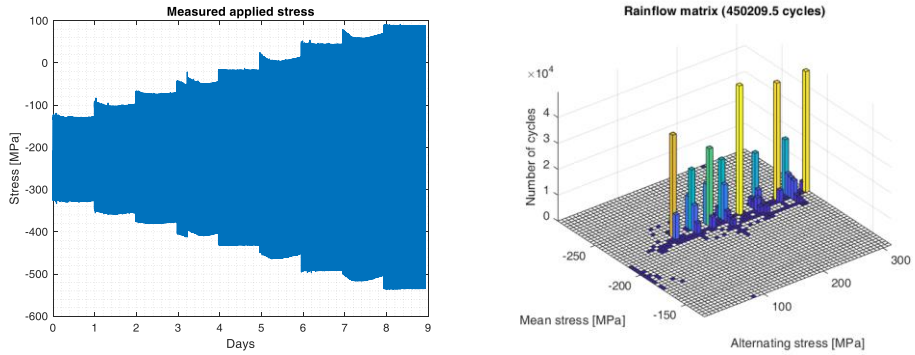

Figure 94. Increasing stress in the first nine steps of fatigue test. Left: time-history of the applied stress at position at the base of the internal spoke. Right: rainflow of the applied stresses.

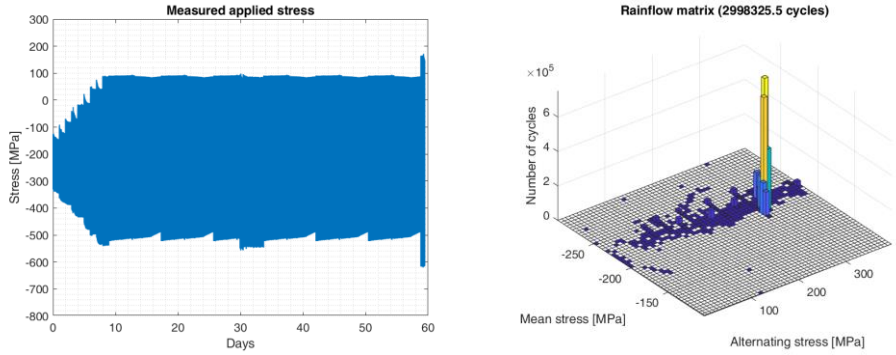

Figure 95. Full fatigue test. Left: time-history of the applied stress at position at the base of the internal spoke. Right: rainflow of the applied stresses.

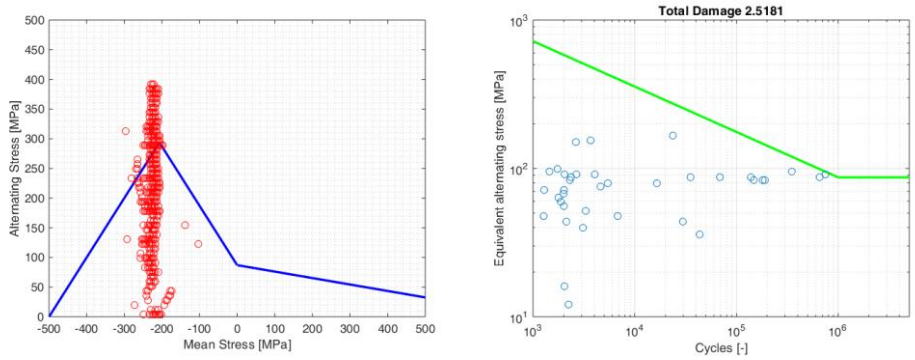

Figure 96. Left: Haigh diagram superposed to the couples of mean and alternating stresses applied during the fatigue test. Right: Equivalent alternating stress, i.e. alternating stress for zero mean stress, plotted against the correspondent applied cycles. Wohler curve is used to calculate the final damage. Both figures are evaluated for the strain gauge applied at the base of the internal spoke.

Figure 97. Application of PT inspection method on the "dummy axle" (left). The crack on the “dummy axle” highlighted by the red liquid and opened by the vertical force applied by the bench.

5.4.3. Impact on noise emission

It is known that the rolling noise emitted by a railway vehicle is due to both track and wheel in different way depending on the speed and the frequency range. Roughness of wheel and rail is the input of vibrations and therefore noise emission, while the wheel-rail contact patch introduces further damping, called *rolling damping*, which is much greater than the modal damping of the free wheel, introduced in paragraph 5.4.1 [127]. Usually the noise emitted by the track is related to low frequencies, while the contribution of the wheel is usually relevant starting from 1 and 2 kHz. Figure 98 shows the predicted rolling noise for a vehicle running at 100 km/h, considering the contribution of the different noise sources. Sleepers could be important below 250 Hz, but at these frequencies the level reduction due to A-weighting filter is quite high, while noise emitted by rail is dominant between 500 and 2000 Hz. Then the wheel noise has a relevant contribution. However, no relevant literature can be found about the noise emission of tyred wheels and spoked wheel centres.

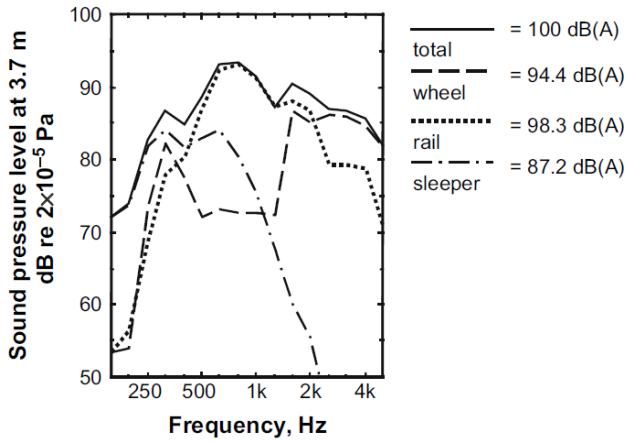

Figure 98. Predicted rolling noise for a freight vehicle at 100 km/h, showing the contribution of the different sources [127].

After the assembly of the first prototype wheelset with Liberty Wheels described in paragraph 5.3, another wheelset has been assembled in order to equip a complete bogie of the DMU. On-track tests were performed in May 2019, making sure that the two bogies, one equipped with Liberty Wheels and the other one with the original solution have the same tread roughness to get valid noise data during the pass-by measurements. Figure 99 shows the complete set of wheelsets to be mounted on the DMU. Ancillary measurements, i.e. rail and wheel roughness and track decay rate, were also performed.

Figure 99. Left: The complete set of wheelsets for the tests. Front with Liberty Wheels, rear with conventional wheels. Right: One wheelset with Liberty Wheels mounted on a bogie.

The tests have been performed in the closed line between Bornato-Calino and Rovato Borgo, which are visible in Figure 100, according to the requirements of ISO 3095:2013 [129] with additional measuring points at the axlebox level close to the vehicle. The measurement configuration is described in Figure 101 and Figure 102. The sound pressure recorded by the microphones has been processed according to a third-octave analysis to evaluate the sound pressure level in the thirty-one frequency bands between 20÷20000 Hz. Four runs (two southbound and two northbound) were performed with a target speed of 80 km/h. Actual speed V has been estimated by the peaks of the microphones corresponding to the passage of the two

bogies, and the A-weighted sound pressure levels are corrected to get the value for V_0= 80 km/h according to equation (14). In Figure 103 the sound pressure level is plotted as function of the frequencies, while the total values are summarized in Table 23.

(14) $$L_{p0} = L_p - 30\log_{10}\left(\frac{V}{V_0}\right)$$

Figure 100. Fist part of the old railway line Iseo-Cremona closed in 1956. Today the section between Bornato-Calino and Iseo is integrated in Brescia-Iseo-Edolo line[28].

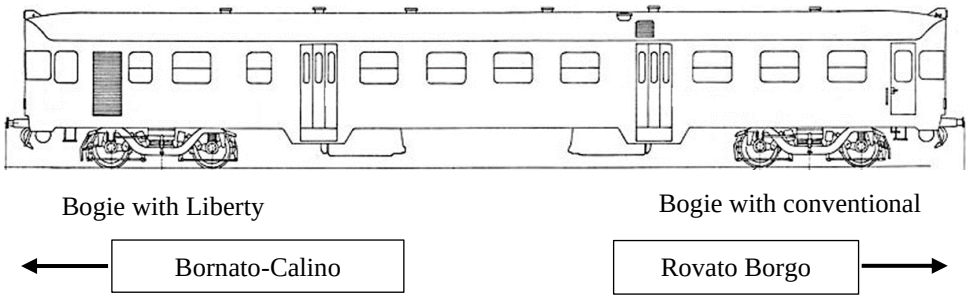

Figure 101. Vehicle configuration during the tests with indication of the bogie position respect to the running direction.

[28] Map by Arbalete - Own work by uploader - CC BY-SA 3.0 https://it.wikipedia.org/wiki/Ferrovia_Cremona-Iseo#/media/File:Mappa_ferrovia_Cremona-Iseo.png (accessed on 24/10/2019)

Figure 102. Microphone configuration for the pass-by noise test. The microphones at the axlebox level M0 and M1 were positioned at 1.5 m distance from the center of the track, while the third one M2 was at 7.5 m.

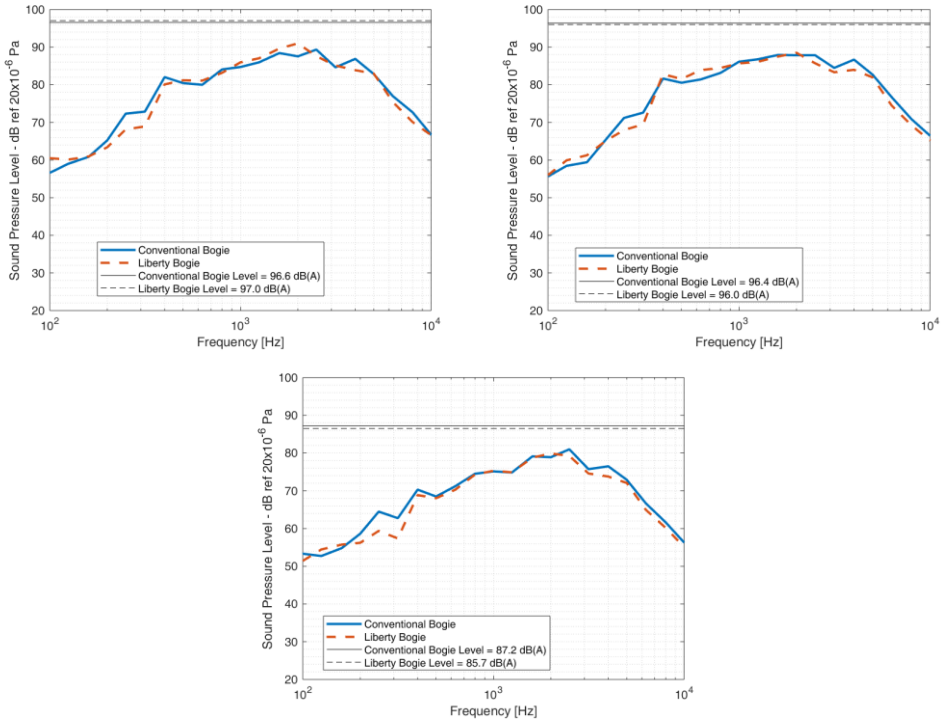

Figure 103. Third octave sound pressure levels for RUN2. Total level is plotted with black lines. Up-left: M0, up-right: M1, below M2.

It should be noted that the track, considering rails, fastening systems, sleepers and ballast, was not in perfect conditions to perform a noise test. In fact, the Track Decay Rate (TDR for short) has been evaluated after the measurement runs. The TDR, measured in dB/m, is the parameter used to estimate the dynamic properties of the track, with reference to its damping behavior. The greater is the damping, the greater is the decay rate. If the decay is low

it means that the bending vibration waves (vertical and horizontal) can propagate along the rails, and the noise emitted is directly proportional to the distance of waves propagation. The TDR is evaluated by the measurement of the frequency response of the track using an instrumented roving hammer and a couple of fixed accelerometers (one for the vertical direction and another for the lateral direction). The full description of the test can be found in [128], while according to [129], the TDR values must comply with a lower limit, in order to avoid that the track noise emission influences the measurement of the noise emitted by the vehicle. This lower limit, which is given as function of the frequency, is shown in Figure 105 and compared to the decay rate measured on test site. For frequencies below 600 Hz the vertical decay rate is very low, resulting in a longer propagation of track vibration and therefore a greater contribution of the track to the total sound emission.

Figure 104. Lateral Track Decay Rate measurement configuration.

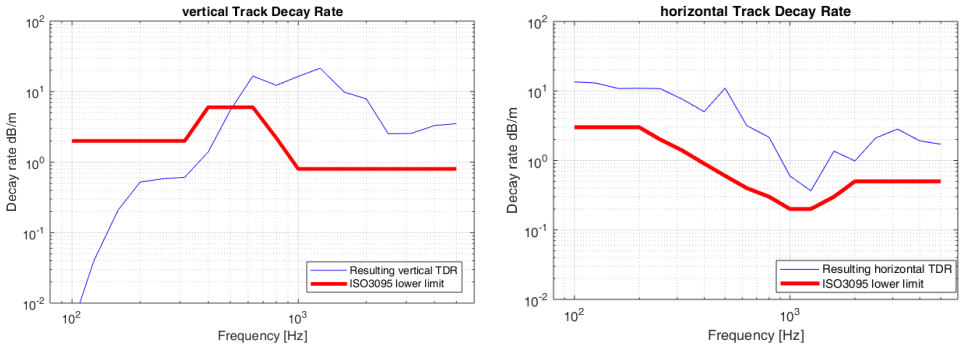

Figure 105. Track Decay Rate evaluated at the test site and compared to the limit of [129]. Left: Vertical Right: Lateral. Vertical TDR does not respect the minimum dynamic properties in terms of damping assessment.

Table 23**.** Total and average values of sound pressure levels for each run and each microphone. Above the values for whole range of frequencies, below the values for the range 2÷10 kHz.

	RUN1 - *V*=90 km/h		RUN2 - *V*=67 km/h		RUN3 - *V*=86 km/h		RUN4 - *V*=73 km/h		Avarage		
	Southbound		Northbound		Southbound		Northbound				
	LW	CW	LW	CW	LW	CW	LW	CW	LW	CW	
M0	96.7	95.3	97.0	96.6	96.8	96.0	96.2	95.8	96.7	95.9	0.8
M1	97.5	95.5	96.0	96.4	97.5	95.7	95.9	96.1	96.7	95.9	0.8
M2	82.3	82.2	86.5	87.2	86.7	86.2	86.2	86.6	85.4	85.6	-0.2
	Sound pressure levels in the range 2÷10 kHz										
M0	90.9	91.1	91.8	92.8	90.7	92.0	91.2	91.4	91.2	91.8	-0.6
M1	91.4	91.3	90.5	92.2	91.3	90.6	89.8	91.8	90.8	91.5	-0.7
M2	71.5	72.9	82.0	83.3	81.0	81.3	81.3	82.6	79.0	80.0	-1.0

Average values do not show clear advantages or disadvantages for the new solution respect to the current one. In the whole range of frequencies sound pressure level is a bit lower for the bogie with conventional wheels (0.8 dB) but considering only the frequency range for which wheel contribution is more relevant (2÷10 kHz) the bogie with Liberty Wheels is lower for all the microphones, with reduction up to 1 dB. Even if the advantages in terms of noise reduction are not the expected one, the results can be considered a good starting point for further evaluations, for example adding to the comparison also monobloc wheels and finding a better test site to perform the noise measurements.

However, the on-track tests ended smoothly with high satisfaction[29], without structural problems neither on the wheel centre, neither in the new coupling. Therefore, it is possible to conclude that the solution of the Liberty Wheel is practically feasible.

[29] A video about the on-track tests is available at https://www.youtube.com/watch?v=3QWGHSY_4zo (accessed on 25/10/2019)

6. Conclusions and final remarks

The development of a new product for railway vehicles has been presented in this thesis. The present three years project started with the necessity to find new applications in the railway field for a recent material called *Austempered Dutile Iron* (ADI), which is obtained by the heat treatment of a conventional ferritic-pearlitic spheroidal Ductile Iron. The improved mechanical properties of ADI are comparable with those of high strength steels and are therefore suitable for the replacement of standard steels usually used for structural components of railway vehicles. During the research various applications have been taken in consideration without neglecting the regulation frame in which the design and the production of a railway vehicle is located. The state-of-the-art analysis has therefore involved a review of the current standards applied during the design process, a market analysis of typical casted components and finally a technical review of the possible new applications. Tyred wheels have been critically analyzed to understand the reasons that bring that kind of wheels out of the business of wheelsets manufactures.

While monobloc wheels are in a continuous development to withstand the increasing necessity of railway industry, tyred wheels has never been revised since their development. Nowadays, due to this missing technology growth, the concept of a removable tyre is not an advantage anymore. Lighter and cheaper monobloc wheels are in fact the preferred solution of all vehicles manufactures and railway operators, while tyred wheels survive only in old vehicles. Long and expensive mounting and dismounting processes, the unsuitable design to withstand high thermal loads and the high stresses to which the wheel centres are subjected during tyre fitting, are the main issues related to the current design of tyred wheels, which is clearly over-dimensioned for application such as light DMU or metro vehicles. The present research demonstrates that a new concept of tyred wheel can be conceived, and a design optimization in terms of tyre thickness, mating interference can be performed to reduce the mass while keeping enough coupling pressure between tyre and wheel centre.

In this context, ADI castings were considered as the best way to improve the design of old-fashioned tyred wheels, replacing the bulk and highly stressed wheel centre with an optimized lightweight spoked one. The innovative wheel centre with two ranks of inclined spokes has been developed thank to easiness to cast complex shapes using cast-iron. This casted wheel centre, together with the new concept of a self-locking conical coupling between the tyre and the wheel centre in order to reduce maintenance costs, led to development of a new product called the *Liberty Wheel*. The main advantages of this product is to simplify the availability of components needed to assembly a tyred wheel and to reduce purchasing and maintenance costs.

It was demonstrated that fully finished tyres can be mounted and dismounted without the need of special tools, and that casted wheel centres can be successfully used opening the market to several new possible suppliers. A replacing wheel for the existing tyred wheel of a DMU has been therefore designed and developed. Two complete wheelsets have been then assembled in order to demonstrate the feasibility of the new products. Tests have included pass-by noise measurements, full-scale fatigue tests and vibration analysis, showing that tyred wheel can be interesting again and that ADI castings can be successfully applied in highly stressed components of railway vehicles.

Figure 106. The Liberty Wheels on display at the Italian trade fair “ExpoFerroviaria”, held in Milan between 1 and 3 October 2019.

Acknowledgements

The present thesis work was carried out in the Department of Industrial Engineering of the University of Florence.

The first acknowledgement is deserved to my supervisor *Prof. Andrea Bracciali*, whose enthusiasm has always been of great inspiration for me. I am also very grateful to *Zanardi Fonderie S.p.A.*, that founded this research, with a special mention to *Franco Zanardi*, *Enrico Veneri* and *Stefano Masaggia*.

Special thanks are needed also for all the people that have contributed to this project with their precious time, starting from *Lucio Rota*, *Paolo Petreschi*, *Alberto Minoia* and *Marco Chiudinelli*, who let this project to pass from theory to practice, passing through *Elia Temporin*, *Gennaro Caianiello*, *Rosario De Marco* and the other guys who physically manufactured the wheels, and arriving to *Luca Bocciolini*, *Riccardo Mastandrea*, *Simone James Sabetti*, *Riccardo Bovì* and *Marco Tombelli*, who gave us the opportunity to perform the fatigue tests. A special thank also goes to *Vincenzo Orazzo*, who firstly trusted in the Liberty Wheel idea.

List of publications

A. Bracciali and G. Megna. Stresses and strains in tyred wheels during tyre fitting process. In: *Proceedings of The Fourth International Conference on Railway Technology (Railways 2018)*, 3-7 September 2018, Sitges, Barcelona, Spain.

A. Bracciali and G. Megna. Tyred wheels without braking: structural optimization. In: *Proceedings of The Fourth International Conference on Railway Technology (Railways 2018)*, 3-7 September 2018, Sitges, Barcelona, Spain.

A. Bracciali and G. Megna. Re-design of tyred wheels to optimize maintenance. In: *Proceedings of The Fourth International Conference on Railway Technology (Railways 2018)*, 3-7 September 2018, Sitges, Barcelona, Spain.

A. Bracciali and G. Megna. Track friendliness of an innovative freight bogie. In: *Proceedings of the 11th International Conference On Contact Mechanics and Wear of Rail/Wheel System (CM2018)*, Delft, The Netherlands, 24-27 September 2018.

L. Bocciolini, R. Bovì, A. Bracciali, G. Caianiello, G. Megna, L. Rota, E. Temporin and E. Veneri. Manufacturing and testing of a tyred wheel with casted ADI wheel centre. In: *Proceedings of the International Wheelset Congress (IWC2019).* 16-19 September 2019, Venice, Italy.

A. Bracciali, S. Masaggia, G. Megna and E. Veneri. Quiet and light spoked wheel centres made of Austempered Ductile Iron. In: *Proceedings of the International Wheelset Congress (IWC2019).* 16-19 September 2019, Venice, Italy.

A. Bracciali, G. Caianiello, G. Megna, P. Petreschi and L. Rota. Dovetail Tyred Wheels – Application to a DMU. In: *Proceedings of the International Wheelset Congress (IWC2019).* 16-19 September 2019, Venice, Italy.

G. Megna, H. Magalhaes, Y. Bezin and A. Bracciali. Running dynamics and contact mechanics comparison of two freight bogies running in plain line and through switches and crossings. In: *Lecture Notes in Mechanical Engineering, Proceedings of the IAVSD2019*, Gothenburg, Sweden, 12-16 August 2019.

A. Bracciali and G. Megna. A Really Innovative Freight Bogie. In: *Proceedings 11th International Conference on Railway Bogies and Running Gears (BOGIE19)*, 9 - 12 September 2019, Budapest, Hungary.

A. Bracciali and G. Megna. The Liberty Wheel. In: *Proceedings 11th International Conference on Railway Bogies and Running Gears (BOGIE19)*, 9 - 12 September 2019, Budapest, Hungary.

A. Bracciali and G. Megna. New wheels, new wheelsets, new bogies. In: *Proceedings 24th International Conference on Current Problems in Rail Vehicles (PRORAIL 2019)*, 17 - 19 September 2019, Zilina, Slovakia.

Bibliography

[1] 2002/735/EC, Commission decision of 30 May 2002 concerning the technical specification for interoperability relating to the rolling stock subsystem of the trans-European high-speed rail system referred to in Article 6(1) of Directive 96/48/EC. Official Journal of the European Communities, L 245/402, 2002, Brussels.

[2] A. Ekberg and B. Pålsson. The Role Of Contact Mechanics In Multiscale Modelling Of Train–Track Interaction Phenomena. In: *Proceedings of the 11th International Conference On Contact Mechanics and Wear of Rail/Wheel System (CM2018)*, Delft, The Netherlands, 24-27 September 2018.

[3] COMMISSION REGULATION (EU) No 1302/2014 of 18 November 2014 concerning a technical specification for interoperability relating to the 'rolling stock — locomotives and passenger rolling stock' subsystem of the rail system in the European Union.

[4] A. Orlova and Y. Boronenko. The Anatomy of Railway Vehicle Running Gear. In: S. Iwnicki (ed) *Handbook of Railway Vehicle Dynamics*. 1st edition. CRC Press - Taylor & Francis Group, 2006, pp. 40-83.

[5] A. Bracciali. Railway wheelsets: history, research and developments. *International Journal of Railway Technology*, 5(1), 23-52, 2016. doi:10.4203/ijrt.5.1.2.

[6] A. Steimel. *Electric Traction – Motive Power and Energy Supply*. Oldenbourg Industrieverlag, 1st edition, 2008, ISBN 978-3-8356-3132-8.

[7] E.Andersson, A. Orvnäs and R. Persson. On the optimization of a Track-Friendly bogie for High Speed. In: *Proceedings of the 21st International Symposium on Dynamics of Vehicles on Roads and Tracks, IAVSD 2009*, Stockholm, August 17-21, 2009

[8] E. Searanke, FLEXX Eco: The leading lightweight passenger bogie design. *Global Ralway Review*, issue 2 (2014).

[9] J. Tunna, S. Clark and C. Urban. A Study of Freight Vehicle Effects on Rail Surface Damage, TTCI (UK) Ltd, 31 May 2006.

[10] I. Poschmann, E. Tschapowetz and H. Rinnhofer. Heat Treatment Process and Facility for Railway Wheels. *HTM Härtereitechnische Mitteilungen*, Vol. 62, No. 1, pp 19-21, 2007.

[11] J. Gordon and J. A. Jones. Evaluation of service-induced residual stresses in railroad commuter car wheels. In: *Proceedings of the International Mechanical Engineering Congress and Exhibition (IMECE1998)*, ASME RTD Vol. 15, Anaheim, CA, November 1998.

[12] K. Wang, R. Pilon. Investigation Of Heat Treating Of Railroad Wheels And Its Effect On Braking Using Finite Element Analysis. 2002 Ansys Conference.

[13] N. E. Dowling. *Mechanical Behaviour of Materials - Engineering Methods for Deformation, Fracture and Fatigue*. Pearson Education Limited, 4th edition, 2013, ISBN: 978-0131395060.

[14] ASTM E399. Standard Method For Plane-Strain Fracture Toughness Of Metallic Materials. *Annual Book Of Astm Standards*, Vol 03.01, ASTM.

[15] Fatigue and Fracture, Volume 19. In: *ASM Metal Handbook.* ASM International, 1996.

[16] X. Zhu and J. A. Joyce. Review of fracture toughness (G, K, J, CTOD, CTOA) testing and standardization. In: *Engineering Fracture Mechanics*. Vol 85 (2012), pp. 1–46.

[17] ORE B169 Rp. 3. Limites thermiques des roues and des sabots - Recherche du seuil de rupture. Utrecht, October 1991.

[18] M. Diener and A. Ghidini. *Reliability and Safety in Railway Products - Fracture Mechanics on Railway Solid Wheels*. LRS-Techno, Vol. 1, 2008.

[19] UIC 510-5. Technical approval of solid wheels. 1st edition, 2003.

[20] I. V. Papadopulos et al. A comparative study of multiaxial high-cycle fatigue criteria for metals, *International Journal of Fatigue*, Vol. 19, No. 3, pp. 219-235, 1997.

[21] S. Cantini and S. Beretta. *Structural Reliability assessment of railway axles*. LRS-Techno, Vol. 4, 2011.

[22] U. Zerbst et al. The development of a damge tolerance concept for railway components and its demonstration for a railway axle. In: *Engineering Fracture Mechanics*, Vol. 72, (2005), pp. 209–239.

[23] ASTM E647 - 15e1 - Standard Test Method for Measurement of Fatigue Crack Growth Rates.

[24] S. Cantini et al. Ultrasonic inspection of solid railway axles by a phased array rotating probe applied to blind holes manufactured at their ends. In: *Proceedings of the International Wheelset Congress (IWC2019).* 16-19 September 2019, Venice, Italy.

[25] EN15085. Railway applications - Welding of railway vehicles and components. October, 2007.

[26] G. Mancini and A. Cera. Design of railway bogies in compliance with new EN 13749 European standard. In: *Proceedings of 7th World Congress on Railway Research*

(WCRR06), 4-8 June, Montreal, Canada.

[27] A. Bracciali. Analisi critica delle procedure di calcolo FEM dei telai carrello e delle casse dei rotabili ferroviari. In: Atti del XXXIX Convegno Nazionale AIAS (Associazione Italiana Per L'analisi Delle Sollecitazioni), 7-10 Settembre 2010, Maratea.

[28] DVS1612. Design and endurance strength evaluation for welded steel joints in railway vehicle construction. August 2009.

[29] C. Casanueva et al. On integrated wheel and track damage prediction using vehicle–track dynamic simulations. In: *Proc IMechE Part F: Journal of Rail and Rapid Transit*, 2017, Vol. 231(7), pp. 775–785.

[30] O. Polach and D. Nicklisch. Wheel/railcontact geometry parameters in regard to vehicle behaviour and thei ralteration with wear. In: *Wear*, 2016, 366-367, pp. 200–208.

[31] A. Mysliński and A. Chudzikiewicz. Wear evolution in wheel-rail contact problems using dissipated energy approach. In: *Proceedings of the 11th International Conference On Contact Mechanics and Wear of Rail/Wheel System (CM2018)*, Delft, The Netherlands, September 24-27, 2018.

[32] M. Faccoli et al. Rolling Contact Fatigue and Wear Behavior of High-Performance Railway Wheel Steels Under Various Rolling-Sliding Contact Conditions. In: *Journal of Materials Engineering and Performance*, 2017, 26(7-8).

[33] N. Farhat et al. The benefits of mechatronically-guided railway vehicles: A multi-body physics simulation study. In: *Mechatronics*, 2018, 51, pp. 115–126.

[34] T. Ozaki et al. Evaluation of a steering bogie about running resistance and power consumption. In: *Proceedings of 10th international conference on railway bogies and running gears (BOGIE16)*, Budapest, 12-15 sept. 2016.

[35] G. I. Alarcón et al. The influence of rail lubrication on energy dissipation in the wheel/rail contact: A comparison of simulation results with field measurements. In: *Wear*, 2015, 330-331, pp. 533–539.

[36] N. Bosso, A. Gugliotta and N. Zampieri. Design and testing of an innovative monitoring system for railway vehicles. In: *Proc IMechE Part F: Journal Rail and Rapid Transit*, 2018, Vol. 232(2), pp. 445–460.

[37] A. Bracciali. Wayside Train Monitoring Systems: A State-of-the-Art and Running Safety Implications. In: *International Journal of Railway Technology*, 2012, Vol. 1(1),pp. 231-247.

[38] K. Andreas et al. Innovative ultrasonic testing technology guarantees higher sensitivity for production testing of railway wheels. In: *Proceedings of the International Wheelset Congress (IWC2019)*, 16-19 September 2019, Venice, Italy.

[39] S. Cantini et al. Ultrasonic inspection of solid railway axles by a phased array rotating probe applied to blind holes manufactured at their ends. In: *Proceedings of the*

International Wheelset Congress (IWC2019), 16-19 September 2019, Venice, Italy.

[40] M. Hassan and S. Bruni. Experimental and numerical investigation of the possibilities for the structural health monitoring of railway axles based on acceleration measurements. In: *Structural Health Monitoring*, 2019, Vol. 18(3), pp. 902–919.

[41] I. Nerlich. Benefits of "track gentle rolling stock" – expected track maintenance costs of new services in the future. In: *Proceedings of 10th international conference on railway bogies and running gears (BOGIE16)*, Budapest, 12-15 sept. 2016.

[42] E. J. Searancke. The B5000 bogie development. In: *Wheels and Axles cost-effective engineering*. IMechE Seminar Publication 2000-20.

[43] A. Ekberg, E. Kabo, J. Nielsen and J. Ringsberg. Researchers on the track of wheel–rail interaction. In: *Railway Gazette International*, 2003, 159(6), pp. 397–399.

[44] W. Geuenich , C. Günther and R. Leo. The Dynamics of Fiber Composite Bogies with Creep-controlled Wheelsets. In: *Vehicle System Dynamics*, 1983, Vol.12, pp. 134-140.

[45] J-S Kim. W-G. Lee and I-K. Kim. Manufacturing and testing of a GFRP composite bogie frame with straight side beam members. In: *Journal of Mechanical Science and Technology*, 2013, Vol. 27 (9), pp. 2761-2767.

[46] D. J. Thompson and P-E. Gautier. Review of research into wheel/rail rolling noise reduction. In: *Proc. IMechE Part F: Journal of Rail and Rapid Transit*, 2006, Vol. 220.

[47] A. Bracciali, M. Pippert and S.Cervello. *Railway noise: the contribution of wheels*. LRS-Techno, Vol.2, 2009.

[48] P.A. Meehan and X. Liu. Modelling and mitigation of wheel squeal noise amplitude. In: *Journal of Sound and Vibration*, 2018, 413, pp. 144-158 .

[49] T. Vernersson, E. Ekberg and R. Lunden. Railway freight braking and LL brake blocks − Three remaining challenges. In: *Proceedings of the International Wheelset Congress (IWC2019)*, 16-19 September 2019, Venice, Italy.

[50] A. Ronchi. *Thermostable wheels*. LRS-Techno, Vol.11, 2018.

[51] J. Csiba. Bogie Type Anniversary: the Bogie Type Y25 is over 50 Years. In: *Proceedings of 10th international conference on railway bogies and running gears (BOGIE16)*, Budapest, 12-15 sept. 2016.

[52] SUSTRAIL Project. Concluding Technical Report. June 2011 - May 2015. Available at www.sustrail.eu/IMG/pdf/sustrail_final_book_web.pdf (accessed 24.07.2019).

[53] M. Hecht and R. König. White Paper Innovative Rail Freight Wagon 2030 – The future initiative "5L" as a basis for growth in rail freight transportation. Berlin/Dresden, September 2012. Available at http://www.innovative-freight-wagon.de/wp-content/uploads/TIS_White-Paper.pdf (accessed 24.07.2019).

[54] Iwnicki S D, Stichel S, Orlova A, Hecht M. Dynamics of railway freight vehicles. In: *Vehicle System Dynamics*, 2015, 53(7), pp. 995-1033.

[55] M. Hecht and A. Schirmer. The 'LEILA DG' project: a quiet, light-weight bogie for freight wagons. In: *Railway Technical Review*, 2004, pp. 33–38.

[56] prTS 13103-2. Railway applications — Wheelsets and bogies — Part 2: Design method for axles with internal journals. 2019.

[57] EN 15437-2. On-board axlebox temperature monitoring. 2012.

[58] J. Campbell. *Complete Castings Handbook - Metal Casting Processes, Metallurgy, Techniques and Design.* Elsevier Ltd., First edition, 2011.

[59] R. Elliot. *Cast Iron Technology*. Butterworth & Co. Ltd, First Edition, 1988.

[60] ISO 1083. Spheroidal graphite cast irons - Classification. 2018.

[61] EN 1563. Founding - Spheroidal graphite cast irons. 2018

[62] J. R. Keough and K. L. Hayrynen. Designing with Austempered Ductile Iron (ADI). In: *Proceedings of American Foundry Society*, Schaumburg, Illinois, USA, 2010.

[63] SKF. *Railway technical handbook - Volume 1 - Axleboxes, wheelset bearings, sensors, condition monitoring, subsystems and services.* SKF Group, 2011.

[64] W. Menk. A New High Strength High Ductile Nodular Iron. In: *Materials Science Forum*, 2018, Vol. 925, pp. 224-230.

[65] F. Zanardi, F. Bonollo and G. Angella. A contribution to new material standards for ductile irons and austempered ductile irons. In: *International Journal of Metalcasting*, 2017, 11(1), pp. 136-147.

[66] F. Zanardi. The development of ADI, IDI™ and ADIWR™ in Italy. In: *Proceedings of 70th World Foundry Congress (WFC2012)*, 25-27 April 2012, Monterrey, Mexico.

[67] J. R. Keough, K. L. Hayrynen and V. M. Popovski. Continuing Developments in the Science and Application of Austempered Ductile Iron (ADI) In: *Proceedings of 70th World Foundry Congress (WFC2012)*, 25-27 April 2012, Monterrey, Mexico.

[68] ISO 17804. Founding - Ausferritic spheroidal graphite cast irons - Classification. 2005.

[69] EN 1564. Founding - Ausferritic spheroidal graphite cast irons. 2011.

[70] SAE J2477. Automotive Austempered Ductile (Nodular) Iron Castings (ADI). 2004.

[71] ASTM A897/A 897M-06. Standard Specification for Austempered Ductile Iron Castings.

[72] L. Meier et al. In-situ measurement of phase transformation kinetics in austempered ductile iron. In: *Material Characterization*, 2013, Vol. 85, pp. 124-133.

[73] M. Nili-Ahmadabadi and H. Shirazi. Austempered Ductile Cast Iron: Bainitic Transformation in. In: R. Colas and G. E. Totten (eds) *Encyclopedia of Iron, Steel, and Their Alloys*, 1st edition, CRC Press - Taylor & Francis Group, 2016, pp. 217-230.

[74] F. Zanardi. The development of ADI and IDI in Italy. In: *Proceedings of the 4th Keith Millis Symposium on Ductile Cast Iron*, 20-22 October 2008, Las Vegas, Nevada.

[75] H. R. Zambrano, G. Härkegård and K. F. Stärk. Fracture toughness and growth of short and long fatigue cracks in ductile cast iron EN-GJS-400-18-LT. In: *Fatigue & Fracture of Engineering Materials & Structures*, 2011, Vol. 35, pp.374-388.

[76] M. Srinivasan and S. Seetharamu. Fracture Toughness of Metal Castings. In : M. Srinivasan (ed.) *Science and Technology of Casting Processes*, 1st edition, IntechOpen, 2012, Chapter 10.

[77] K. E. McKinney et al. An Evaluation of the Toughness of Ductile Iron vs Cast Steel Using Modified Charpy Test Specimens. In: *Transactions of the American Foundrymen's Society*, 1984, Vol. 92, pp. 239-250.

[78] S-C. Lee, C-H. Hsu, C-C. Chang, and H-P. Feng. Influence of Casting Size and Graphite Nodule Refinement on Fracture Toughness of Austempered Ductile Iron. In: *Metallurgical and Materials Transactions A*, 1998, 29(10), pp. 2511-2521.

[79] A. H. Elsayed, M.M. Megahed, A.A. Sadek and K.M. Abouelela. Fracture toughness characterization of austempered ductile iron produced using both conventional and two-step austempering processes. In: *Materials and Design*, 2009, Vol. 30, pp. 1866–1877.

[80] R.A. Martinez, R.E. Boeri and J.A Sikora. Impact and Fracture Properties of ADI, compared with SAE 4140 Steel. In: *Transactions of the American Foundrymen's Society*, 1998, Vol. 106, pp. 1-26.

[81] F. Zanardi. Ductile Iron, Isothermed Ductile Iron, and Austempered Ductile Iron Material Structural Design. In: *Proceedings of the 5th Keith Millis Symposium on Ductile Cast Iron*, 2013, 15-17 October 2013, Nashville, USA.

[82] W. Böhme and L. Reissig. Capability of New High Strength ADI-Materials for Automotive Components under Crash Loading. In: *Advanced Engineering Materials*, 2015, 17(8), pp.1189-1196.

[83] G. Ianniti et al. Micromechanical modelling of constitutive behavior of austempered ductile iron (ADI) at high strain rate. In: *Theoretical and Applied Fracture Mechanics*, 2017, Vol. 92, pp-351-359.

[84] A. Ruggiero et al. ADI 1050-6 Mechanical Behavior at Different Strain Rates and Temperatures. In: *Material Science Forum*, 2018, Vol. 925, pp. 196-202.

[85] R. I. Stephens, A. Fatemi, R. R. Stephens and H. O. Fuchs. *Metal fatigue in engineering*. 2nd edition, JOHN WILEY & SONS, 2000.

[86] R. E. Peterson. *Stress Concentration Factors.* 1st edition, JOHN WILEY & SONS, 1974.

[87] B. Atzori, P. Lazzarin and G. Meneghetti. Fracture mechanics and notch sensitivity. In: *Fatigue & Fracture of Engineering Materials & Structures*, 2002, 26(8), pp. 257-267.

[88] ASTM E647 - 15e1. Standard Test Method for Measurement of Fatigue Crack Growth Rates. 2015.

[89] S. Masaggia. The development of ADI and IDI in Italy. In: *Procedia Engineering*, 2010, 2(1), pp. 1459-1476.

[90] W. Bauer. Bending Fatigue Behaviour of Ductile Iron – Effects of As-Cast Surface – Microstructure and Quality. In: *Giesserei Rundschau*, 2005, 52(1/2), pp. 17-28.

[91] EN 1370. Founding – Examination of surface condition. 2011.

[92] S. Beretta, M. Carboni, S. Cantini and A. Ghidini. Application of fatigue crack growth algorithms to railway axles and comparison of two steel grades. In: *Journal of Rail and Rapid Transit*, 2004, Vol. 218, pp. 317-326.

[93] A. Ghidini, M. Diener and F. Lombardo. Development of an innovative wheel materials for High Speed Service. In: *Proceedings of International Conference On High Speed Rail Travel: Low Cost Solutions*, 29-30 October 2013, New Delhi, India.

[94] K. Brandenberg. Successfully Machining Austempered Ductile Iron (ADI). *Applied Process Inc. Technologies*, 2001. Available at https://www.appliedprocess.com/document/233948_machining_adi_final_revision/ (accessed on 24.09.2019).

[95] J. R. Keough and K. L. Hayrynen. Automotive Applications of Austempered Ductile Iron (ADI): A Critical Review. In: *Proceedings of SAE World Congress*, 6-9 March 2000, Detroit, Michigan.

[96] R. A. Harding. The production, properties and automotive applications of austempered ductile iron. In: *Metallic Materials*, 2006, Vol. 45, pp. 1-6.

[97] C. Gorla et al. Contact and bending fatigue behaviour of austempered ductile iron gears. In: *Proc IMechE Part C: Journal of Mechanical Engineering Science*, 2018, Vol. 232(6), pp. 998–1008.

[98] Q. Wu, Y. Sun, M. Spiryagin and C. Cole. Methodology to optimize wedge suspensions of three-piece bogies of railway vehicles. In: *Journal of Vibration and Control*, 2018, Vol. 24(3), pp. 565–581.

[99] Back to the future for spoked wheels. *International Railway Journal*, 2019, Vol. 59(6), pp. 50-51.

[100] K. Jokipii. KYMENITE in Railway application. In: *International ADI-seminar: Austempered Ductile Iron*, 1991.

[101] K. Mädler. On On the Suitability of ADI as an Alternative Material for (Railcar) Wheels. In: *Proceedings of CIATF 99 Technical Forum*, 10-11 June 1999, Düsseldorf,

Germany.

[102] K. Mädler and M. Bannasch. Materials used for wheels on rolling stock. In: *Proceedings of the 7th World Congress on Railway Research* (*WCRR 2006)*, 4-8 June 2006, Montréal, Canada.

[103] M. Kuna et al. Fracture mechanics based design of a railway wheel made of austempered ductile iron. In: *Engineering Fracture Mechanics*, 2005, Vol. 72, pp. 241–253.

[104] R. Boelen and P. J. Mutton. A Comparison of the Thermal Transient Response and Deformation of Austempered Ductile Iron and Standard Tramcar Tyre Material. Internal Report of Institute of Railway Technology, Department of Mechanical Engineering, Monash University, 2001.

[105] N. Zhang et al. Wear and friction behavior of austempered ductile iron as railway wheel material. In: *Materials and Design*, 2016, Vol. 89, pp. 815-822.

[106] EN 10293. Steel castings - Steel castings for general engineering uses. 2015.

[107] G. Meneghetti et al. Fatigue properties of austempered ductile iron-to-steel dissimilar arc-welded joints. In: *Structural Integrity Procedia*, 2019.

[108] Y.Sun, M. Spiryagin, Q.Wu and C. Cole. Determination of dynamic characteristics of draft gears of heavy haul train using collision simulations. In: *Proceedings of 11th IHHA Conference*, 21 – 24 June 2015, Perth, Australia.

[109] Association of American Railroads. Manual of Standards and Recommended Practice - Section S Castings details. 2016.

[110] K. Gonzales, K. Koch, D. Carter and S. Kalay. Effects of Heavy Axle Loads on Car Coupling Systems. In: *Proceedings of 10th International Heavy Haul Association Conference*, 4-6 February 2013, New Delhi, India.

[111] J. Steed and R. Kimpton. Improving the 10" Head Alliance Coupler and Knuckle. In: *Proceedings of 11th IHHA Conference*, 21 – 24 June 2015, Perth, Australia.

[112] A. Khan and B. K. Chen. Evaluation Of Grade 1 Austempered Ductile Iron For Application To Rail Cast Components. In: *Proceedings the 5th Asia Pacific Industrial Engineering and Management Systems Conference*, 30 November 2004, Gold Coast, Australia.

[113] O.V. Makhnenko, G.Yu. Saprykina, I.V. Mirzov and A.D. Pustovoj. Prospects For Development Of Load-Carrying Elements of Freight Car Bogie. In: *The Paton Welding Journal*, 2014, Vol. 3.

[114] K. Jones, M. Degeorge and M. Stewart. Improved Steels for Freight Vehicle Bogie Castings. In: *Proceedings of the International Wheelset Congress (IWC2019)*, 16-19 September 2019, Venice, Italy.

[115] EN15313. In-service wheelset operation requirements - In-service and off-vehicle wheelset maintenance. 2016.

[116] ORE Question B64 Composite Brake Blocks. B64/RP 5/E - Limits of energy dissipation during braking with tyred wheels. 1968.

[117] K. Sachs. *Elektrische Triebfahrzeuge - Band 1*. 1st edition, Springer-Verlag, 1973.

[118] M. Große-Hovest and G. Fischer. Development of an innovative high performance railway wheelset. In: *Proceedings of the 7th World Congress on Railway Research (WCRR 2006)*, 4-8 June 2006, Montréal, Canada.

[119] Y. Okagata. Design Technologies for Railway Wheels and Future Prospects. In: *Nippon Steel & Sumitomo Metal technical report*, No. 105, December 2013.

[120] H. Anscombe and K.L. Johnson. Slip of a thin solid tyre press-fitted on a wheel. In: *International Journal of Mechanical Sciences*, 1974, Vol. 16, pp. 329-331.

[121] S. Reina, D. A. Hills and D. Dini. Incipient slip conditions in the rolling contact of tyred wheels. In: *Proceedings of the Institution of Mechanical Engineers, Part C: Journal of Mechanical Engineering Science*, 2010, Vol. 224. pp. 2049-2054.

[122] M. Tiryakioglu, E. Tiryakioglu and D. R. Askeland. Statistical investigation of the effects of the shape, size and superheat on solidification times of castings. In: *ASF Transaction*, 1997, pp. 907-913.

[123] T-Y. Hsu and Z. Wang. Fatigue crack initiation at notch root under compressive cyclic loading. In: *Procedia Engineering*, 2010, Vol. 2 , pp. 91–100.

[124] R. I. Stephens. *Metal fatigue in engineering*. 2nd edition, Wiley-Interscience publications, 2000.

[125] ERRI B169 Rp.9. Définition du cahier des charges des roues – Dimensionnement mécanique; tenue a la fatigue.

[126] A. Brand, J.F. Flavenot, R. Gregoire and C. Tournier. Donneés technologiques sur la fatigue. CETIM, France, pp. 97-119, 1989.

[127] D. Thompson. *Railway noise and vibration*. Elsevier Ltd, 2009.

[128] EN15471. Characterisation of the dynamic properties of track sections for pass by noise measurements. 2011.

[129] ISO3095. Measurement of noise emitted by railbound vehicles. 2013.